

POLITECNICO DI TORINO

Corso di Laurea in Ingegneria Energetica e Nucleare

Master thesis

**Sizing of solar-based hydrogen
production systems in North Africa and
transportation of hydrogen-natural gas
blend to Italy**



Supervisors

Prof. Pierluigi Leone

Phd Marco Cavana

Candidate

Diego Alonzo Llerena Cordova

Academic Year 2018–2019

Summary

The objective of this master thesis regards the technical assessment of hydrogen production and transportation from North Africa to Italy by using the already existing infrastructures conveying natural gas. Specifically, solar-derived hydrogen is intended to be produced by means of centralized production facilities composed of integrated photovoltaic-electrolyzer systems. For what concerns the transportation, Transmed and Greenstream pipelines have been considered in this study.

Due to contractual and design constraints, an initial evaluation of the main gas indicators has been performed to find the suitable hydrogen share for natural gas blends in both pipelines. Three countries including Algeria, Tunisia and Libya have been involved in the simulations. The areas for the installation of dedicated hydrogen production systems have been selected according to their solar resources, as well as their proximity with respect to strategic points of the pipelines. The corresponding solar irradiation data has been extracted from Meteonorm.

Subsequently, by means of MATLAB, it has been built a model to estimate the required photovoltaic capacity to obtain a blend with 5%vol of H_2 . Several configurations have been evaluated in this part: constant imported gas volume; constant imported energy and additional injection of hydrogen by keeping constant the import of natural gas. All these scenarios have been studied both in the hypothesis of constant gas flow rate and using the real gas flow rate extracted from ENTSOG database, considering 2018 as year of reference. Moreover, in order to keep 5%vol of H_2 as maximum production threshold, it has been also investigated the sizing of hydrogen storage facilities. Finally, it has been analyzed the effect of hydrogen injection on the performance of compressor stations placed along natural gas pipeline networks.

The findings of this study provide an overall perspective of the potentiality of renewable-based hydrogen production systems and the viability of hydrogen transportation in energy terms. From these results, further developments could focus on the economic feasibility of hydrogen importation in Italy.

Sommario

Lo scopo del presente lavoro di tesi consiste nella valutazione tecnica della produzione e del trasporto di idrogeno da paesi del Nord Africa in Italia, attraverso le reti di condotte attualmente adibite al trasporto di gas naturale. In dettaglio, si intende produrre idrogeno di origine solare mediante impianti di produzione centralizzata composti da sistemi integranti pannelli fotovoltaici ed elettrolizzatori. Per quanto riguarda il trasporto di idrogeno, si è considerato l'utilizzo dei gasdotti Transmed e Greenstream.

A causa dei vincoli dettati dalle normative e dalla resistenza dei materiali usati nelle condotte, è stata compiuta una valutazione iniziale dei principali indicatori dei gas con l'obiettivo di trovare la percentuale di idrogeno tale da poter essere impiegata in miscele con gas naturale. I paesi coinvolti nelle simulazioni sono Algeria, Tunisia e Libia, mentre i luoghi di installazione dei sistemi dedicati alla produzione di idrogeno sono stati selezionati in base alle risorse di energia solare ed alla posizione rispetto ai nodi strategici delle condotte. I dati di radiazione solare corrispondenti sono stati ricavati dai database del software Meteonorm.

Successivamente si è realizzato un modello per la stima della capacità installata di solare fotovoltaico richiesta per ottenere una miscela con 5% in volume di idrogeno. Partendo da questo dimensionamento, sono state analizzate diverse configurazioni del sistema: volume del gas importato costante, energia del gas importato costante e aggiunta di idrogeno al quantitativo di gas naturale importato in origine. Questi scenari sono stati studiati sia nell'ipotesi di flusso di gas costante sia rispetto al flusso di gas reale fornito dai database di ENTSOG, considerando il 2018 come anno di riferimento. Inoltre, al fine di mantenere il 5% in volume di idrogeno come soglia massima di produzione, è stata studiata l'integrazione di impianti di stoccaggio di idrogeno. Infine, è stata valutata l'incidenza dell'iniezione di idrogeno sulle prestazioni delle stazioni di compressione che si trovano lungo le reti di gasdotti.

I risultati di questo lavoro forniscono un quadro generale sulle potenzialità dei sistemi di produzione di idrogeno rinnovabile e sulla realizzazione del suo trasporto in termini energetici. Ulteriori sviluppi e studi futuri potrebbero focalizzarsi sulla effettiva sostenibilità economica dell'importazione di idrogeno in Italia.

Contents

List of Figures	V
List of Tables	VII
1 Introduction	1
1.1 Thesis purpose	3
1.2 Methodology	4
1.3 Structure	5
2 Hydrogen production techniques	7
2.1 Hydrogen from natural gas	8
2.2 Hydrogen by electrolysis	10
2.3 Electrolyzer technologies	10
3 Analysis of solar potential in North Africa	15
3.1 Literature review	15
3.2 Site selection	17
3.2.1 Algeria	18
3.2.2 Tunisia	20
3.2.3 Libya	21
4 Gas transmission networks connected to Italy	25
4.1 Transmed	26
4.2 Greenstream	27
4.3 Gas flow rates	28
5 Sizing of solar-based hydrogen production systems	31
5.1 Choice of hydrogen share	31
5.2 PV sizing	34
5.3 Case studies	36
5.3.1 Constant imported gas volume	36
5.3.2 Constant imported energy	41

5.3.3	Additional hydrogen injection to the gas imported	44
5.4	Findings and discussion	47
6	Integration of storage facilities	51
6.1	Complete supply systems	51
6.2	Partial supply systems	58
6.3	Findings and discussion	61
7	Analysis of compression stations	63
7.1	Model description	63
7.2	Operational logic of compressors	66
7.3	Findings and discussion	67
7.3.1	Greenstream	67
7.3.2	Transmed	73
8	Conclusions	79
	Bibliography	81
	Appendix A	85
	Appendix B	87

List of Figures

2.1	Different routes to hydrogen production.	7
2.2	Schematic illustrations of the main electrolyzer technologies.	11
3.1	Map of global horizontal irradiation in Algeria.	19
3.2	Solar irradiation in Hassi R' Mel, extracted from Meteonorm.	19
3.3	Map of global horizontal irradiation in Tunisia.	20
3.4	Solar irradiation in Borj Cedria, extracted from Meteonorm.	21
3.5	Map of global horizontal irradiation in Libya.	22
3.6	Solar irradiation in Wafa, extracted from Meteonorm.	23
4.1	Route followed by the Trans-Mediterranean pipeline.	26
4.2	Route followed by the Greenstream pipeline.	28
4.3	Hourly volumetric gas flow rates for the algerian gas.	29
4.4	Hourly volumetric gas flow rates for the libyan gas.	30
5.1	Gas Gravity with different hydrogen shares.	32
5.2	Gross Calorific Value with different hydrogen shares.	33
5.3	Wobbe Index with different hydrogen shares.	34
5.4	Hourly mass flow rate of H_2 in the complete supply configuration for Hassi R'Mel.	37
5.5	Hourly H_2 share in the blend in the complete supply configuration for Hassi R'Mel.	37
5.6	Hourly mass flow rate of H_2 in the partial supply configuration for Hassi R'Mel.	38
5.7	Hourly H_2 share in the blend in the partial supply configuration for Hassi R'Mel.	38
5.8	H_2 produced with respect to the real trend of the gas flow rate in the complete supply configuration for Hassi R'Mel.	39
5.9	H_2 produced with respect to the real trend of the gas flow rate in the partial supply configuration for Hassi R'Mel.	40
5.10	H_2 shares produced by the downsized system in Hassi R'Mel.	41

5.11	Hourly mass flow rates of H_2 before and after the downsizing for Borj Cedria.	42
5.12	Hourly H_2 shares in the blend before and after the downsizing for Borj Cedria.	42
5.13	H_2 produced with respect to the real trend of the gas flow rate in the complete supply configuration for Borj Cedria.	43
5.14	H_2 shares produced by the PV system of 2.56 GW in Borj Cedria. .	44
5.15	Hourly mass flow rates of H_2 before and after the downsizing for Wafa. .	45
5.16	Hourly H_2 shares in the blend before and after the downsizing for Wafa.	46
5.17	H_2 produced with respect to the real trend of the gas flow rate in the complete supply configuration for Wafa.	46
5.18	H_2 produced with respect to the real trend of the gas flow rate in the partial supply configuration for Wafa.	47
6.1	Volume of hydrogen stored in Hassi R' Mel over the year.	52
6.2	Daily stock of H_2 in Hassi R' Mel.	53
6.3	Integration of seasonal storage in Hassi R' Mel.	54
6.4	Volume of hydrogen stored in Borj Cedria over the year.	55
6.5	Daily stock of H_2 in Borj Cedria.	55
6.6	Volume of hydrogen stored in Wafa over the year.	56
6.7	Daily stock of H_2 in Wafa	57
6.8	Integration of seasonal storage in Wafa.	57
6.9	Volume of H_2 stored daily in Hassi R' Mel and coupling between PV system and storage facilities.	59
6.10	Storage utilization during summer and winter seasons in Hassi R' Mel. .	59
6.11	Volume of H_2 stored daily in Wafa and coupling between PV system and storage facilities.	60
6.12	Storage utilization during summer and winter seasons in Wafa. . . .	60
7.1	Simplified scheme of the elements represented in the model.	64
7.2	Gas flow rates through Greenstream in the Base case.	69
7.3	Pressure trends registered at Gela.	69
7.4	Pressure trends along Greenstream in the base case.	70
7.5	Characteristic of operation for the Mellitah CGS.	70
7.6	Gas consumption of turbines at Mellitah CGS.	72
7.7	Percent variance of the transport efficiency for Greenstream.	72
7.8	Gas flow rates through Transmed in the Base case.	74
7.9	Pressure trends registered at Mazara del Vallo.	74
7.10	Pressure trends along Transmed in the base case.	75
7.11	Frequencies of operation for all CGS.	76
7.12	Gas consumption of turbines for all the CGS.	77
7.13	Percent variance of the transport efficiency for Transmed.	77

List of Tables

2.1	Techno-economic characteristics of the main electrolyzer technologies.	13
4.1	Composition of the Algerian gas.	27
4.2	Composition of the Libyan gas.	28
5.1	Quantities involved for the complete supply of 5% of H ₂ in the various scenarios.	48
5.2	Results obtained for the sizing of PV systems in the various scenarios.	50
6.1	Results obtained for the integration of storage facilities in the various scenarios.	62
7.1	Input parameters regarding pipe elements for Greenstream.	68
7.2	Input parameters regarding Non-pipe elements for Greenstream. . .	68
7.3	Input parameters regarding pipe elements for Transmed.	73
7.4	Input parameters regarding Non-pipe elements for Transmed.	73

Chapter 1

Introduction

Currently, the majority of the global energy demand is supplied by fossil fuel resources. With the continuous world growing population, the energy consumption is expected to rise more and more. Thus, by considering their non-renewable origin, it is necessary to plan a future energy scenario in the scarcity of fossil fuels. This necessity is even more important due to the increasing levels of greenhouse gas (GHG) emissions associated with the intensive consumption of fossil fuels, which have led to the advancement of climate change.

To deal with these issues, the market is interested in developing alternative fuels to diversify the energy supply. Specifically, the technological interest is focus on renewable energy sources such as solar and wind energy. Indeed, after years of significant development efforts, electricity from photovoltaic (PV) systems and from wind turbines is partly economically competitive with fossil fuel based electricity at many locations.

Regarding Central Europe, renewable energy sources (RES) are of moderate quality and their availability is limited with respect to other areas with higher potentials, such as North Africa. For instance, Algeria is characterized by a very high solar potential, with yearly average direct normal irradiation (DNI) values around 2000 kWh/m², but so far it has only 350 MW of PV installed capacity on a total area of around 2382000 km² [25]. Compared to that, Italy features relatively low values of DNI, namely less than 1300 kWh/m², but at least around 20 GW of PV capacity are already installed on 301340 km² [24]. As the population density of Algeria (18 people/km²) is much smaller compared to that of Italy (201 people/km²), renewable resources should be able to meet the local energy demand and also be available for exportation in the future.

One possibility for the energy import from areas with beneficial renewable resources consists in the electricity transportation. The idea went viral in 2009 with the

Desertec Industrial Initiative (DII), a large-scale project which aimed at creating a power grid connecting North Africa and Europe. Along with power lines, it was expected the installation of solar thermal power plants including heat storage facilities in order to fulfill the energy demand also in absence of solar irradiation. However, the realization of this concept would have required significant investments for both solar power plants and power lines. Moreover, due to its non-mobile nature, the power grid would have made Europe's electricity supply partly dependent on North African and Middle Eastern countries, which represented a strong challenge with the beginning of the Arab spring in 2010 [14]. Thus, up to date none of the planned power lines have been realized.

An alternative to the electricity transport consists in the conveyance of hydrogen, which is regarded as one of the most promising energy vectors to replace fossil fuels in the near future. This energy rich gas has considerable potential because it features a flexible utilization for a range of applications including fuel for mobility, raw material in chemical and processing industries or energy storage for heat and power generation. However, like electricity, hydrogen is a secondary form of energy that has to be produced from other resources such as fossil fuels and renewable energies. The latter approach is emerging progressively as solution for the reduction of greenhouse gas emissions.

The best option for hydrogen transportation in large quantities consists in the usage of pipelines. However, installation costs associated to a pipeline network specifically designed for hydrogen are considerable and, to have low levelized transport costs, high utilization factors should be guaranteed. For this reason, it has been studied the opportunity to using existing infrastructure such as natural gas supply systems for hydrogen transportation. For instance, there are continuously operating pipeline networks connecting North Africa with Europe that should be able to transport hydrogen blended with natural gas. Such concept has been addressed by the MedHySol (Mediterranean Hydrogen Solar) project, which proposed the idea to inject hydrogen in Algeria into natural gas pipelines to be exported to Europe [16]. Even though it has not been further investigated for the time being, the development of this idea is justified by the following reasons:

- Electricity production from renewable resources, especially photovoltaic systems, has seen considerable cost reductions in recent years. That is highlighted by several low price records such as the bid of 1.79 ¢/kWh to supply power from a 300 MW PV plant in Saudi Arabia [6].
- New methodologies are needed to fulfill the target set by the Paris Agreement, which aims to keep global average temperature rise below 2 °C [20]. The provision of renewable electricity is already at the state-of-the-art and providing renewable fuels will be the next challenge in order to contribute to GHG reduction in the chemical industry, transportation and heating sector.

- The conversion techniques of electrical energy into hydrogen become more and more technologically mature and feature increasingly lower specific investment costs. Thus, the chances to implement such concepts successfully are continuously growing.

Against this background, this master thesis aims at determining the potential for solar-based hydrogen production in North Africa and assessing the possibility of hydrogen transportation in Italy by means of existing natural gas pipeline networks.

1.1 Thesis purpose

This work intends to conduct a technical assessment of the potential for hydrogen production from solar energy in some countries of North Africa. It also investigates the subsequent transport of the hydrogen produced to Italy, by blending it with natural gas in existing pipeline networks.

A preliminary issue that has been addressed regards the evaluation of the bearable shares of hydrogen within the blend with natural gas. The analysis has considered the impact related to the injection of hydrogen on the main gas indicators which determine the quality of a gas. Once the interval of hydrogen shares corresponding to the range of acceptability of such indicators has been detected, it has been chosen the hydrogen quota to be blended with natural gas (i.e. 5%vol of H_2).

The first objective of this study concerns the sizing of PV plants producing the electricity that is requested by PEM electrolyzers in order to produce the amount of hydrogen corresponding to the share adopted in the blend with natural gas. To this end, it has been considered the amount of natural gas transported by pipeline networks connecting North Africa to Italy.

Secondly, this work investigates the opportunity for integrating storage facilities in order to modulate the hydrogen supply. As the systems involved in this study are exclusively dedicated for hydrogen production, it is necessary to deal with the fluctuating nature of renewable resources such as solar energy. For this reason, it has been determined the amount of hydrogen that could be stored both in case of daily and seasonal storage.

The final goal of this thesis consists in estimating the power required by the compression stations placed along the pipeline networks in order to convey a natural gas blend with the hydrogen produced by the integrated photovoltaic-electrolyzer systems. To do that, the technical parameters of pipelines and compression stations have been analyzed in detail prior to use them in pipeline model which estimates the pressure losses associated to the injection of hydrogen.

1.2 Methodology

The hydrogen production systems considered in this study are composed of electrolyzers directly powered by solar PV plants, without connection to the local electric grid. Thus, hydrogen is solely produced from a renewable resource and therefore very low GHG emissions are involved. PV technology has been selected as their related costs have experienced sharp reductions in the last years. Moreover, this trend is set to continue over the next years [12].

Electricity generation from solar energy is performed by using hourly irradiation data extracted from the Meteonorm software and referred to a near future scenario (i.e. year 2020). The sites involved in the simulations are Hassi R'Mel (Algeria), Borj Cedria (Tunisia) and Wafa (Libya). These locations have been chosen after an accurate literature review, focusing on the most suitable areas for the installation of solar energy systems. Another important aspect that has been regarded is the proximity of the areas to the ducts used for the natural gas exportation to Italy, namely Transmed and Greenstream pipelines.

The overall amount of hydrogen that can be produced in North Africa and transferred to Italy has been calculated based on the natural gas import in 2018, reported in [4]. Specifically, three different cases have been considered:

- **Constant volume.** The gas volume conveyed stays constant and 5% of hydrogen is injected into the gas stream. The limiting factor is represented by the pipeline capacities in the reference year. In this case the export of natural gas and especially of energy decreases.
- **Constant energy.** The amount of energy transported in the reference year remains constant and 5% of hydrogen is added to the gas stream. In this scenario the energy trade is limited by the energy demand of consumers and consequently the natural gas exported reduces.
- **Additional H₂.** The amount of imported natural gas in the reference year is kept constant and 5% of hydrogen is blended to it. This case takes into account the common practice in the natural gas industry to set a certain amount of natural gas trade through long-term contracts.

Furthermore, two scenarios for the hourly gas flow rate have been assumed:

- **Constant trend.** The hourly mass of hydrogen to be produced is the same over the entire year. It has been calculated by dividing the amount of natural gas imported in the reference year by the number of annual hours.
- **Import trend.** The amount of hydrogen produced varies with the trade of natural gas on hourly basis, registered in Italy at the receiving terminals of Mazara del Vallo and Gela. Such data have been extracted from the database

of ENTSOG [7].

Finally, in the analysis of compression stations, a pipeline model has been used in order to evaluate the response of compression stations to the hydrogen blending with natural gas. In input, design parameters of pipeline networks are required, such as diameters, roughness, pipe lengths and the minimum pressures that have to be maintained throughout the route. In output, it provides the pressure trend along pipelines, and quantifies the compressor utilization in terms of switch on frequency and number of full load hours. Eventually, it also allows to estimate the transport efficiency for all the scenarios of hydrogen injection.

1.3 Structure

The contents of this master thesis are structured as follows:

- Chapter 2 proposes a review of the most conventional method for hydrogen production, based on fossil fuels, and introduces the alternative pathway which is at the basis of this thesis, that is water electrolysis. A brief description of the main electrolyzers and the differences between them is also provided.
- Chapter 3 presents the areas of North Africa that have been involved in the simulations of this investigation. The chapter opens with a recap of similar studies that have been previously conducted, from which the process of site selection has started. Afterwards it analyzes the solar potential of each area and explains the reasons behind their choice.
- Chapter 4 describes the features of the gas pipeline networks through which the hydrogen produced in North Africa could be imported in Italy. This also includes the gas composition and the hypotheses on the hourly gas flow rate that have been considered in this work.
- Chapter 5 focuses on the solar-based hydrogen production systems. Specifically, it explains the choice of the hydrogen share assumed and describes the procedures followed for the sizing of the solar PV systems feeding the electrolyzers. Moreover, the chapter shows the findings obtained in the simulations for the different scenarios that have been regarded.
- Chapter 6 investigates the integration of storage facilities to the PV systems sized in the previous chapter. In particular, the results attained for the various scenarios considered are presented in two possible configurations: seasonal and daily storage.

Chapter 7 analyzes the performance of compression stations along both the pipeline networks regarding the transportation of natural gas blends with hydrogen. The chapter starts with a description of the simulation tool used to

evaluate the pressure trend along pipeline networks. Moreover, it introduces the operational logic of compressors considered in all simulations.

Chapter 2

Hydrogen production techniques

As electricity, hydrogen is not an energy source but an energy carrier. In fact, hydrogen does not exist in nature in its molecular form and therefore it must be produced. There are several methods to produce hydrogen (Fig. 2.1). It can be mainly extracted from fossil fuels and from water. Currently, natural gas is the primary source for hydrogen generation, as it accounts for around 75% of the annual global production. Coal comes next, representing about 23% of the raw materials to produce hydrogen. Finally, oil and electricity account for the remainder of the dedicated production [27].

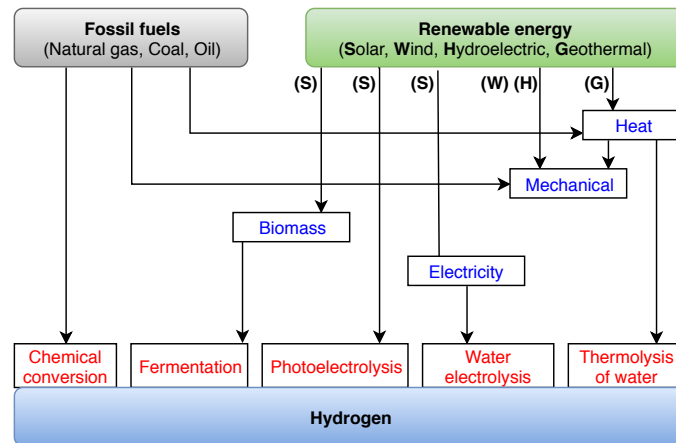


Figure 2.1. Different routes to hydrogen production.

The role played by natural gas and coal in the production of hydrogen implies that

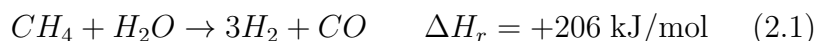
considerable CO₂ emissions are generated during this process. Although part of this CO₂ can be stored in Carbon Capture and Sequestration (CCS) systems to be used later on either industrial or chemical applications, most of it is emitted in the atmosphere. Conversely, electrolytic hydrogen plays only a minor role, despite it is able to provide low-carbon hydrogen by using electricity from renewable sources.

This chapter presents an overview of the hydrogen production methods, focusing mainly on the most conventional techniques and on those emerging of greater interest in the last years.

2.1 Hydrogen from natural gas

There are four processes for producing hydrogen from natural gas: steam reforming (using water as oxidant and source of hydrogen), partial oxidation (using oxygen as oxidant), autothermal reforming (using both water and oxygen as oxidants) and dry reforming (using CO₂ as oxidant). In all cases a synthesis gas, also known as syngas, is formed and it is mostly composed of hydrogen and carbon monoxide. The main difference between these methods regards their hydrogen to carbon monoxide ratios: steam reforming has the highest ratio (H₂/CO = 3), followed by partial oxidation (H₂/CO = 2) and dry reforming (H₂/CO = 1). For what concern the enthalpy of the reactions involved (Eqs. 2.1–2.3), steam reforming and dry reforming are endothermic processes, while partial oxidation is exothermic. Thus, steam reforming shows itself as the best technique to produce hydrogen and therefore it will be analyzed more in detail in the next paragraphs.

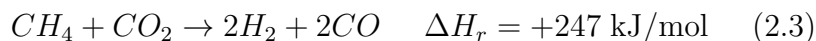
Steam reforming:



Partial oxidation:



Dry reforming:



Steam Methane Reforming (SMR) is indeed the most widespread technology for hydrogen production from natural gas at large scale. To obtain hydrogen of a certain purity, steam reforming involves several steps in which natural gas and water are both fuels and feedstocks.

The first step consists in the clean up of the starting natural gas, specifically to remove their sulphur compounds. In fact, these substances represent a poison for

nickel, which is used as catalyst in the subsequent step of steam reforming. The desulphurization process can be performed through two ways: chemical absorption (sulphur content > 100 ppm) and physical adsorption (sulphur content < 100 ppm).

After the clean up section, the natural gas is sent to the reformer, along with large amounts of water in order to have a complete reaction. Specifically, water must be added in the form of steam, otherwise the heat coming from the burner - useful to drive the endothermic reaction at about 800 °C - will be absorbed by water, decreasing the process efficiency. A fraction of the starting natural gas is oxidated with air in the combustor, together with residual combustibles exiting the final section of the process. Instead, the heat necessary for the phase change of water is retrieved from the subsequent units of the plant, which work at lower temperatures.

The syngas produce by steam reforming is characterized by a too high CO concentration (about 7%). To increase the hydrogen content, a process known as Water Gas Shift (WGS) must be performed. It is an exothermic reaction (Eq. 2.4) occurring at low temperatures, comprised between 200–350 °C. Since the syngas coming from the reformer is at higher temperatures, it must be cooled down before entering the WGS reactor. The recovered heat is used for water vaporization at the inlet of the reformer. However, to improve conversion efficiency, the WGS reaction is often divided into two stages: high temperature shift (HTS) and low temperature shift (LTS), each separated by an intercooler. The first reactor has fast kinetics, but is limited by thermodynamics to the amount of CO that can be shifted. Thus, the second reactor is necessary to reduce the CO content down to the order of 0.3%.

Water Gas Shift:



The gas mixture obtained, called reformat, still contains an amount of CO too high for most industrial applications, which typically require a high purity hydrogen. For this reason a final clean-up step is performed, namely the Pressure Swing Adsorption (PSA) process. Before entering this unit, the reformat is cooled down and its water content is removed through a condensation process. The heat retrieved is used for water pre-heating at the inlet of the reformer. PSA consists in cycles of pressurization and depressurization of a vessel containing adsorption beds, through which the dry reformat flows. Generally, at the outlet of this unit, Hydrogen 4.0 - which means a purity higher than 99.99% - is obtained, and the residual substances that can be still burned are sent to the burner.

With an estimated overall energy efficiency of about 80%, SMR is likely to remain the dominant technology for large-scale hydrogen production in the near term, due to its favourable economics and the large number of plants in operation. One

option to produce low-carbon hydrogen while still relying on fossil fuels might be the integration of CCS systems, which can lead to a reduction in carbon emissions of up to 90% [26].

2.2 Hydrogen by electrolysis

Another pathway for hydrogen generation is via electrolysis of water. It is an electrochemical process in which hydrogen and oxygen are dissociated by the application of electricity using an electrolytic cell. Although it was a major source of industrial hydrogen in the 1920s to 1960s, using hydroelectricity, electrolysis currently accounts for approximately 2% of global hydrogen production, typically in small scale systems [26]. However, there is a growing interest in this technology as it is able to provide more low-carbon hydrogen than the existing infrastructure, if surplus electricity from renewable sources is used. Declining costs for solar photovoltaic and wind generation are a further reason to consider it as a valid option for hydrogen production in the long term.

To produce 1 kg H_2 almost 9 litres of water are needed, obtaining 8 kg O_2 as by-product [27]. The latter can be used in the health care sector (at smaller scale) or for industrial purposes (at larger scale). Such considerable request of freshwater could be an issue in water-stressed areas. However, using seawater might become an alternative in coastal areas. The electricity demand for desalination - for instance using reverse osmosis - has only a minor impact on the total costs of water electrolysis. Direct use of seawater currently provokes corrosive damage to the electrolytic cell, but there are ongoing researches to make it possible and easier in the future.

Electrolysis is performed in an electrochemical device called electrolyzer. It is composed of two electrodes, namely anode and cathode, in which the oxidation and reduction reactions take place respectively. A third component, called electrolyte, is responsible for the ion migration between electrodes. Currently, three main types of electrolyzer exist: alkaline electrolytic cell (AEC), proton exchange membrane (PEM) and solid oxide electrolytic cell (SOEC). Each of them is characterized by a specific configuration (Fig. 2.2) and unique technical features (Table 2.1).

2.3 Electrolyzer technologies

Alkaline electrolysis represents the most mature and cost-efficient technology [8], which has been applied for large-scale hydrogen production (e.g. in the fertiliser and chlorine industries) since the beginning of the 20th century. In its configuration, the electrodes are immersed in an aqueous electrolyte solution of approximately 25–30 wt% KOH or NaOH, separated by a microporous diaphragm. The most common cathode material is nickel with a catalytic coating, such as platinum; for

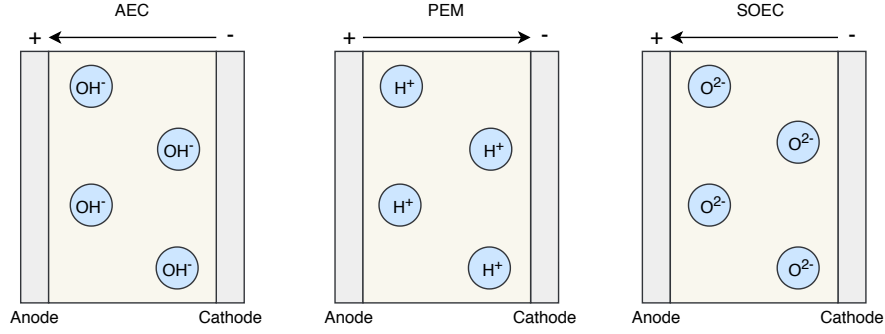
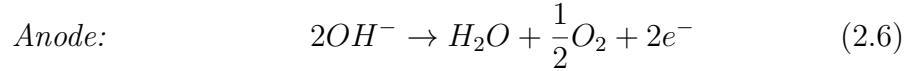
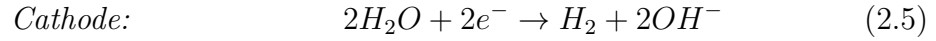


Figure 2.2. Schematic illustrations of the main electrolyzer technologies.

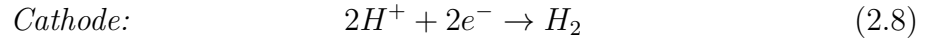
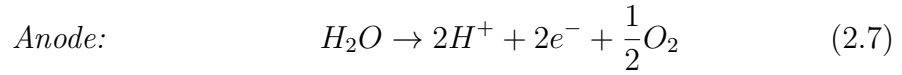
the anode, nickel or copper coated with metal oxides, such as manganese, tungsten or ruthenium, are used. Although the liquid electrolyte is not consumed in the reaction, it must be replenished over time, mainly due to other system losses during hydrogen recovery. The reactions occurring at the electrodes are:



Water is introduced in the cathode, where it is decomposed into hydrogen and hydroxide ions. The OH^- travel through the electrolyte to the anode, where O_2 is formed. The produce hydrogen is left in the alkaline solution, from which is then extracted by using a gas-liquid separation unit placed outside of the electrolyzer. Operating temperatures are below 100°C , while the standard pressure can be up to 30 bar. The minimum load of these electrolyzers is limited to 20–25%, but the hydrogen production capacities are in the order of thousands Nm^3/h [5]. Finally, the nominal stack efficiencies are between 60–70%.

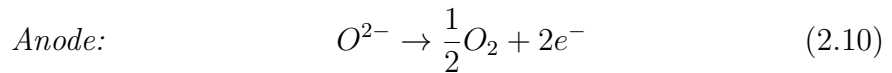
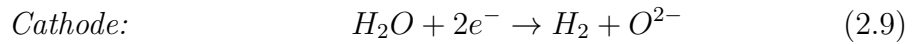
PEM electrolyzers were first introduced by General Electrics in the 1960s, to overcome some of the operational drawbacks of alkaline electrolysis. The component which brings many advantages to this technology is the electrolyte. It is composed of a solid polymeric material - also known as NafionTM membrane - which leads to a compact design. It resolves the leaking issue which AEC suffers from, due to the liquid nature of its electrolyte. Moreover, due to the solidity of the membrane, its thickness reduces leading to lower ohmic losses and consequently to higher current densities. Thanks to the solidity of the electrolyte the strength of the cell structure grows as well, and so higher operating pressures - up to 200 bar in some systems [17] - could be used. Generally, PEM electrolyzers are more suited to be coupled with intermittent renewable electricity, as there is no technical limit of minimum

load due to the low gas permeability of the membrane [5]. Several tests have even demonstrated the possibility of overload operation, up to 160% of the design capacity [27]. However, among the drawbacks, PEM electrolyzers suffer from the necessity of using expensive materials to operate under acidic regime and high voltages. Usually noble metal catalysts like iridium for the anode and platinum for the cathode are used, leading to overall costs higher than those of alkaline electrolysis. They also present a shorter lifetime and lower hydrogen production capacities, below 500 Nm³/h. Finally, the nominal stack efficiency is slightly lower with respect to those of AEC, while the operating temperatures are very similar. The reactions occurring at the electrodes are shown below.



Water is sent to the anode, where it splits into protons and oxygen. The H⁺ travel through the membrane towards the cathode, where they recombine with electrons to produce hydrogen. The O₂ exits the anode along with the unreacted water.

SOECs are the newest developed technology and still in a pre-commercial phase. Unlike the previous types of electrolyzer, operating temperatures of the SOEC are much higher, in the range of 650-900 °C, which replace part of the required electrical energy with thermal energy. For this reason SOEC is suited to being combined with heat sources like nuclear and solar thermal plants with large waste heat production. High temperature operation results in higher efficiencies - up to 80% - than AEC or PEM electrolyzer, due to improved kinetics, internal heat utilization and conversion of steam rather than liquid water. Conversely, it implies the usage of costly materials which increase the capital cost of the system. The electrolyte is made up a solid material deriving from the mixture of two ceramic powders, namely yttria stabilized zirconia (YSZ). The anode is composed of porous cermet, an alloy of nickel and YSZ, while the cathode is constituted by metal oxide doped lanthanum. The most important drawback of the SOEC is the long term degradation, whose causes are still unknown and so subject of research. The reactions occurring at the electrodes are:



Water is fed to the cathode side, where it receives electrons and forms hydrogen and oxygen ions. The O²⁻ transfer through the electrolyte and reach the anode, where they convert into oxygen.

	AEC	PEM	SOEC
Operating parameters:			
Temperature [°C]	60–80	50–80	650–900
Pressure [bar]	10–30	30–80	1–15
Current density [A/cm ²]	0.25–0.45	1.0–2.0	0.3–1.0
Flexibility:			
Load range [% of the nominal capacity]	25–110	0–160	20–100
Cold start-up time	1–2 h	5–10 min	hours
Warm start-up time	1–5 min	< 10 s	15 min
Electrical efficiency:			
Stack efficiency [%, LHV]	63–71	60–68	>95
System efficiency [%, LHV]	51–60	56–60	76–81
Available capacity:			
Max. nominal power per stack [MW]	6	2	< 0.01
H ₂ production per stack [Nm ³ /h]	1400	400	< 10
Cell area [m ²]	3.6	0.13	< 0.06
Durability:			
Stack lifetime [operating hours]	60000– 100000	30000– 90000	10000– 20000
Efficiency degradation [%/a]	0.25–1.5	0.5–2.5	< 3–50
Economic parameters:			
Investment costs [€/kW]	800–1500	1400–2100	> 2000
O&M costs [% of investment costs per year]	2–3	3–5	n.a.

Table 2.1: Techno-economic characteristics of the main electrolyzer technologies.

Chapter 3

Analysis of solar potential in North Africa

One of the first tasks addressed in this study has been the accurate research of similar works in the literature. To have a complete understanding of the topic, several studies performed worldwide evaluating both the potential generation of solar hydrogen and its economic integration have been investigated, focusing as much as possible on those carried out in northern african countries. Therefore, a review including various solar energy systems for the production of hydrogen will open this chapter.

Subsequently, there will be a section dedicated to the locations involved in the simulations of this study. Here the procedures adopted for their selection will be described and for each of them it will be proposed a more detailed analysis regarding the solar resources and the predisposition for the arrangement of dedicated solar-hydrogen production systems.

3.1 Literature review

Touili et al. [28] estimated the hydrogen production potential of Morocco from a large scale grid independent system composed of PEM and PV panels for electricity generation. First, they stated that an adequate way to assess the solar potential for large areas consists in using a combination between data from satellite and ground measurements. For this reason, they performed an uncertainty analysis of satellite data, characterized by a large spatial coverage and valid for a long-time period, with respect to data from meteorological stations, which provide information with higher resolution for only small areas in the space. Results indicated that satellite data were very acceptable and therefore suitable for simulating the electricity and

hydrogen production in the country, by means of a GIS software. Finally, they performed a technical and economical assessment, finding out that Morocco has a huge potential for hydrogen production from solar energy. The daily annual production varies between 6489 and 8308 tons/km², with the southern part of the country displaying a higher potential than northern parts. Besides, the cost of electricity and hydrogen production are in the range of 7.7–9.9 c\$/kWh and 4.64–5.79 \$/kg respectively.

Sayedin et al. [22] examined the technical and economical production of hydrogen using small scale direct-coupled PV-PEM systems throughout six cities in Iran, to investigate the impact of different climate conditions. Moreover, they considered two scenarios to carry out a system optimization: minimization of energy transfer losses and minimization of the LCH. It was found that northern cities are characterized by lower energy losses, but higher hydrogen production cost. This is due to the design variables of the first scenario, that are the number of electrolyzer cells in series and parallel. In order to match with the PV, the size of electrolyzer has to be increased and consequently the cost of the system. Conversely, southern cities have the lowest LCH, due to the better solar radiation, but higher energy losses, since the size of optimal systems is smaller than in the first scenario. The hydrogen production cost of both scenarios is in the range of 7.32–9.46 €/kg.

Koumi Ngoh et al. [15] designed and optimized a large scale hybrid system in Cameroon. It is composed of a SOEC coupled to both a PV array through a Direct Current converter and to a Parabolic Trough Collector (PTC) through a heat exchanger network. The sizing of the system was performed according to the project capacity of the largest PV power plant to be installed in the country in horizon 2020. The cost of hydrogen production from such system is 5.24 \$/kg.

Shaner et al. [23] conducted a techno-economic analysis of renewable solar hydrogen production systems in California, USA. Among several configurations examined, the large scale hybrid PV-PEM showed the most remarkable results. Two operation modes of this kind of configuration were considered: grid-independent and grid-supplemented. In the first scenario, electrolyzer units were directly connected to PV modules without a DC-DC converter to avoid additional costs. It was possible because the efficiency losses due to non-optimal operation were similar to those incurred with the converter unit. For the second scenario, the configuration was similar to the previous one, but an AC-DC rectifier along with a DC-DC converter were included for a proper electrical control; grid electricity and solar energy had production shares of 79% and 21% respectively. The main difference between these operation modes regards the capacity factor of electrolyzers: while in the first scenario it was the same as for the PV modules (~ 0.20), in the second one the capacity factor reached its maximum value (~ 0.97). Results showed a hydrogen production cost of 12 \$/kg for the grid independent operation and 6.1 \$/kg for the

grid connected scheme.

Rahmouni et al. [19] evaluated the solar hydrogen production potential in Algeria. Solar irradiation data were obtained from satellite database, meteorological stations and technical models. These values vary in a quite small interval, between 1692–2413 kWh/m²/year, with southern regions being more promising for the exploitation of solar resources for hydrogen production. The total annual solar electricity potential is ranged between 250–370 GWh/km² and the corresponding hydrogen production potential is comprised between 4437–6327 tons/km². They concluded that the Algerian Sahara is optimal for large scale solar projects.

More studies were conducted in Algeria by Boudries [1–3]. In order to evaluate the impact of climate conditions, two cities were considered, located in southwest and coastline of the country. He performed techno-economic assessments of hydrogen production from low temperature electrolyzers coupled to three different technologies: hybrid solar parabolic trough-gas power plant, conventional photovoltaic (PV) and concentrator photovoltaic (CPV). Results showed that the first configuration has LCH values in the range of 6–7 \$/kg. From a sensitivity analysis, it turned out that by increasing the solar fraction the cost of hydrogen production increases, while it decreases with higher values of direct normal irradiance. The second scheme has hydrogen production costs between 9.5–13 \$/kg, with the lower values corresponding to the addition of tracking systems. Finally, LCH values ranging between 1.5–4.5 \$/kg were found for the third layout. Lower costs correspond to higher values of concentration ratio and PV cell efficiency. Overall, it was concluded that south of Algeria is more suitable for the installation of those systems, particularly for CPV-electrolysis technology.

3.2 Site selection

Several factors have to be considered for choosing the sites in which the simulations of solar-hydrogen production will take place. The gathered information during literature review has played a fundamental role, primarily because it has been possible to compare the results obtained in different locations in order to focus on the most interesting.

The first aspect that has to be considered is the global horizontal irradiation. For this reason the maps showing the solar potential in each site selected will be presented. Another important factor that will be addressed is the water availability, which is necessary in order to perform the water electrolysis for hydrogen production. Finally, also the proximity of the sites with respect to the pipeline networks conveying natural gas - described in Chapter 4 - has been evaluated, in order to take advantage during the injection of the blends.

The sites considered in this study to perform the simulations are located in Algeria,

Tunisia and Libya. In the following sections, a more detailed description will be presented for each of them.

3.2.1 Algeria

Several studies consider Algeria as the most appropriate site for massive production of solar hydrogen. Indeed, this country features all the feasibility elements of such project, including important potential of solar resources, considerable amounts of groundwater exploitable, and the presence of gas pipeline networks connected to the European market.

According to the German Aerospace Center (DLR), Algeria has the most important solar potential in the Mediterranean basin, with around 13.9 TWh/year for solar photovoltaic and 169440 TWh/year for solar thermal [16]. As shown in Fig. 3.1, the country present irradiation rates comprised between 1700–2400 kWh/m².

Regarding the water resources, the algerian territory comprises 70% of the North Western Sahara Aquifer System (NWSAS), which covers an extension of about 1000000 km² [9]. This basin is one of the largest groundwater layers in the world and one of the three hydrous resources whose the Arab world intends to rely in the future (the other two being the aquifer of the Nubian Sandstone located in Libya and Egypt, and aquifers on Saudi Arabia). The average annual recharge amount of water is estimated to be around 1 bcm/year, but at the present time it is still subject of research.

Lastly, the geographical position of Algeria plays a fundamental role in the energy provisioning of the European Union. Indeed, Algeria is the main gas provider for Europe in the Mediterranean, where at present there are three pipelines in operation delivering natural gas:

- Maghreb-Europe Gas (MEG) pipeline, connected to Spain via Morocco;
- Medgaz, connected directly to Spain;
- Transmed, connected to Italy via Tunisia.

The site selected in Algeria corresponds to Hassi R' Mel, which represents the hub for all the pipelines listed above. Located at a latitude of 32.94° N, this town is characterized by the presence of the largest gas field of the country, with an extension of 70 kilometers from north to south and 50 kilometers from east to west. The solar irradiation data for this location has been extracted from the Meteonorm software in both hourly and monthly basis. The data are referred to the optimized values of slope and orientation of the PV panels, that are 33° and -2° respectively. The hourly data have been integrated to obtain daily values, in order to make a comparison with respect to the mean values provided by the monthly basis (Fig. 3.2). It is observed that the average daily values are mostly comprised between

6–7 kWh/m² along the year, being slightly higher during the spring and summer seasons.

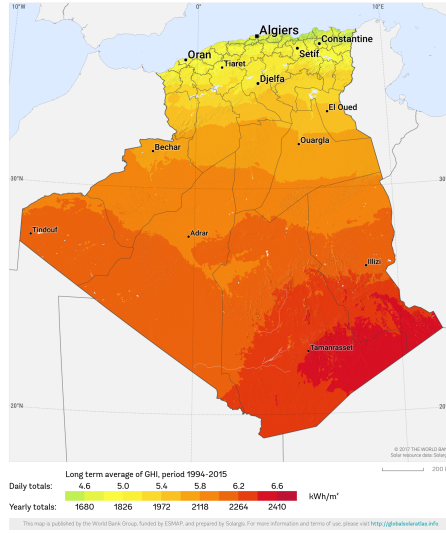


Figure 3.1. Map of global horizontal irradiation in Algeria.

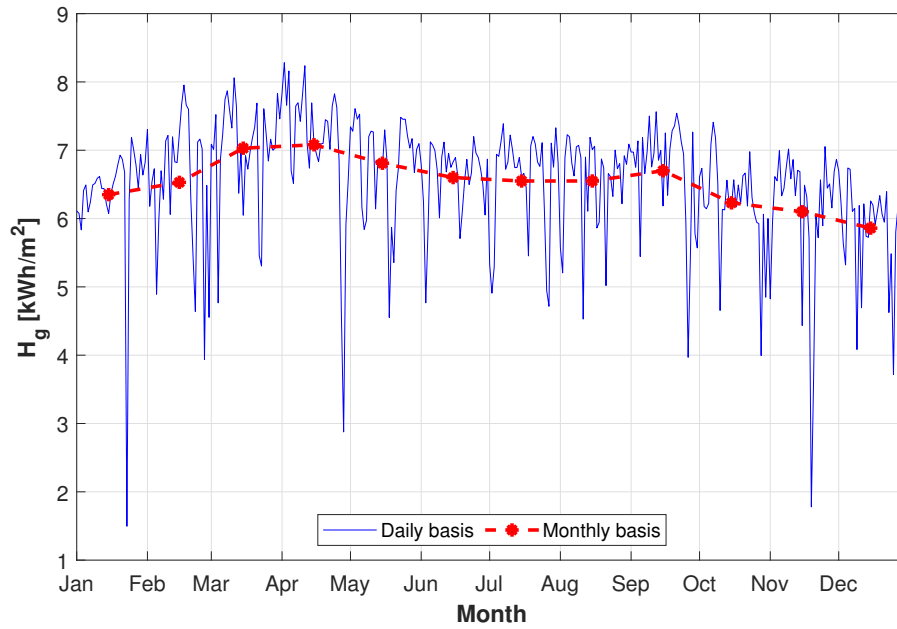


Figure 3.2. Solar irradiation in Hassi R' Mel, extracted from Meteonorm.

3.2.2 Tunisia

Tunisia is an energy-dependent country with modest oil and gas reserves. However, the rapid expansion of the global renewable market has permit the recognition of its significant solar energy potential, resulting in an strong commitment by the country in the diversification of the power generation portfolio.

Regarding the solar energy market, in 2009 the Tunisian government adopted the "Plan Solaire Tunisien", which aims to achieve 4.7 GW of renewable energy capacity by 2030, including the use of solar photovoltaic systems, solar water heating systems and solar concentrated power units. On international level, Tunisia is also involved in the early stages of the Mediterranean Solar Plan (MSP), a separate EU-backed scheme that envisions to create 20 GW of new solar generation around the Mediterranean Sea on the horizon 2020–2030 [13].

In Fig. 3.3, it is shown that the irradiation rates for Tunisia range between 1600–2200 kWh/m², with more favorable values in the south of the country. However, in this study a north-eastern town near to the gulf of Tunis has been considered, namely the Borj Cedria area. This is a well-watered site is located at a latitude of 36.68° N, being the most northerly place in which the simulations have been performed. Moreover, its choice has been also done based on its proximity to one of the compressor stations along Transmed (described in Section 4.1).

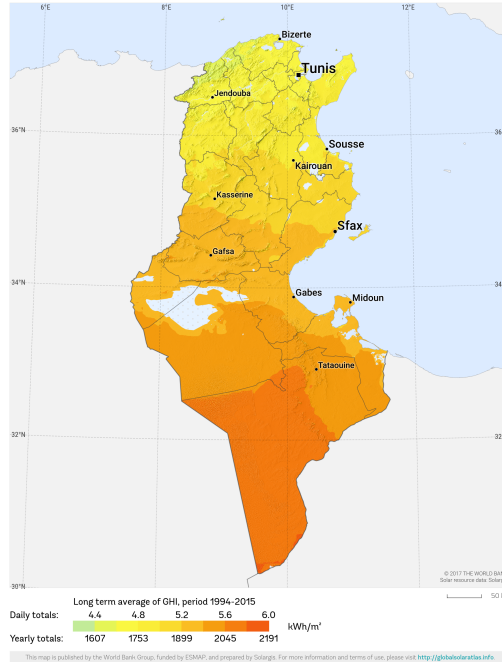


Figure 3.3. Map of global horizontal irradiation in Tunisia.

The solar irradiation data (Fig. 3.4) are referred to a slope of 32° and an orientation of -5° , being the values which optimize the production of solar panels in this site. Unlike the other two locations, the solar irradiation trend in this site has a more evident contrast between warmer and colder seasons: it reaches average daily peaks near to 7 kWh/m^2 during summer, while the lowest values correspond to around 4 kWh/m^2 during winter.

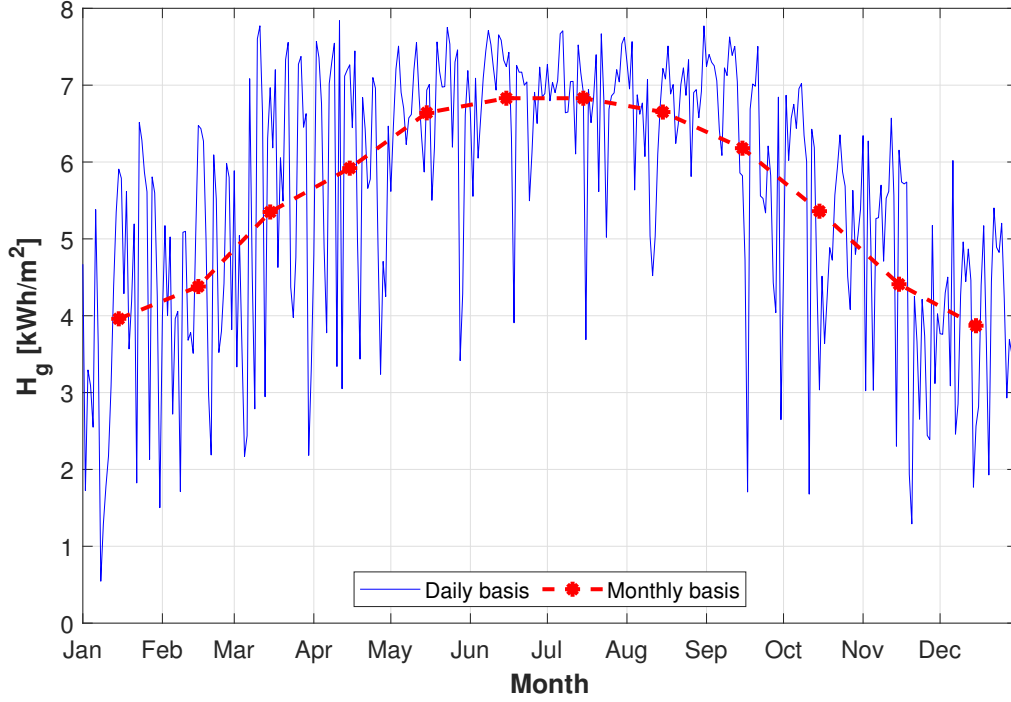


Figure 3.4. Solar irradiation in Borj Cedria, extracted from Meeonorm.

3.2.3 Libya

The major source of income in Libya is primarily represented by the oil exporting. However, according to researchers, Libya could generate approximately five times the amount of energy from solar power than it currently produces in crude oil. This is because the Libyan desert accounts for almost 88% of the total area [21]. Thus, Libya is considered as an excellent candidate to be one of the major countries that generates energy by renewable techniques for itself as well as for other countries simultaneously.

Libya boasts the highest daily solar radiation rates among the sites considered in this study: on the flat coastal plain it is about 5.5 kWh/m^2 , while in the south region values up to 7 kWh/m^2 can be reached (Fig. 3.5).

For what concern the water resources, very large quantities of fresh water are available in the Libyan desert. Indeed, 250000 km² of the NWSAS are in Libya. Another groundwater layer located in this country is the Nubian Sandstone Aquifer System (NSAS), which covers the land area in south-eastern Libya. From this fossil aquifer, the largest irrigation project in the world, known as the Great Man-Made River, supplies water to the Sahara in Libya, extracting roughly 2.4 km³ per year [18].

The place that has been selected in Libya to perform the simulations is the Wafa field, located about 540 km southwest of Tripoli, along the Libyan-Algerian border. At a latitude of 28.89° N, this place is a gas-condensate reservoir with a thin oil leg, whose production is sent to the Mellitah plant to be treated before the exportation to Italy through Greenstream (described in Section 4.2).

Also in this case the solar irradiation data are referred to a tilted plane, namely to a slope of 29° and an orientation of -3°. As shown in Fig. 3.6, the average daily values range between 6–7 kWh/m² along the year, with very similar and slightly higher values from April to September.

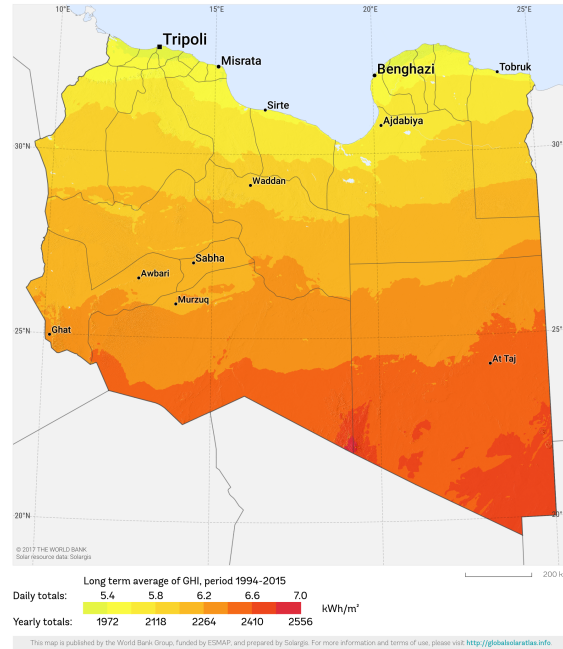


Figure 3.5. Map of global horizontal irradiation in Libya.

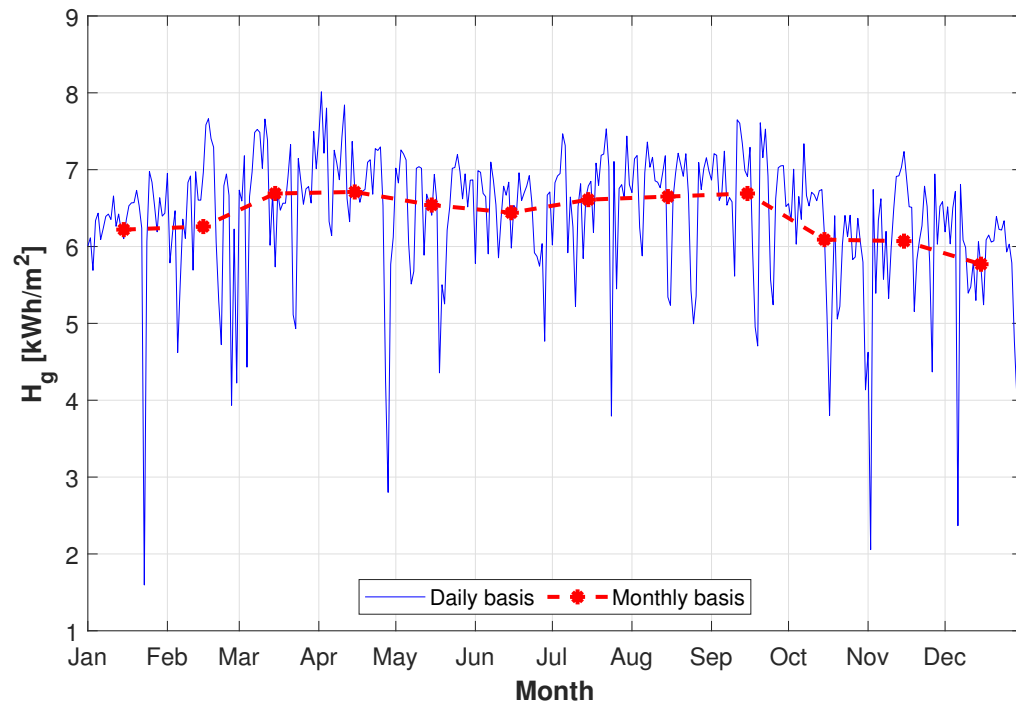


Figure 3.6. Solar irradiation in Wafa, extracted from Meteonorm.

Chapter 4

Gas transmission networks connected to Italy

On a large scale, hydrogen has to be transported by using pipeline networks. However, specifically designed pipelines for pure hydrogen transportation require high levels of initial investment. At present there exist only micro-networks of these pipelines on a regional level, primarily in US and Europe. The most widespread distribution network is operated in western part of Europe including France, Belgium, Netherlands, Germany, Switzerland and Italy, with a length of 1351 km [11].

Another transportation method consists in blending hydrogen into natural gas pipeline networks. In correspondence of the points of end use, hydrogen can be extracted from the natural gas blend by using separation and purification technologies (e.g. PSA, membrane separation, etc). As a hydrogen delivering method, blending represents an interesting solution to avoid the cost of building dedicated hydrogen pipelines during the early market development phase.

This chapter will present the two pipeline networks connecting North Africa with Europe that have been involved in this study. Such pipelines are designed for conveying natural gas, but in theory they are technically able to transport a certain amount of hydrogen in the form of blend. The discussion will consider the countries crossed and the distances covered, as well as the compressor stations located along the pipelines. The latter information will be particularly useful for the assessment of the power required by the compressor stations, that will be treated in Chapter 7. It will be also provided the composition of the original gases transported by each pipeline and, in the final section, the two scenarios assumed in this investigation for the gas flow rate will be explained.

4.1 Transmed

The Trans-Mediterranean pipeline, also known as the Enrico Mattei gas pipeline, is a natural gas transmission network connecting Algeria to Italy via Tunisia. With an overall length of almost 2490 km, this pipeline network is managed by a joint venture composed of the Algerian state-owned company Sonatrach, the Tunisian state-owned company Sotugat and the Italian company ENI. Currently, the maximum pipeline capacity is 33.5 billion cubic meter (bcm) of natural gas per year, but in 2018 only 16.3 bcm were transported [4].



Figure 4.1. Route followed by the Trans-Mediterranean pipeline.

As shown in Fig. 4.1, the pipeline begins from Hassi R' Mel in Algeria and runs for 550 km to Safsaf El Ouesra, located towards the Tunisian border. This section is composed of a compressor station placed at Ain Naga, and involves two lines with 48 inches diameter. In the Tunisian territory, the pipeline network runs for about 370 km, from the Algerian border to El Haouaria, on the Mediterranean coast. In Tunisia, the system includes five compression stations located at Feriana, Sbeitla, Sbikha, Korba and Cap Bon, involving again two lines with 48 inches diameter. The offshore section of Transmed crosses the Channel of Sicily for 155 km and lands in Mazara del Vallo, an entry point to the Italian gas pipeline network. This branch is composed of five lines with diameters comprised between 20–26 inches. Once arrived to the Italian coast, the pipeline continues for 340 km in Sicily, 15 km across the Strait of Messina and 1055 km in Italian mainland towards the northern part of the country. The Italian section is characterized by two lines with diameters ranging between 42–48 inches.

The Algerian gas is subjected to different pressures along the pipeline: in the onshore section, the gas pressure is comprised between 45–71 bar, whereas in the offshore section pressures up to 120 bar can be reached. The gas composition referred to the import year 2018 is presented in Table 4.1.

Composition	%vol
Methane	86.364
Ethane	8.693
Propane	1.355
i-Butane	0.126
n-Butane	0.176
i-Pentane	0.034
n-Pentane	0.029
Hexanes +	0.026
Nitrogen	1.300
Carbon dioxide	1.809
Helium	0.088

Table 4.1: Composition of the Algerian gas.

4.2 Greenstream

The Greenstream pipeline is a natural gas offshore pipeline connecting Libya and Italy directly. It is part of the Western Libyan Gas Project (WLGP), which is a 50-50 joint venture between the Libyan National Oil Corporation (NOC) and ENI. Although the maximum pipeline capacity is 11 bcm of natural gas per year, in 2018 just 4.3 bcm were carried [4]. The water depths along the route can exceed 1100 m.

The submarine pipeline runs for 520 km from Mellitah, on the Libyan coast to the receiving terminal of Gela, in Sicily, and is composed of a single line with a diameter of 32 inches. However, the pipeline is supplied with the natural gas extracted from two deposits: Bahr Essalam, an offshore field located at about 110 km from Tripoli coast, and Wafa, an onshore gas reservoir situated in the Libyan desert near to the Algerian border, 530 km southwest from Mellitah (Fig. 4.2). From the first field the gas is transported through a pipeline with 36 inches diameter, while from the second one it is pumped through a 32 inches pipeline.

Mellitah plays a fundamental role for the exportation of the Libyan gas. Indeed, aside the gas treatment plant, the complex also includes the compression station needed to increase the gas pressure up to 212 bar, the maximum allowable operating pressure suitable for the export to the Italian market. The gas composition referred

to the import year 2018 is also shown in this case (Table 4.2).

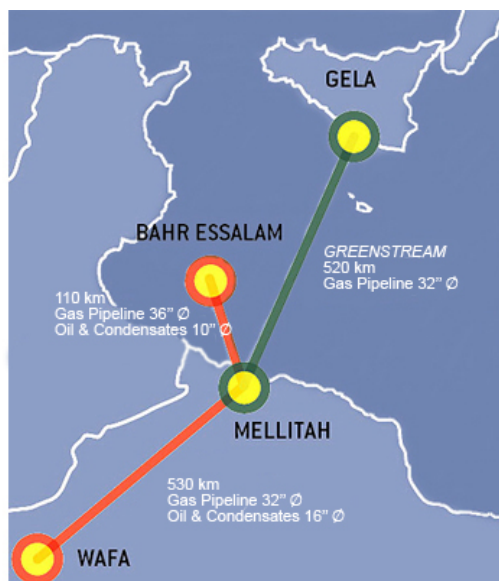


Figure 4.2. Route followed by the Greenstream pipeline.

Composition	%vol
Methane	85.306
Ethane	6.486
Propane	2.058
i-Butane	0.280
n-Butane	0.437
i-Pentane	0.099
n-Pentane	0.063
Hexanes +	0.015
Nitrogen	3.882
Carbon dioxide	1.268
Helium	0.106

Table 4.2: Composition of the Libyan gas.

4.3 Gas flow rates

In this study, all the simulations have been conducted by considering two situations: constant gas flow rate and real gas flow rate. The first scenario was determine by

starting from the total natural gas volume imported in Italy from North Africa, referred to 2018 and provided by the BP Statistical Review of World Energy [10]. According to this technical report, 16.3 billion cubic meter (bcm) of natural gas - measured at the standard conditions - were imported from Algeria, while only 4.3 bcm came from Libya. These quantities have been divided by the total annual hours of the same year of reference to find the hourly volumetric gas flow rate. On the other hand, for the second scenario these data have been retrieved from the ENTSOG database, which collect information on gas supply and demand for the European market. The difference between these layouts is reported below.

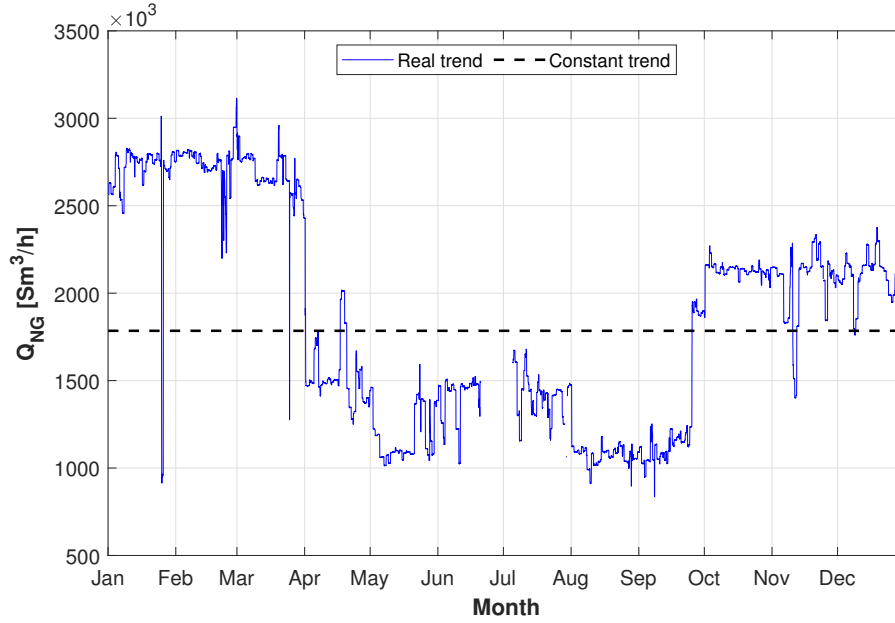


Figure 4.3. Hourly volumetric gas flow rates for the algerian gas.

The blue curve in Fig. 4.3 represents the actual annual trend of the algerian gas registered at Mazara del Vallo, one of the Italian gas network entry points. It is possible to distinguish three main zones: from January to March there is the highest import of natural gas, due to the energy consumption associated to the winter season; between April and September there is the lowest import of natural gas, because of the lower energy demand corresponding to the spring and summer seasons; finally, in the fall months the gas flow rate grows up considerably, but the amounts imported are still lower than in winter. The difference with respect to the constant trend is relevant, especially for the colder months of the year.

Less evident is the contrast between the constant trend and the real trend of the libyan gas recorded at Gela (Fig. 4.4), another entry point of the Italian gas grid. However, even if the course is quite similar from January to August, the total

volume of gas imported during the winter and fall season is considerably higher than the corresponding value for the warmer months of the year. In fact, the minimum points in the central zone of the graph are larger and sometimes there is not even an import of natural gas, as highlighted in April and late June.

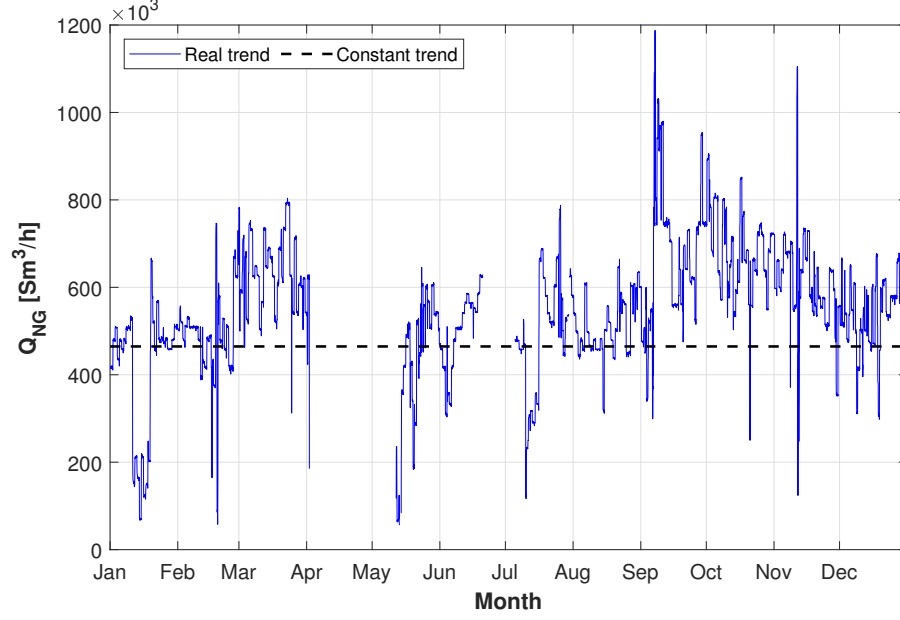


Figure 4.4. Hourly volumetric gas flow rates for the libyan gas.

Chapter 5

Sizing of solar-based hydrogen production systems

This chapter will present the procedures adopted for the sizing of solar-based hydrogen production systems. First, it will be justified the hydrogen share deployed in the blend, providing a brief review of the parameters playing a major role in the choice. After that, the formulas and assumptions used to sizing the solar PV systems will be introduced. Finally, the system configurations analyzed in this study will be described and the results obtained for the different locations will be discussed and compared between them.

5.1 Choice of hydrogen share

Existing pipeline networks conveying natural gas are designed for bearing specific chemical compositions. Additionally, regulations regarding natural gas composition set a range of values that can be assumed by the gas quality indicators. There exists three main parameters considered to describe the quality of a gas: Gas Gravity (GG), Gross Calorific Value (GCV) and Wobbe Index (WI).

Gas Gravity, or relative density, is given by the ratio between the gas density and the air density at the same specified conditions of temperature and pressure. In this study the standard conditions ($T = 15\text{ }^{\circ}\text{C}$, $p = 1\text{ atm}$) have been considered as reference. Typical values of GG for natural gas are comprised between 0.6–0.7.

Gross Calorific Value, also known as Higher Heating Value (HHV), represents the amount of heat released by the complete combustion of a gas with oxygen,

when all the products are brought to the same conditions of the reactants. The acceptable values of GCV for natural gas are strongly tied to those of GG and WI. Thus, in this work the tolerated GCV values are included between 35–45 MJ/Nm³.

Wobbe Index is the primary indicator considered to assess the interchangeability of fuel gases supplied for end-use applications. It is defined as:

$$WI = \frac{GCV}{\sqrt{GG}} \quad (5.1)$$

In the case of natural gas, typical WI values range between 40–55 MJ/Nm³, but for high quality gas the acceptability range is narrowed to 47–52 MJ/Nm³. The latter interval has been considered in this study.

The variation of these indicators with the hydrogen share in both the algerian and libyan gas compositions are described below.

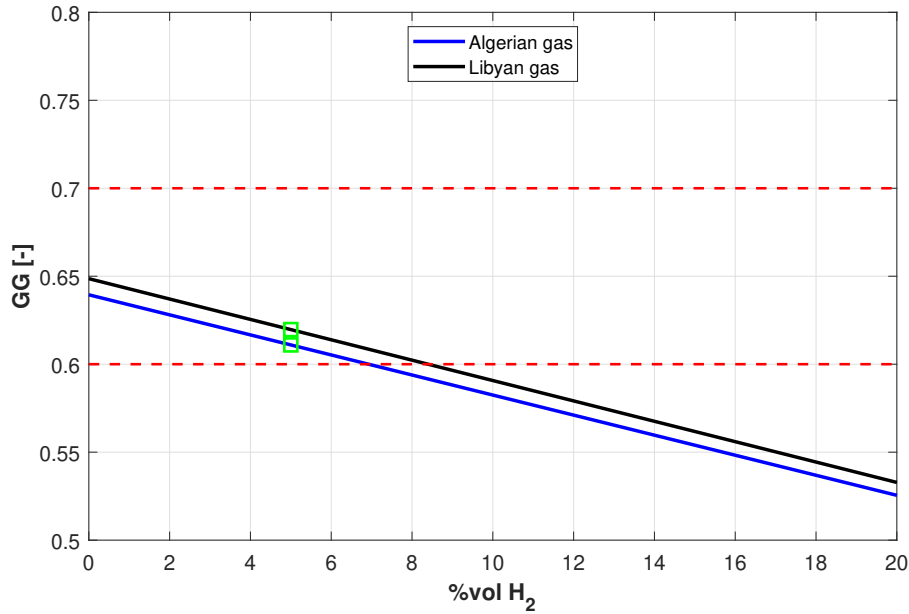


Figure 5.1. Gas Gravity with different hydrogen shares.

Higher concentrations of hydrogen determine lower values of gas gravity (Fig. 5.1). This is due to the molecular weight of hydrogen, which is considerably lower with respect to those of the other gas components. At constant hydrogen share, the libyan gas shows higher values of GG than the algerian gas, due to its slightly higher density. However, both gas compositions can accept a maximum injection of 6% of H₂ to be within the limits of gas gravity.

A similar decreasing trend is reflected for the gross calorific value of the blends, as shown in Fig. 5.2. In fact, hydrogen has a higher energy content in terms of mass, but a lower energy content in terms of volume than natural gas, due to its extremely low density. The graph exhibits higher GCV for the algerian gas, and both the compositions are within the limits for hydrogen shares below 8%.

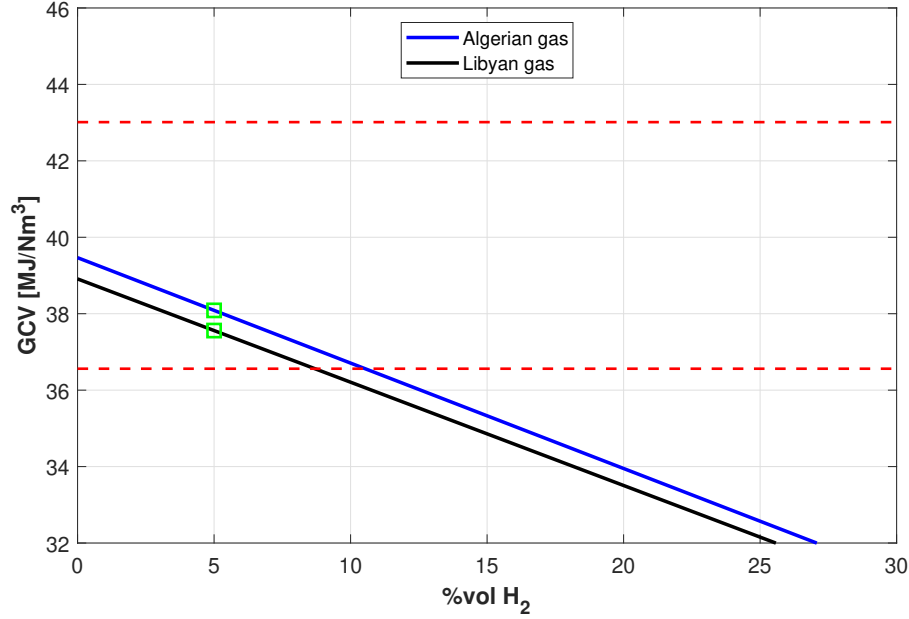


Figure 5.2. Gross Calorific Value with different hydrogen shares.

Again, a diminishing tendency is described by the Wobbe index (Fig. 5.3). It is due to its definition, as both quantities decrease with increasing levels of hydrogen. Higher values of GCV and lower values of GG give higher WI values for the algerian gas. The boundaries of this indicator are respected for hydrogen shares up to 9% in both gas compositions.

From these results it is evident that the upper limit is set by the value corresponding for the gas gravity. Thus, it can be concluded that the choice of 5% H₂ - green markers in the graphs - to be included in natural gas blends is acceptable.

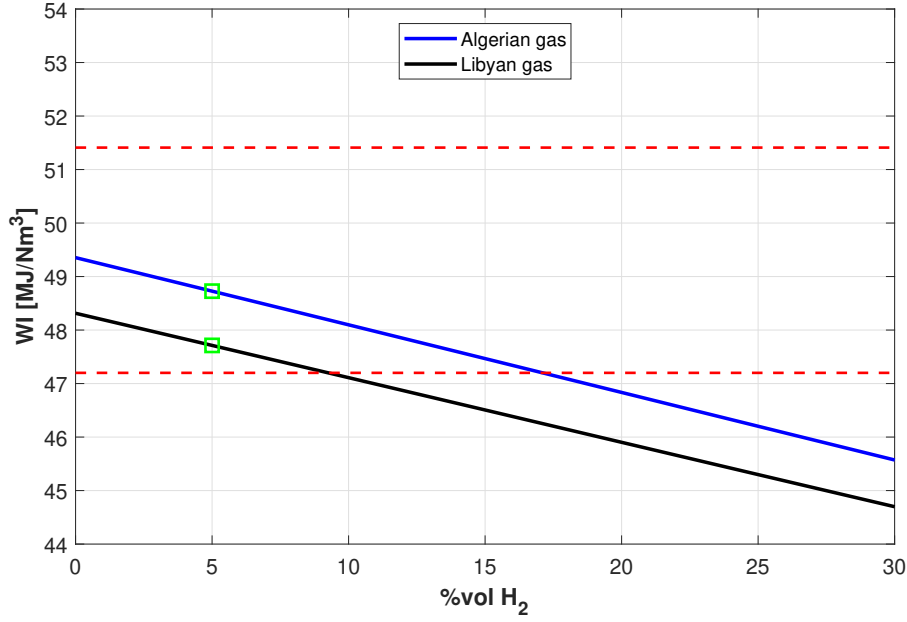


Figure 5.3. Wobbe Index with different hydrogen shares.

5.2 PV sizing

In this section the procedures followed for sizing the solar photovoltaic capacity will be discussed.

As the total blend volume is provided in input, from the previous step the volume of hydrogen to be produced is known. By means of the ideal gas law, it is possible to find the corresponding mass of hydrogen that has to be produced by the electrolyzer:

$$M_{H_2} = n_{H_2} \cdot MW_{H_2} = \frac{p_{std} V_{H_2}}{R T_{std}} \cdot MW_{H_2} \quad [\text{kg}] \quad (5.2)$$

where

n_{H_2} is the number of H₂ moles to be produced, in kmol.

MW_{H_2} is the molecular weight of H₂, equal to 2.016 kg/kmol.

p_{std} and T_{std} are the pressure and temperature in standard conditions, that are 101325 Pa and 288.15 K.

V_{H_2} is the volume of hydrogen that has to be produced, in Sm³.

R is the gas constant, equal to 8314.472 J/(kmol K).

The energy required by the electrolyzer to produce the mass of hydrogen from Eq. 5.2 is given by:

$$E_{ely,in} = \frac{M_{H_2} HHV_{H_2}}{3.6 \eta_{ely}} \quad [\text{kWh}] \quad (5.3)$$

where

HHV_{H_2} is the higher heating value of H_2 , equal to 141.91 MJ/kg.

η_{ely} is the efficiency of the electrolyzer, assumed equal to 75% for the PEM technology in the mid term.

The electricity needed by the electrolyzer has to be produced by the PV field. This energy is referred to an specific time interval (e.g hour, day, year, etc) and is given by the formula:

$$E_{ely,in} = E_{PV,out} = H_g S_{PV} \eta_{stc} PR \quad [\text{kWh}] \quad (5.4)$$

where

η_{stc} is the rated efficiency of PV modules, measured at standard test conditions ($T = 25^\circ\text{C}$ and $G_{stc} = 1 \text{ kW/m}^2$). The solar panel that has been considered in this study is reported in Appendix A.

PR is the performance ratio, assumed equal to 70%. It includes losses typical of outdoor operation.

$H_g = \int G(t)dt$ is the global irradiation on tilted plane, in kWh/m^2 . It is given by the integration of irradiance $G(t)$ over a specified period.

By inverting equation 5.4 it is possible to find the photovoltaic area corresponding to such an energy production:

$$S_{PV} = \frac{E_{PV,out}}{H_g \eta_{stc} PR} \quad [\text{m}^2] \quad (5.5)$$

Finally, it is possible to calculate the total installed PV power by knowing the number of modules corresponding to the total photovoltaic area:

$$N_{modules} = \frac{S_{PV} \eta_{stc} G_{stc}}{P_{peak}} \quad (5.6)$$

$$W_{PV} = P_{peak} N_{modules} \quad [\text{W}] \quad (5.7)$$

where P_{peak} is the peak power of the single PV module, in W.

5.3 Case studies

For what concern the total volume of natural gas imported by Italy from North Africa, three case studies have been considered in this work: constant volume of the gas imported, constant energy of the gas imported and additional injection of hydrogen to the actual import of natural gas. For each of them, it has been first determined the solar PV capacity which guarantees the supply of a blend with 5% of H_2 continuously over the year. Then, starting from these configurations, it has been evaluated the possibility of downsizing, in order to assure the production of the imposed target with the maximum frequency over the sun hours. Finally, the integration of storage facilities has been considered, accumulating hydrogen whenever there is an overproduction.

The three scenarios listed above will be explained hereafter. However, due to the similarities between them, for each scenario the results of one location will be presented, and to conclude a summarizing table collecting all the simulations results will be provided.

5.3.1 Constant imported gas volume

The first scenario assumes the data provided by the technical reports [10] and ENTSOG as referred to the total volume of blend. Therefore, the volume of the original natural gas composition will be reduced as a result of the addition of the hydrogen share. The results obtained for Algeria are presented in this section.

In the hypothesis of constant gas flow rate, the installed capacity of solar PV in Hassi R'Mel corresponding to the annual hydrogen demand is equal to 2.09 GW, with an associated required PV area of around 15.61 km². In Fig. 5.4 it is possible to observe the intermittent behavior of solar energy: during sun hours this plant produces up to 30 ton/h, exceeding considerably the almost 8 ton/h imposed as target. A better understanding on the actual hourly hydrogen shares produced is provided by Fig. 5.5. It is evident that by using a daily sampling the hydrogen shares are closer to the target, but with finer timesteps such as the hourly sampling peaks up to 20% of H_2 can be reached.

Since this study focuses on the stand-alone configuration, one of the solutions proposed could be the downsizing of the system. To do that, the hours of null production have been excluded and the plant has been scaled down in order to have 5% of H_2 in the blend as the most frequent hourly share over the year. The new solar PV installed capacity obtained for Hassi R'Mel is equal to 715 MW, equivalent to 5.34 km² of PV area, and the amount of hydrogen produced hourly by this plant is shown in Fig. 5.6. With this configuration, hydrogen shares up to 7% of H_2 can be reached, but 21% of the sun hours allow to produce the target imposed (Fig. 5.7).

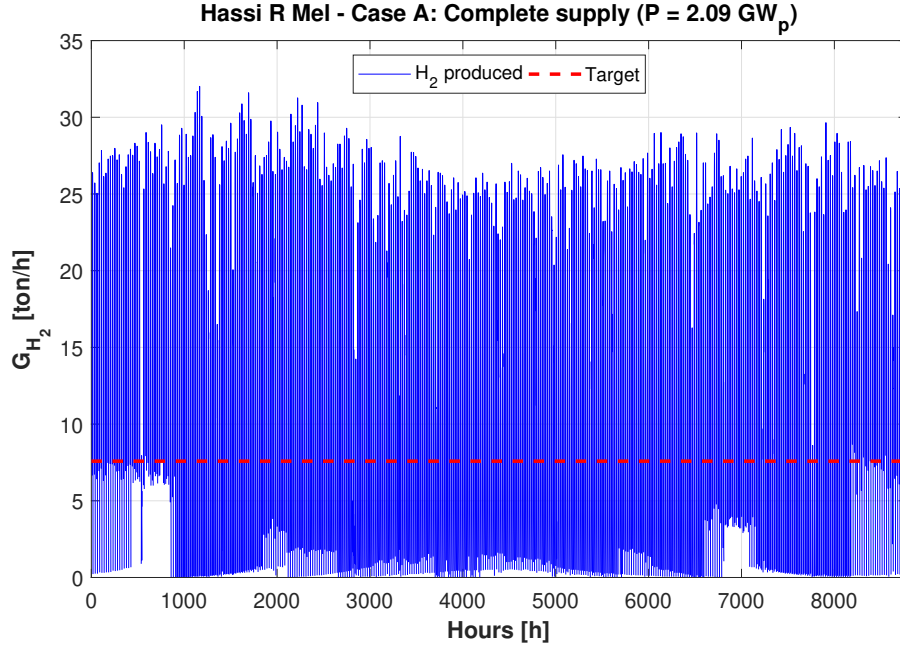


Figure 5.4. Hourly mass flow rate of H_2 in the complete supply configuration for Hassi R'Mel.

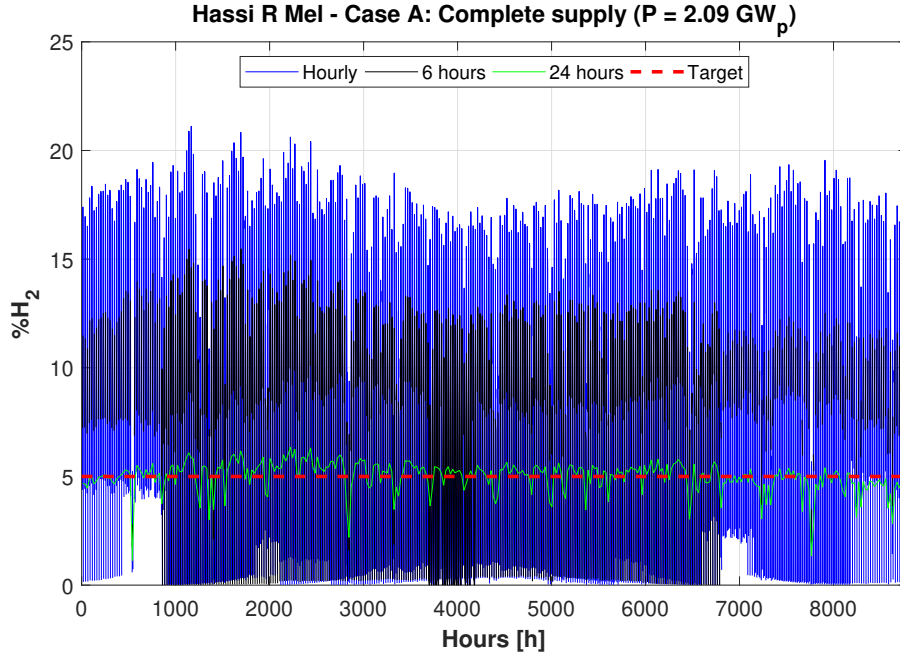


Figure 5.5. Hourly H_2 share in the blend in the complete supply configuration for Hassi R'Mel.

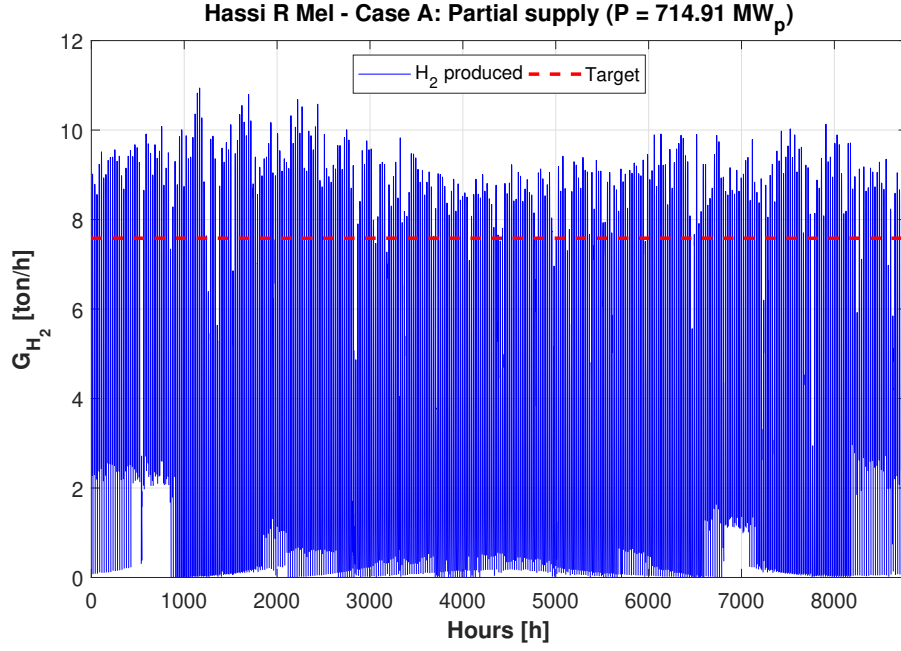


Figure 5.6. Hourly mass flow rate of H_2 in the partial supply configuration for Hassi R'Mel.

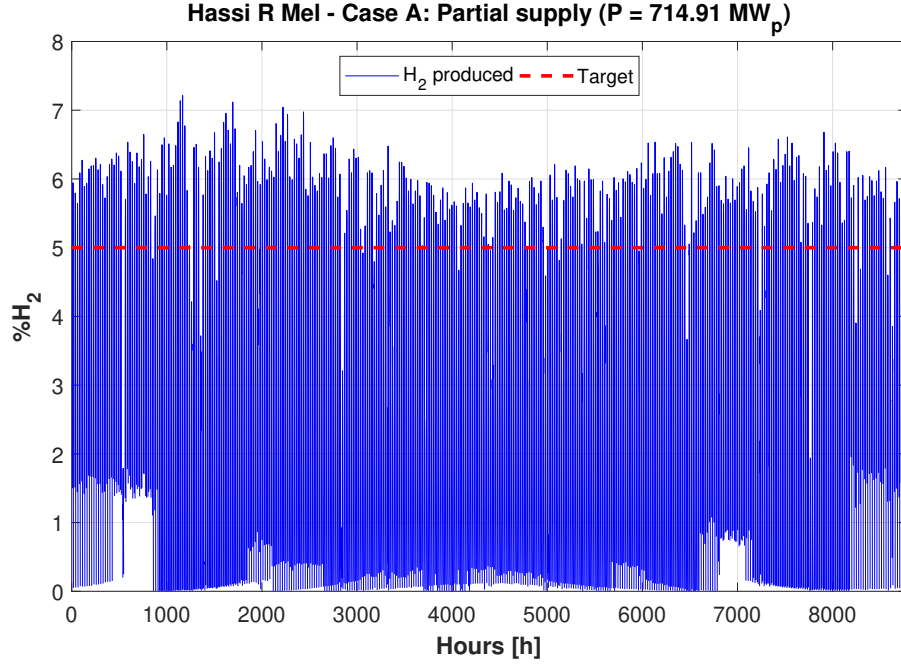


Figure 5.7. Hourly H_2 share in the blend in the partial supply configuration for Hassi R'Mel.

The same approach has been adopted to analyze the hydrogen production with respect to the real trend of the gas flow rate. The upper graph of Fig. 5.8 shows the hourly volumetric flow rates for the solar capacity satisfying the annual hydrogen demand. As before, the plant produces more hydrogen than the actual target during sun hours. However, the main difference regards the hourly hydrogen shares produce by this system. In fact, three zones can be distinguished in the bottom part of the same figure, and they are directly correlated to the trend of the blend. During the first 2000 hours peaks up to 10% of hydrogen are reached. Compare with the previous case, the maximum amount of hydrogen produced has been halved, due to the highest demand of gas during this period. In the warmer months, the supply of gas reduces considerably, and so here the highest hydrogen shares are found. Peaks up to 30% of hydrogen are obtained in the spring and summer seasons. Finally, with the increasing of gas exportation from October, the maximum quota of hydrogen produced decreases down to around 15%.

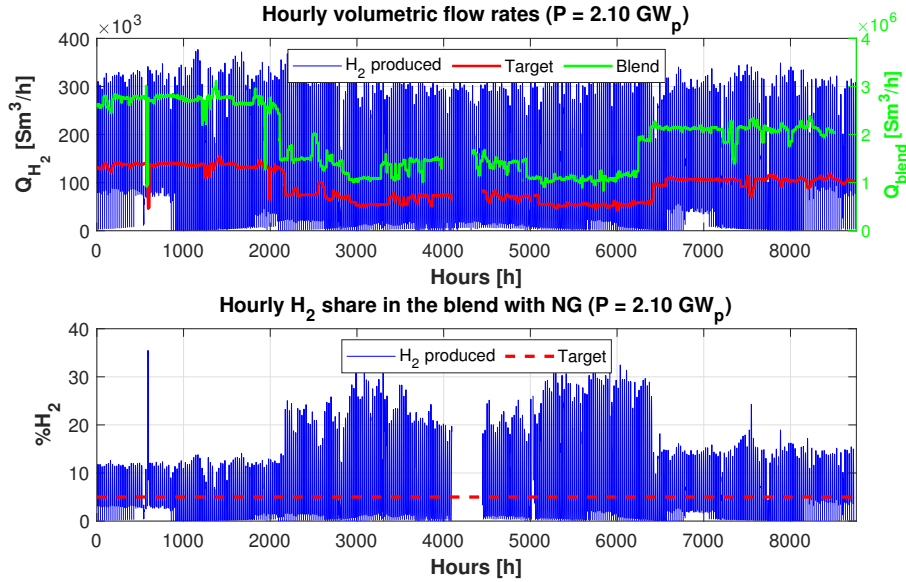


Figure 5.8. H_2 produced with respect to the real trend of the gas flow rate in the complete supply configuration for Hassi R'Mel.

To reduce the hydrogen levels the downsizing of the system has been considered also in this case. The installed capacity of solar PV which guarantees the most frequent production of 5% of hydrogen is equal to 1 GW, corresponding to a surface of 7.53 km². As shown in Fig. 5.9, the production is closer to the target during times of higher demand of gas, but peaks up to 15% of hydrogen can be reached during the warmer months. However, to have a better understanding of the hydrogen produced by this plant it is convenient to quantify the frequency of the hydrogen shares over the operating time (Fig. 5.10). Out of 4531 hours of operation during

the year, around 88% corresponds to a production lower than 10% of hydrogen, of which almost 13% corresponds to the imposed target. The injection of these levels of hydrogen could affect the quality of the gas, as they are outside the range of acceptability of the gas indicators analyzed previously.

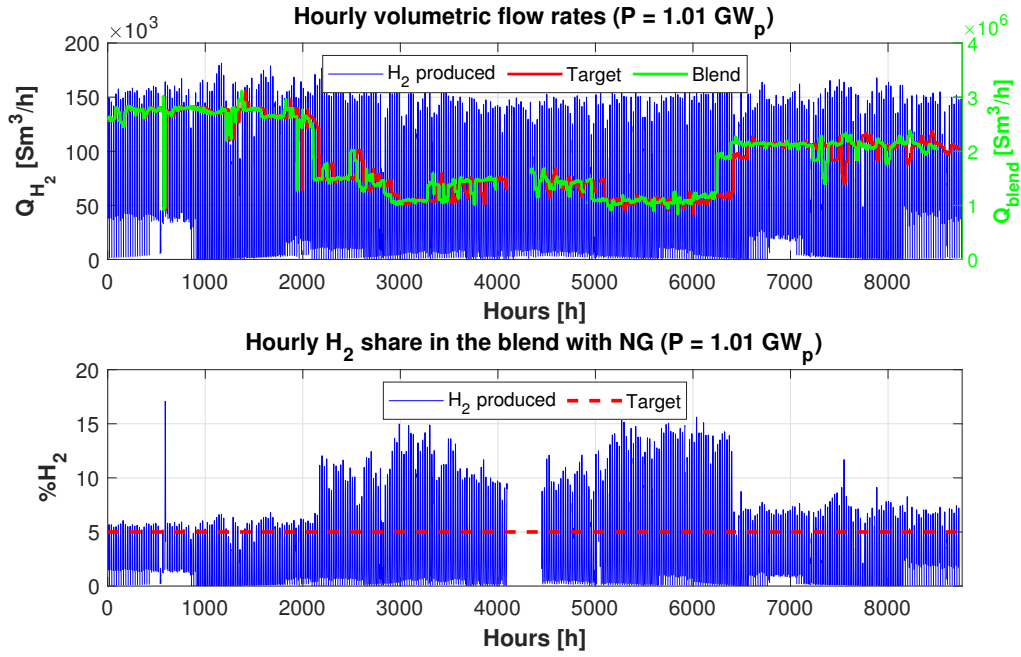


Figure 5.9. H₂ produced with respect to the real trend of the gas flow rate in the partial supply configuration for Hassi R'Mel.

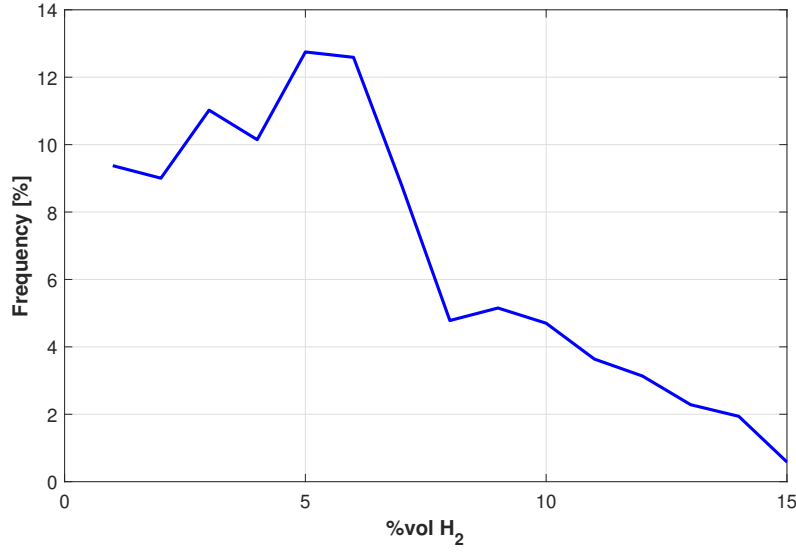


Figure 5.10. H₂ shares produced by the downsized system in Hassi R'Mel.

5.3.2 Constant imported energy

ENTSOG provides data associated to the gas flow rate imported in kWh/h. Thus, the objective of this scenario is to keep constant the energy imported from North Africa. Part of this energy will be supplied by the target of 5% of H₂ considered in this study. The results obtained for Tunisia are presented in this section.

By assuming a constant gas flow rate over the year, Borj Cedria requires a solar PV capacity of 2.56 GW (i.e. an area of 19 km²) to supply the entire annual demand of hydrogen. However, as observed in the upper graph of Fig. 5.11, hourly hydrogen mass flow rates up to 40 ton/h can be reached, exceeding by far the target which is almost 8 ton/h. In terms of hydrogen share, peaks around 20% are obtained with this plant (Fig. 5.12).

After the downsizing, the mass flow rate is closer to the target, reaching maximum flow rates of 10 ton/h. It is also evidenced by the hydrogen shares produced, lower than 8% of H₂. The highest production corresponds to 5% of H₂ and is equal to 17.5%. The solar installed capacity in the new configuration is about 777 MW, employing a surface of 5.8 km².

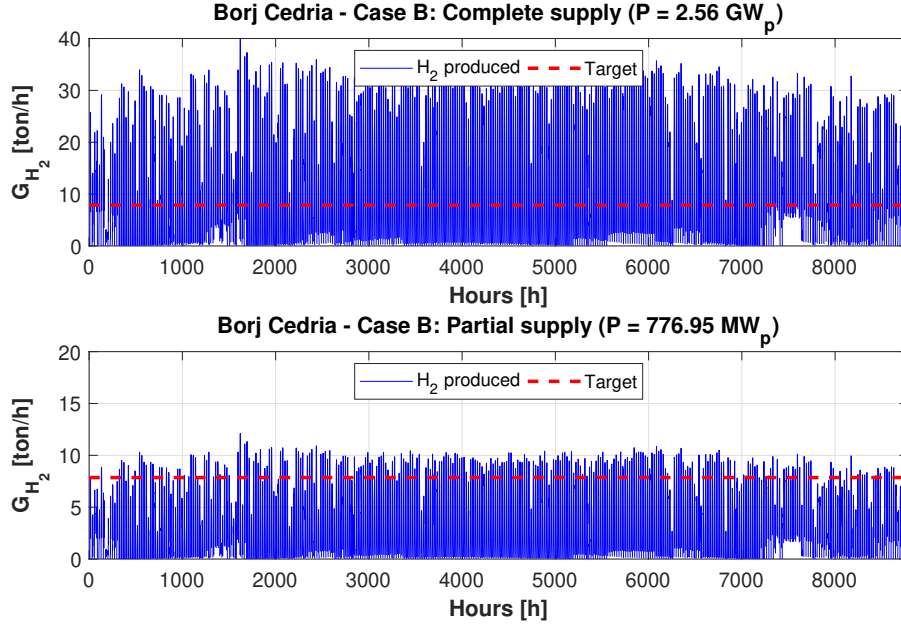


Figure 5.11. Hourly mass flow rates of H_2 before and after the down-sizing for Borj Cedria.

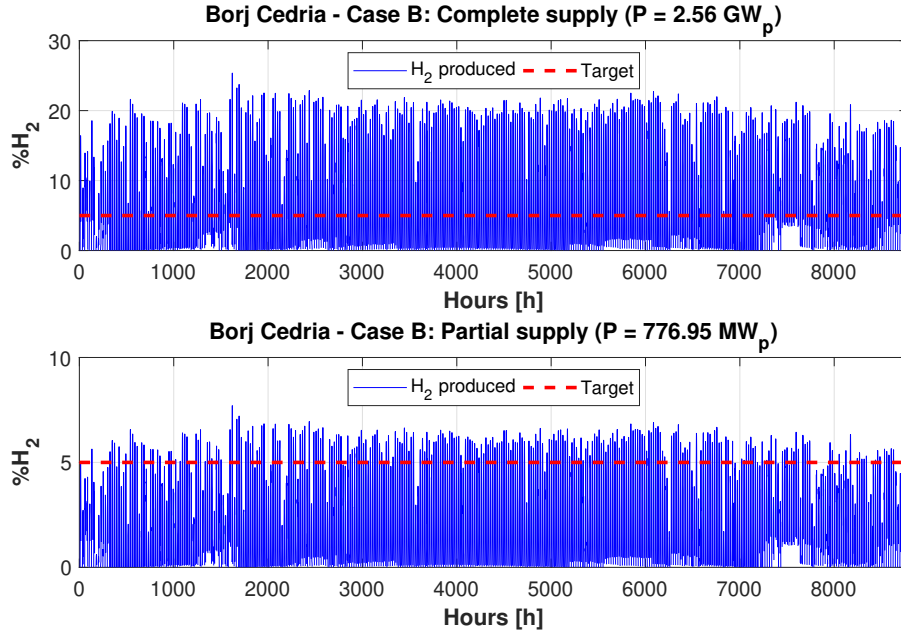


Figure 5.12. Hourly H_2 shares in the blend before and after the down-sizing for Borj Cedria.

The findings obtained by using the real trend of the gas flow rate in Borj Cedria

follow a less predictable pattern with respect to those attained for the other locations. For what concerns the hourly volumetric flow rates of hydrogen, the upper graph of Fig. 5.13 shows that during sun hours the hydrogen production exceeds the imposed target, reaching values up to around 400 thousand Sm^3 per hour. In terms of hydrogen shares, during fall and summer seasons up to 40% of H_2 could be injected to the blend, while during the colder months, except some isolated cases, hydrogen levels lower than 15% are obtained. However, to have a better knowledge of the amount of hydrogen produced, the frequencies of hydrogen levels have been estimated (Fig. 5.14). Out of 4568 hours of operation, the highest frequency of around 6% corresponds to the 4% of H_2 production. For around half of the operating hours the plant produces hydrogen shares lower than 10%, whereas for one fifth its production exceeds the 20% of hydrogen quota. This behavior could be due to the solar irradiation distribution of Borj Cedria. Even though the optimal panel inclination and azimuth have been considered, the values are lower and more irregular than those for Hassi R'Mel and Wafa. Moreover, as the most frequent hydrogen share is already lower than 5%, the downsizing in this case has been not possible.

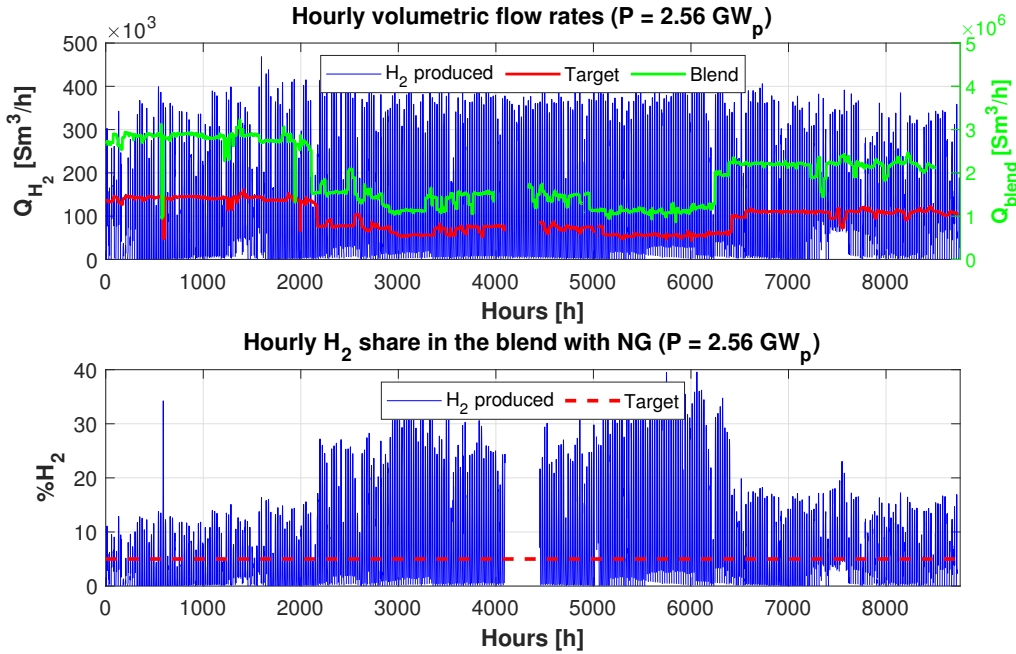


Figure 5.13. H_2 produced with respect to the real trend of the gas flow rate in the complete supply configuration for Borj Cedria.

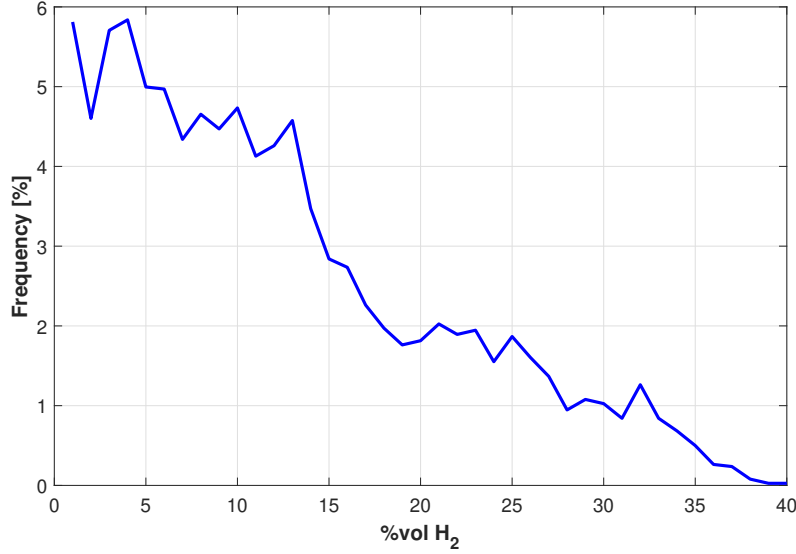


Figure 5.14. H₂ shares produced by the PV system of 2.56 GW in Borj Cedria.

5.3.3 Additional hydrogen injection to the gas imported

The goal of this scenario is to produce a blend in which the volume of natural gas remains constant with respect to the year considered. Thus, hydrogen will be added to this quantity in order to represent 5% of the gas mixture. The results obtained for Libya will be presented hereafter.

In the hypothesis of constant gas flow rate, the PV system which satisfies completely the annual hydrogen demand has an installed capacity of almost 586 MW, requiring a surface of 4.37 km². However, during sun hours this plant produces mass flow rates of hydrogen four times higher than the imposed target of about 2 ton/h, as shown in the upper graph of Fig. 5.15. For what concerns the hydrogen quota, peaks of 20% can be attained.

By downsizing this plant, it is possible to produce hydrogen mass flow rates up to 3 ton/h, which in terms of hydrogen percentages in the blend it is equivalent to values lower than 7% (Fig. 5.16).

If the real trend of the gas flow rate is assumed for Wafa, quite different results are obtained with respect to the other locations. The plant which fulfills the annual demand of hydrogen is able to produce hourly volumetric flow rates up to 100 thousand Sm³ per hour, almost doubling the maximum peak of the target (Fig. 5.17). By looking at the hydrogen quotas, peaks up to 30% can be attained, especially from January to September where there are more periods of lower gas import.

Again, also for this case the downsizing has been considered. The plant able to produce 5% of H_2 with the highest frequency over the year has an installed capacity of almost 272 MW. As observed in the upper graph of Fig. 5.18, this plant is able to produce maximum hourly volumetric flow rates of hydrogen quite similar to those of the target over the entire year. In terms of hydrogen shares, out of 4578 hours of operation, almost 15% corresponds to a production equivalent to the target imposed, while less than 4% of the time a production exceeding the 10% of H_2 occurs.

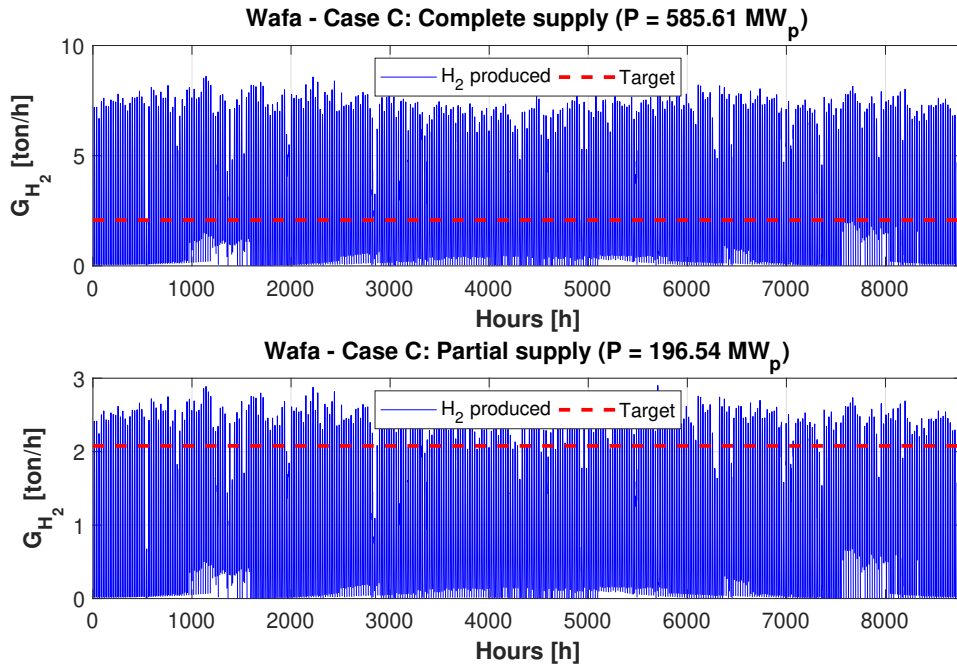


Figure 5.15. Hourly mass flow rates of H_2 before and after the downsizing for Wafa.

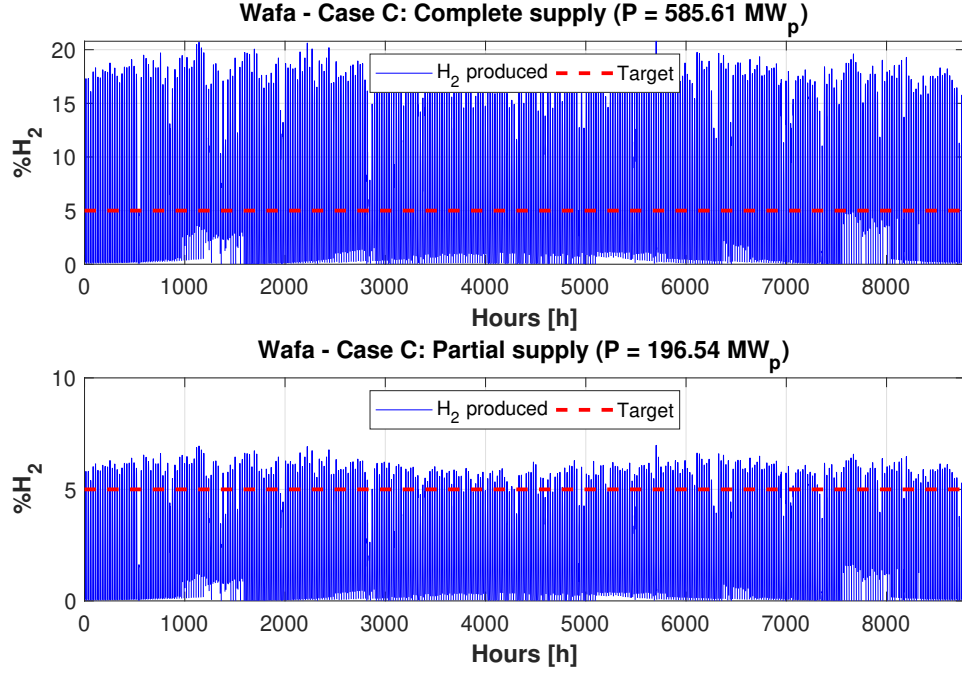


Figure 5.16. Hourly H_2 shares in the blend before and after the downsizing for Wafa.

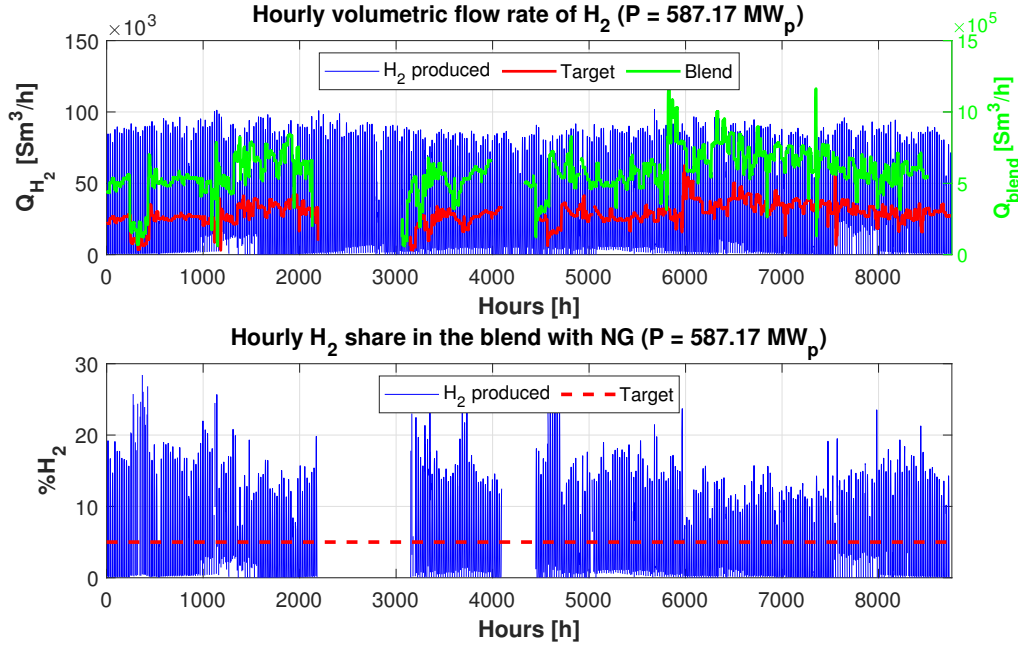


Figure 5.17. H_2 produced with respect to the real trend of the gas flow rate in the complete supply configuration for Wafa.

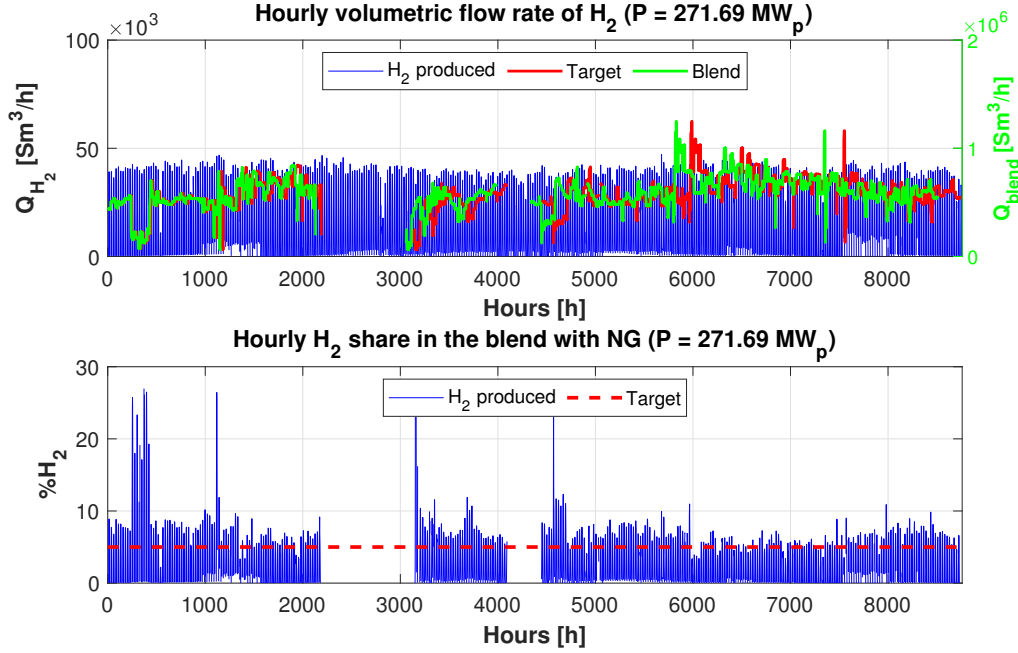


Figure 5.18. H₂ produced with respect to the real trend of the gas flow rate in the partial supply configuration for Wafa.

5.4 Findings and discussion

The main difference between the scenarios explained previously regards the imported energy. In the first case, by keeping constant the volume of the gas imported, the overall energy associated will be diminished when a blend of natural gas and hydrogen is considered. It is due to the higher heating value of hydrogen, which in volumetric terms is less than one third of that for the natural gas. As seen in section 5.1, the higher is the hydrogen share in the blend, the lower will be the higher heating value of the mixture, and so the energy transported. Although the adoption of this configuration implies the saving of natural gas, it seems the least interesting, since investments would be made to obtain a lower amount of energy than the original situation. The second scenario appears more attractive than the previous one. In such configuration there are savings of natural gas without compromising the energy requirements, as hydrogen is used in a complementary way. Finally, the third case is also quite interesting, as it assesses the possibility of a higher energy import by injecting additional hydrogen to the current stream of natural gas.

In table 5.1 the requirements to guarantee the supply of the annual hydrogen demand are shown for the three scenarios. Due to the different capacities of the analyzed pipeline networks, these quantities differ considerably for each of them.

Regarding Transmed, the total volume of gas imported increases at most of 1 bcm (Case C) with respect to the base case, with an associated increment of the imported energy of almost 10 TWh. To accomplish this improvement, around 70 kton of H_2 has to be produced, and this would require a photovoltaic production of 3685 GWh. However, if the imported energy has to be maintain (Case B), more than 1 kton less of hydrogen mass and almost 67 GWh less of photovoltaic energy are required in order to have an imported energy of 3 TWh less than in Case C. For what concerns Greenstream, lower differences are found between the cases, as the volume of gas imported is almost one fourth of that imported through Transmed. To have a blend with 5% of H_2 constantly throughout the year, the total volume imported is at most 20 mcm (Case C) with respect to the base case, which in terms of energy corresponds to 2000 GWh more. Such configuration would require a production of about 18 kton of H_2 and almost 960 GWh of photovoltaic energy.

	A	B	C
TRANSMED			
Annual requirements:			
M_{H_2} [kton/a]	66.6	69.0	70.1
$E_{PV_{out}}$ [GWh/a]	3501.0	3627.7	3685.3
V_{H_2} [Sm^3/a]	$781.7 \cdot 10^6$	$810.0 \cdot 10^6$	$822.9 \cdot 10^6$
V_{NG} [bcm/a]	14.85	15.39	15.63
V_{blend} [bcm/a]	15.63	16.20	16.46
Annual energy imported:			
E_{blend} [TWh/a]	168.3	174.4	177.1
GREENSTREAM			
Annual requirements:			
M_{H_2} [kton/a]	17.3	18.0	18.3
$E_{PV_{out}}$ [GWh/a]	911.7	944.5	959.6
V_{H_2} [Sm^3/a]	$203.6 \cdot 10^6$	$210.9 \cdot 10^6$	$214.3 \cdot 10^6$
V_{NG} [bcm/a]	3.87	4.01	4.07
V_{blend} [bcm/a]	4.07	4.22	4.29
Annual energy imported:			
E_{blend} [TWh/a]	43.2	44.8	45.5

Table 5.1: Quantities involved for the complete supply of 5% of H_2 in the various scenarios.

The findings obtained in all the simulations for each location are presented in table 5.2. Even though having similar sun hours, the results differ substantially for Algeria and Tunisia, which are involved in the same pipeline network. For the complete supply of the annual hydrogen demand, the solar PV capacity ranges between 2.5–2.6 GW for Tunisia in all the scenarios considered, while for Algeria it is comprised between 2.0–2.2 GW. For what concern Libya, the nominal capacities

are much lower, in the range of 560–590 MW, due to the lower amount of hydrogen imported through Greenstream. More observations can be done when it comes to the downsized systems. First, the installed capacities in the hypothesis of constant gas flow rates are lower than for the real trend of the gas, except for Tunisia where the downsizing has not been possible. As observed in the previous sections, it is due to the variability of the gas supply and its coupling with the solar irradiation of the different locations. In order to assure a higher frequency of the 5% of H_2 , higher capacities are required. The difference between these two situations for Algeria is quantified in the range of 250–290 MW, whereas for Libya it is comprised between 70–80 MW. If the constant gas flow rate assumption could be adopted, installed capacities between 750–790 MW would be required in Tunisia for the downsized systems, slightly higher than those for Algeria. For Libya, these plants would have nominal capacities comprised between 190–200 MW. Finally, some remarks should be made for the frequencies of the hydrogen shares produced by the downsized systems. In the constant gas flow rate scenario, both Algeria and Libya are able to supply for near 20% of the operating hours the 5% of H_2 in the blend. Due to its less favorable solar irradiation distribution, Tunisia is able to fulfill the target for around 17% of the time. However, if blends with higher hydrogen shares could be injected into the existing natural gas piping network - as suggested by several studies - all three locations would provide hydrogen quotas lower than 8% for the entire time of operation. For the scenario considering the real trend of the gas, the downsized systems in Algeria and Libya are able to supply for less than 15% of the operating hours the imposed target, but respectively for 88% and 96% of the time they will inject less than 10% of H_2 in the blend. The corresponding results showed for Tunisia are referred to the plant which guarantees the whole supply of hydrogen demand: it satisfies the target for only 5% of the time, and produces hydrogen shares below 10% during half of the sun hours.

	ALGERIA		TUNISIA		LIBYA	
	Const.	Real	Const.	Real	Const.	Real
Operating hours:						
Complete supply	4531		4568		4578	
Partial supply	4304		4341		3807	
CASE A						
Complete supply:						
PV capacity [GW]	2.10		2.47		0.558	
Surface required [km ²]	15.66		18.44		4.16	
Partial supply:						
PV capacity [GW]	0.715	1.01	0.750	n.a.	0.187	0.258
Surface required [km ²]	5.34	7.53	5.60	n.a.	1.39	1.93
CASE B						
Complete supply:						
PV capacity [GW]	2.17		2.56		0.578	
Surface required [km ²]	16.22		19.11		4.31	
Partial supply:						
PV capacity [GW]	0.741	1.05	0.777	n.a.	0.193	0.268
Surface required [km ²]	5.53	7.80	5.80	n.a.	1.44	2.00
CASE C						
Complete supply:						
PV capacity [GW]	2.21		2.60		0.587	
Surface required [km ²]	16.48		19.41		4.38	
Partial supply:						
PV capacity [GW]	0.753	1.06	0.789	n.a.	0.197	0.272
Surface required [km ²]	5.62	7.93	5.89	n.a.	1.47	2.03
Partial supply:						
Frequency % H ₂ = 5 [%]	21.2	12.8	17.4	5	20.6	14.7
Frequency % H ₂ ≤ 10 [%]	100 (max. 7%)	88.3	100 (max. 8%)	50.1	100 (max. 7%)	96.4

Table 5.2: Results obtained for the sizing of PV systems in the various scenarios.

Chapter 6

Integration of storage facilities

The intermittent nature of renewable sources represents one of the main obstacles to the emergence of systems dedicated to the production of renewable-based hydrogen. To deal with this issue, storage facilities could be integrated in order to save hydrogen during periods of overproduction. The stored hydrogen could be then used either to contribute for reaching the imposed target or to fulfill it completely during the night, when no production occurs.

In this chapter the integration of storage facilities will be investigated, starting from the systems sized previously for the scenario of real gas flow rate imported. The analysis will be subdivided for both the plants able to perform the complete supply and partial supply of annual hydrogen demand.

6.1 Complete supply systems

These plants have been sized in order to produce the whole amount of hydrogen that will be necessary to provide a blend with 5% of H_2 constantly throughout the year. However, the hydrogen production will occur during the operating hours of the plant, producing hourly hydrogen shares exceeding the imposed target. To deal with this issue, it has been estimated the hourly mass of hydrogen produced in excess to store it for subsequent periods of shortage. The approach used to achieve this goal consists in the construction of cumulatives, obtained by adding up the differences between the hourly mass of hydrogen produced and the hourly mass of hydrogen required.

The cumulatives have been constructed starting from the beginning of the year.

As shown in the upper graph of Fig. 6.1 for the case A in Algeria, if the plant is started up in January there will be a shortage of hydrogen for the first 5000 hours of the year, corresponding almost to the end of July. That behavior is due to the real trend of the imported gas, which requires the highest amount of hydrogen during winter. Once the demand reduces, in correspondence of the end of March, the excess of production is able to sustain the periods of low or null production until October, when the hydrogen demand increases again considerably. From here to the end of the year, the stored hydrogen is completely consumed.

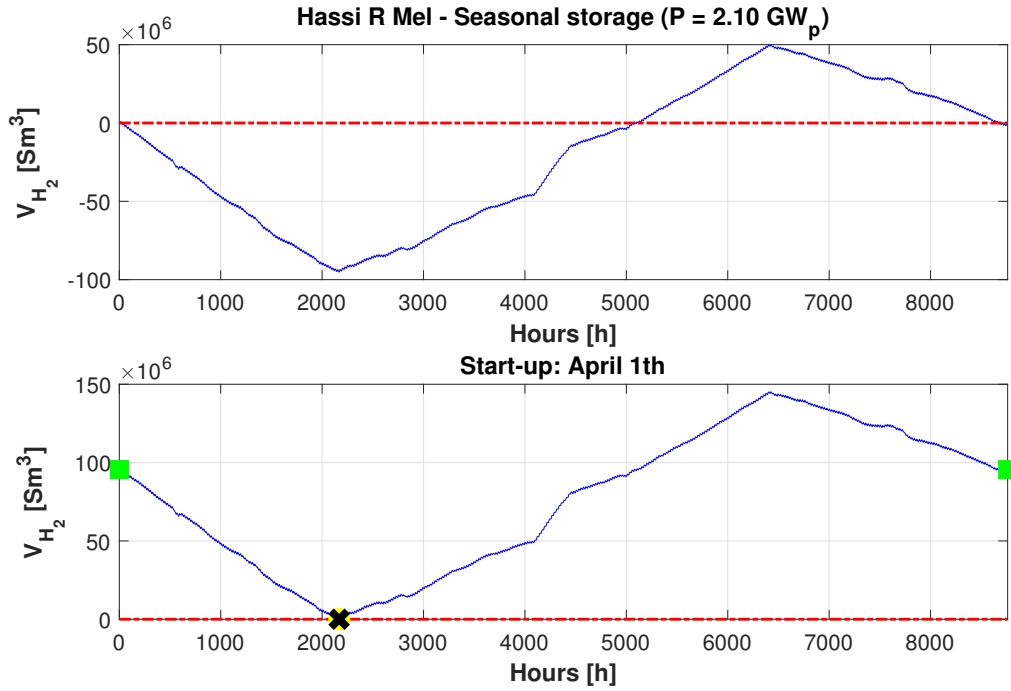


Figure 6.1. Volume of hydrogen stored in Hassi R' Mel over the year.

The solution proposed here consists in setting the start-up of the plant when the hydrogen demand is the lowest (i.e. during the warmer months of the year). Specifically, if the photovoltaic system is started up from the beginning of April, it will be able to produce and store very high amounts of hydrogen that will be used for short periods of shortage (e.g. during nights or cloudy days), but mainly during the fall and winter season, when the request is on average much more higher than the production of the plant. The maximum volume of H_2 to be stored in this scenario would be around 145 million Sm^3 . However, to have a better understanding on how the seasonal storage works, the daily stock of H_2 is displayed in Fig. 6.2. It is observed that from April to September the overproduction of H_2 which is injected in the storage facilities reaches peaks up to 1 million Sm^3 per day with more frequency.

At the end of June, when no importation of natural gas occurs, all the H_2 produced by the plant is stored and for that reason peaks up to 2 million Sm^3 per day can be reached. Conversely, from October to March H_2 is extracted in order to meet the hydrogen demand. The quantities supplied by the storage systems increase from peaks of 500 thousand Sm^3 per day in the last months of the year to peaks of 1 million Sm^3 per day in the winter season. The unusual periods of shortages and accumulation of hydrogen evidenced in the graph correspond to intervals in which the importation of natural gas is particularly different with respect to its regular trend.

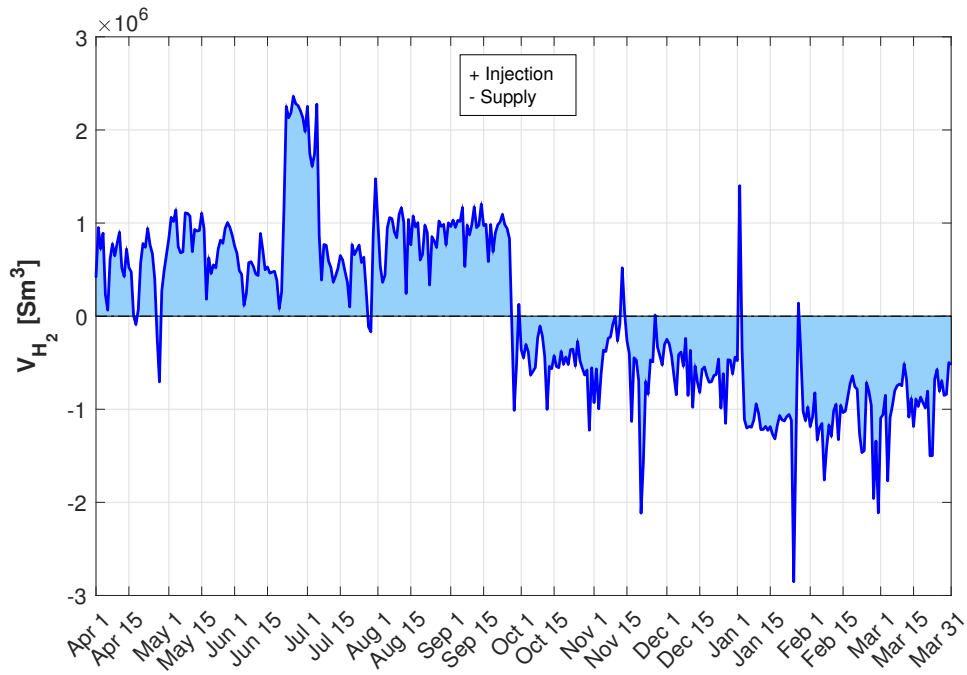


Figure 6.2. Daily stock of H_2 in Hassi R' Mel.

In Fig. 6.3 the coupling between the hydrogen produced and the hydrogen supplied by the storage is provided. In the upper part of the graph it can be observed that the hydrogen demand is never exceeded along the year. To have a more clear vision, in the bottom part the trend of that integration is shown for a restricted interval of time. During the sun hours, the hydrogen demand is fulfilled by means of the photovoltaic panels (blue curve), while the part in excess is stored. Then, during periods of no production, the hydrogen demand is supplied only by the storage system (green curve).

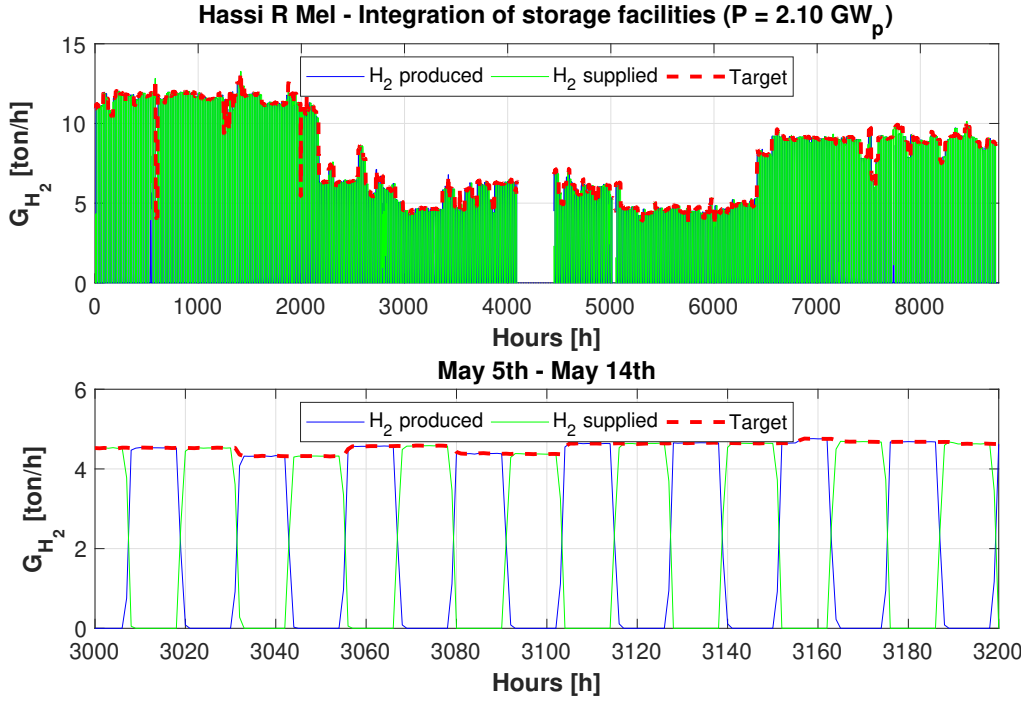


Figure 6.3. Integration of seasonal storage in Hassi R' Mel.

In Fig. 6.4 the cumulative of the hydrogen stored for case B in Borj Cedria is shown. Due to the same pipeline network involved, Tunisia shows very similar results with respect to Algeria. However, the maximum amount of hydrogen that has to be stored in this case increases considerably, to values near 210 million Sm^3 . It is due to the less uniform distribution of the solar irradiation along the year for this location. In fact, to supply the whole demand the required installed PV capacity is much higher than in Hassi R' Mel, and consequently there will be a much more hydrogen production during spring and summer seasons. It is also observed in Fig. 6.5, where the most frequent daily amount of H_2 stored is near to 1.5 million Sm^3 per day with the same exception encountered for Hassi R' Mel, this time storing almost 3 million Sm^3 per day. When it comes to the extraction, during autumn and primarily in winter around 2 million Sm^3 of H_2 are supplied by the storage systems with more frequency.

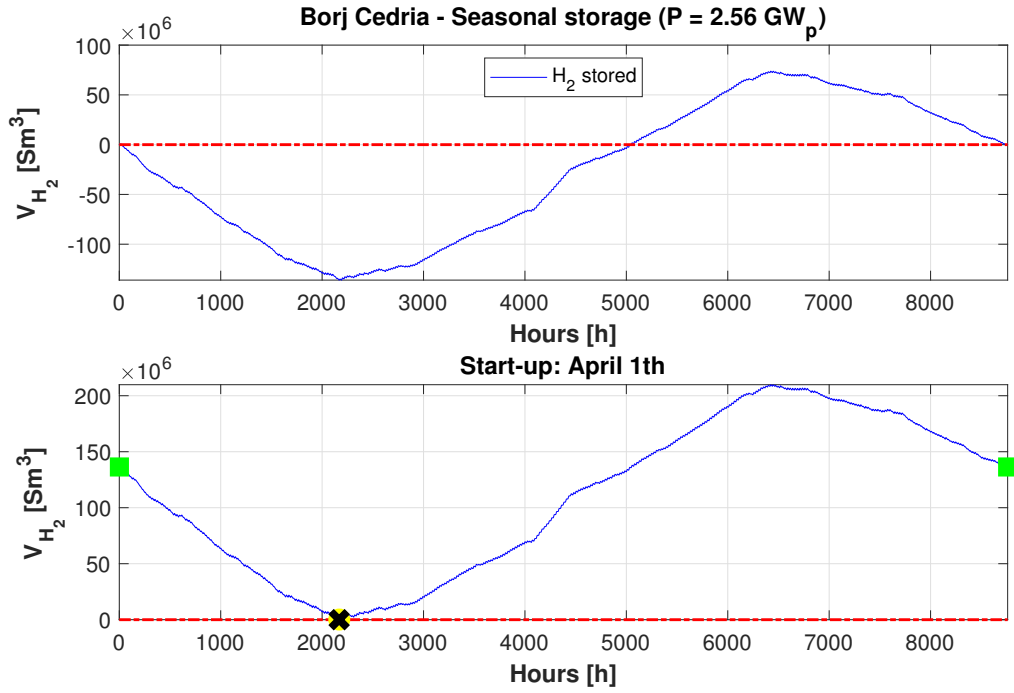


Figure 6.4. Volume of hydrogen stored in Borj Cedria over the year.

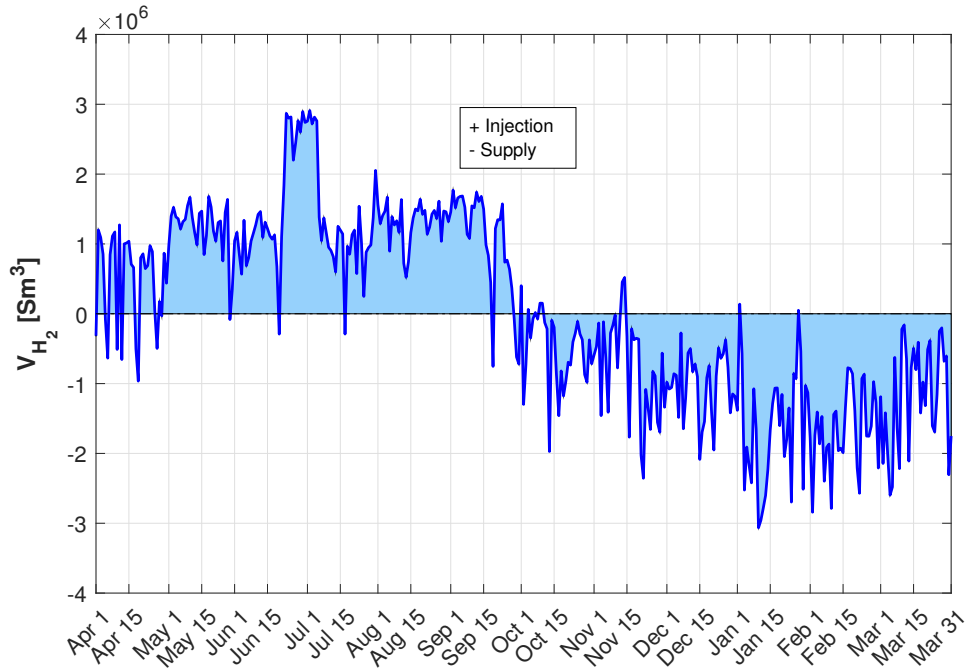


Figure 6.5. Daily stock of H₂ in Borj Cedria.

Some differences are evidenced in the case of Libya. In the upper graph of Fig. 6.6, it can be observed that if the plant is started up from the beginning of the year, there are less hours of shortage than for the other two locations in the same condition. In fact, for less than 1000 hours of the year the plant is not able to supply the entire demand. These hours are distributed for very small intervals during January and for a much wider period including March and half of April. It is due to the real trend of the gas imported, as in the first months of the year there is no the highest gas import from Greenstream. However, in order to use all the hydrogen that can be produced by the system, also in this case the best period for the start-up regards April. The maximum amount of hydrogen that has to be stored in this case corresponds to 35 million Sm^3 . The graph of the daily movement of H_2 (Fig. 6.7) shows a less remarkable contrast between the periods of injection and supply of hydrogen with respect to the previous cases. Again, it is due to the real trend of the natural gas imported through Greenstream, which displays unexpected gas flow rates with respect to its regular trend over the different seasons. It is though evident that from April to August peaks around 600 thousand Sm^3 are injected in the storage facilities with more frequency, while during autumn and winter peaks between 200–400 thousand Sm^3 of H_2 are supplied by the storage facilities. Finally, also here the coupling between storage and PV plant is possible (Fig. 6.8) and never exceeds the amount of hydrogen requested, as shown in the restricted interval between the end of January and the first days of February.

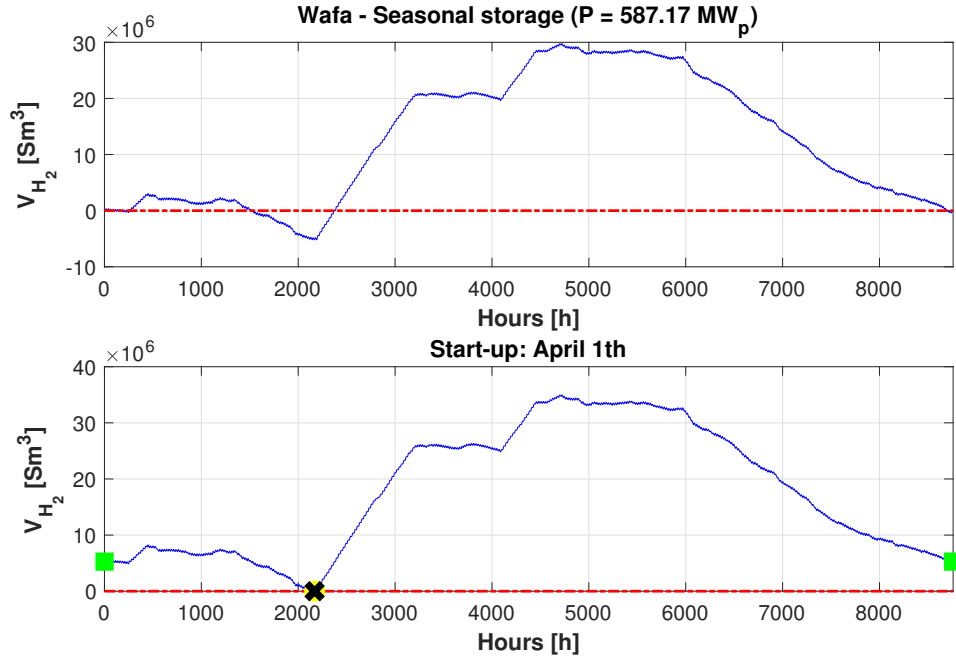


Figure 6.6. Volume of hydrogen stored in Wafa over the year.

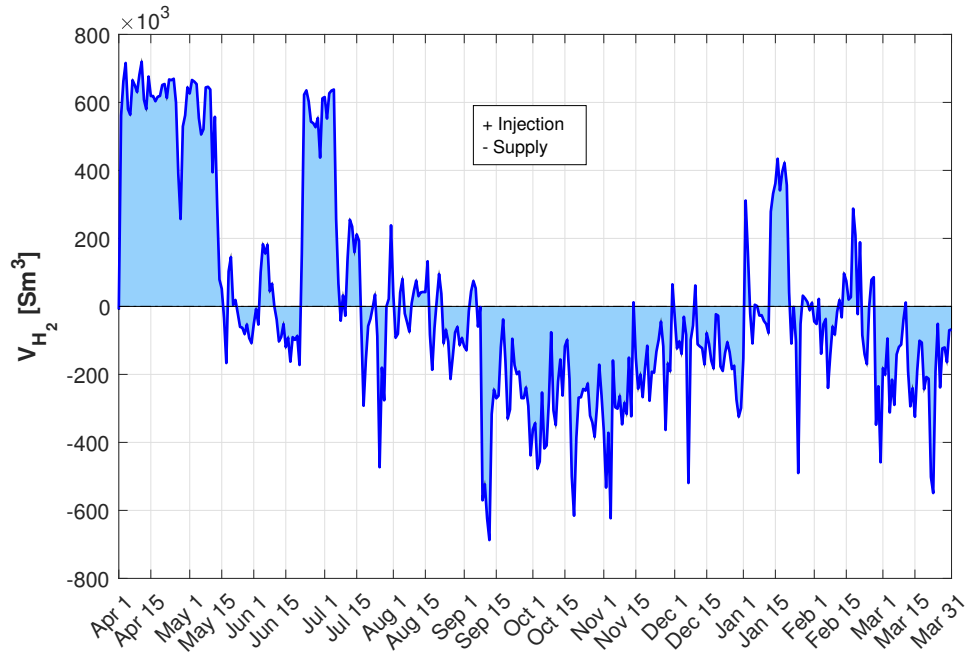


Figure 6.7. Daily stock of H₂ in Wafa

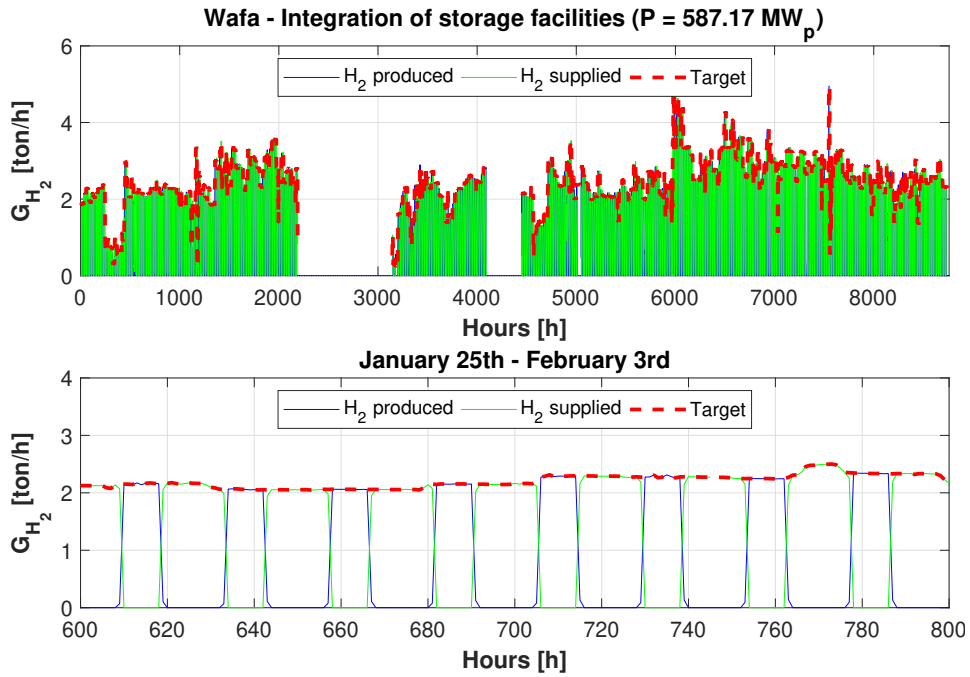


Figure 6.8. Integration of seasonal storage in Wafa.

6.2 Partial supply systems

The systems treated in this section are the result of the downsizing performed on the previous ones. These plants provide a blend with a variable hydrogen share on hourly basis, but most of time the 5% is guaranteed. To quantify the hydrogen mass in excess that can be store to be used subsequently, the same approach involving cumulatives has been adopted in this part.

The results obtained for case A for Algeria are shown in Fig. 6.9. In the upper graph it is observed that the highest mass of hydrogen stored is reached during spring and summer, namely around 640 thousand Sm^3 per day. From autumn to the end of the year the most frequent storage capacity used is around 20 ton per day and lastly during winter this quantity is halved. In the bottom part of the same figure the coupling between the PV system and the storage facilities is displayed. It is clear how during periods of high overproduction the hydrogen share imposed is reached easily, as large amounts of hydrogen are stored and used subsequently as backup. During low overproduction times, the storage is still working, but it does not allow to satisfy completely the hydrogen demand. A clearer picture of this behavior is shown in Fig. 6.10, where two representative time windows are analyzed. During summer the green curves are wider, meaning that the storage is able to fulfill the hydrogen demand for more hours than in winter, where the storage works for less hours and sometimes it is not even enough to reach the hydrogen share imposed.

Some dissimilarities are encountered when analyzing the findings achieved in case C for Libya (Fig. 6.11). It is due to the real trend of the gas imported through Greenstream, in which there is no obvious contrast between the different seasons as in the case of Transmed. In the cited figure, it is possible to observe that widespread peaks in all seasons up to 140 thousand Sm^3 per day of H_2 stored can be achieved. However, the most frequent storage capacity used throughout the year is around 60 thousand Sm^3 per day. The fact that there is no a well defined period of higher hydrogen storage is highlighted by the picture describing the integration of storage facilities. From September to the end of the year, when the highest import of gas takes place, the storage facilities are able to supply very few amounts of hydrogen, most times not enough to reach the 5% of hydrogen in the blend. During other periods of the year the role of storage systems is generally more marked, allowing to reach more times the hydrogen target. Also in this case, it is provided a deeper look of the storage usage in different seasons (Fig. 6.12). Excluding some exceptions, when the hydrogen request is slightly higher with respect to the mean, the storage is able to fulfill the hydrogen share imposed for most of the daily hours in the summer season. Conversely, during winter the contribution of storage facilities is rather scarce, working for less than 3 hours per day without granting the established target.

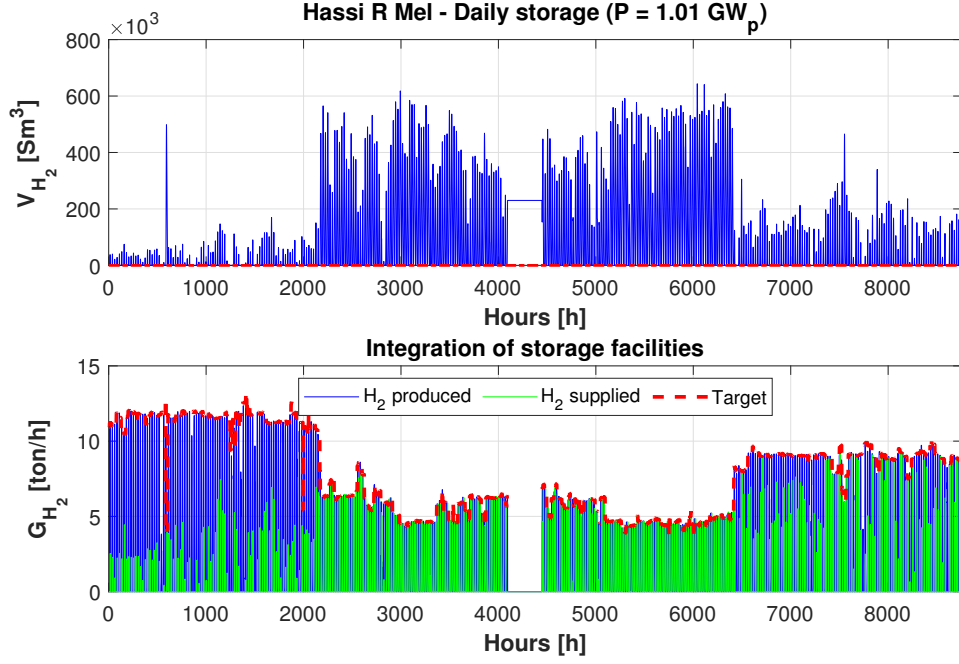


Figure 6.9. Volume of H_2 stored daily in Hassi R' Mel and coupling between PV system and storage facilities.

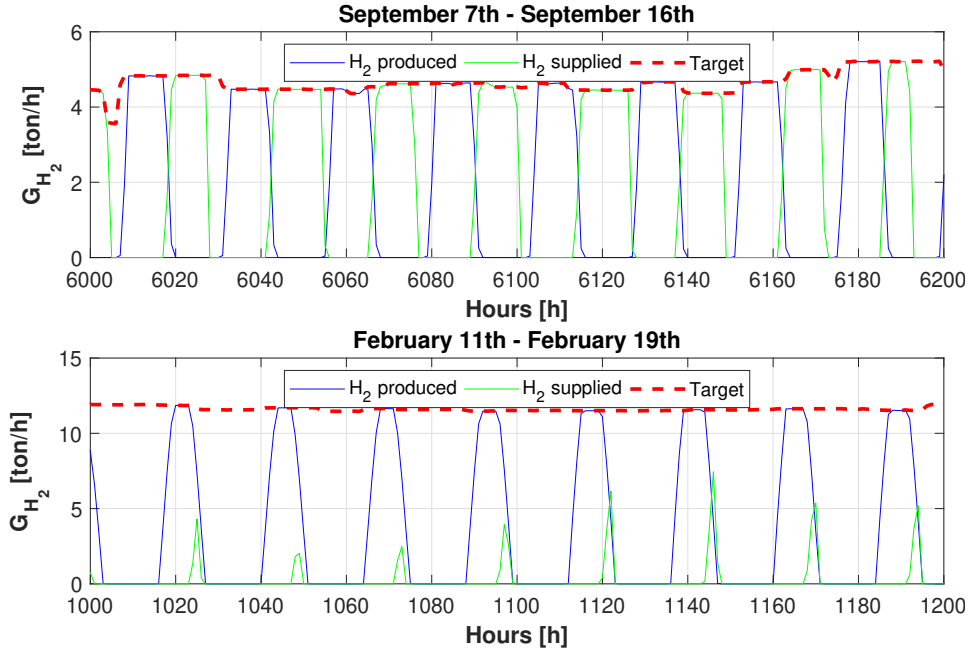


Figure 6.10. Storage utilization during summer and winter seasons in Hassi R' Mel.

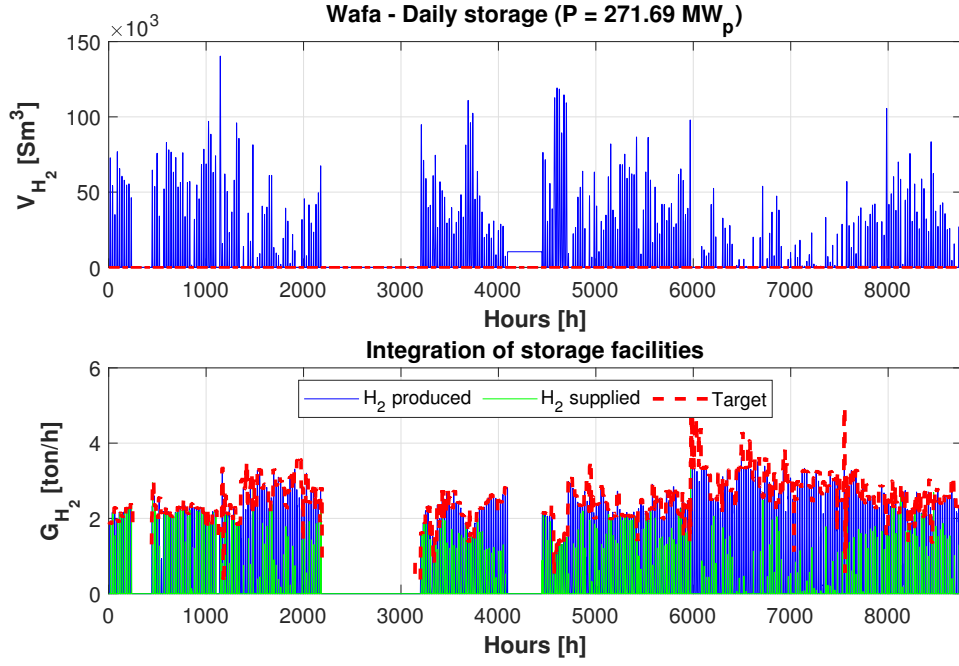


Figure 6.11. Volume of H₂ stored daily in Wafa and coupling between PV system and storage facilities.

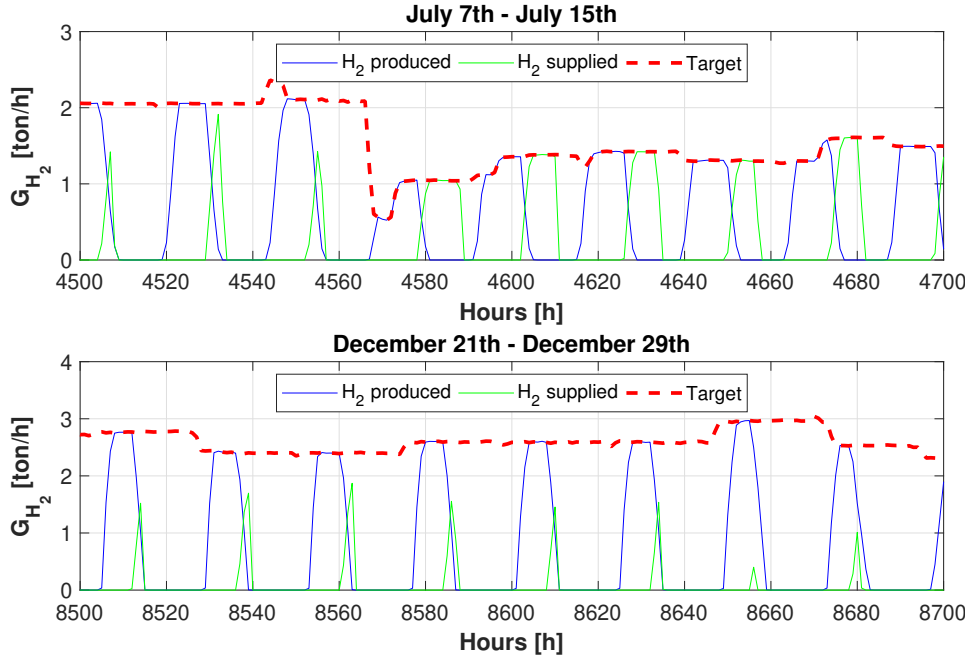


Figure 6.12. Storage utilization during summer and winter seasons in Wafa.

6.3 Findings and discussion

The results attained in all the simulations are summarized in table 6.1. The discussion will be subdivided for the two types of systems described previously, for each location in which it has been possible to obtain significant outcomes.

For what concern the complete supply systems, the integration of storage facilities allows to provide the blend with 5% of H_2 during the whole period of gas import in all the locations. The mass of hydrogen to be stored in all the locations is in the order of kilo tons. Algeria and Tunisia, involved in the same pipeline network, show nominal capacities ranging between 12–13 ktons and 17–18 ktons respectively. The mass of hydrogen stored in Tunisia is higher because of the higher installed capacities required there to produce the total annual hydrogen demand. In the case of Libya the storage capacity required is considerably lower, namely almost 3 ktons in all the scenarios. The difference is due to the amount of gas imported through the two pipeline networks, which for Greenstream is around one forth of that for Transmed. If the storage capacities would be expressed as function of the total mass of hydrogen produced by the plants, in Algeria and Tunisia it would be necessary to store up to 19% and 25% of the total production respectively, while in Libya up to 17%.

The only solution that could be considered for the accumulation of such quantities regards the underground storage. According to several studies, hydrogen could be stored in large amounts within salt caverns, depleted gas fields or aquifers. The latter two options could be examined in Algeria and Libya, as the selected locations are characterized by the presence of gas extraction fields and desert aquifers. On the other hand, geological studies should be performed in Tunisia in order to verify the availability of underground deposits for massive hydrogen storage.

In the case of partial supply plants, the coupling with storage systems allows to satisfy only a fraction of the total demand. In Algeria, the plants are able to provide blends for about 63% of the time, of which 77% represents the imposed target. Less favorable findings are obtained for Libya, where the plants yield blends only for 55% of the time, of which almost 65% represent the desired blend. There are two main causes explaining this difference: the operating hours of the pipeline networks and the real trend of the gas imported through them. Regarding the first point, Transmed has almost 1000 operating hours more than Greenstream over the year. As consequence, a similar difference is reflected in the operating hours of the partial supply systems. For the second point, the algerian gas is characterized by a more relevant contrast in the import trend than that evidenced by the libyan gas over the seasons. Since the downsizing is strictly related to this trend (see Section 5.3), partial supply systems in Algeria are able to produce much more hydrogen in excess, giving rise to more periods in which hydrogen can be accumulated. Therefore, storage facilities in Libya play a minor role in providing

blends.

The amounts of hydrogen to be stored by partial supply systems are remarkably lower with respect to those involved by complete supply systems. The storage capacities are comprised between 55–57 tons and 11–12 tons for Algeria and Libya respectively. As the solution to be adopted in this case regards the daily storage, it has been estimated the number of compressed tanks that would be required to store such quantities of hydrogen. In Algeria, the number of units required is comprised between 13000–13800, whereas in Libya it ranges from 2700–2850. The compressed tank considered in this work is able to store hydrogen at 60 bar and has a capacity of 4.2 kg (see Appendix B).

	ALGERIA	TUNISIA	LIBYA
Operating hours:			
Complete supply	8359	8359	7391
Partial supply	5277	n.a.	4078
CASE A			
Complete supply:			
Mass capacity [kton]	12.37	17.26	2.83
Volume capacity [Sm ³]	145.2·10 ⁶	202.5·10 ⁶	33.2·10 ⁶
Partial supply:			
Mass capacity [ton]	54.8	n.a.	11.4
Volume capacity [Sm ³]	643.4·10 ³	n.a.	133.4·10 ³
N° tanks	13053	n.a.	2707
CASE B			
Complete supply:			
Mass capacity [kton]	12.82	17.88	2.93
Volume capacity [Sm ³]	150.5·10 ⁶	209.8·10 ⁶	34.4·10 ⁶
Partial supply:			
Mass capacity [ton]	56.8	n.a.	11.8
Volume capacity [Sm ³]	666.5·10 ³	n.a.	138.5·10 ³
N° tanks	13521	n.a.	2810
CASE C			
Complete supply:			
Mass capacity [kton]	13.03	18.16	2.98
Volume capacity [Sm ³]	152.9·10 ⁶	213.2·10 ⁶	35.0·10 ⁶
Partial supply:			
Mass capacity [ton]	57.7	n.a.	12.0
Volume capacity [Sm ³]	677.5·10 ³	n.a.	140.4·10 ³
N° tanks	13744	n.a.	2848
Partial supply:			
Frequency % H ₂ = 5 [%]	77.0	n.a.	64.8

Table 6.1: Results obtained for the integration of storage facilities in the various scenarios.

Chapter 7

Analysis of compression stations

Due to the difference in the physical and chemical parameters of hydrogen with respect to the characteristics of natural gas, the work of gas compressors for blends with a certain hydrogen content will be different. In this chapter it will be presented how the injection of hydrogen in natural gas pipeline networks affects the performance of compressor stations, by analyzing the change of the main energetic parameters characterizing transportation of blends from the selected areas in the scenarios presented in Section 5.3.

This investigation has been conducted by means of a simulation tool developed at *Politecnico di Torino*, which describes the operation of the most important facilities involved in natural gas transport systems, such as pipelines and compressor stations, as well as the interconnection between them. Thus, a brief presentation of the model will be firstly afforded, focusing primarily on the assumptions adopted and input parameters that have to be provided. Subsequently, it will be explained the operational logic of compressors established for all the simulations conducted and, lastly, the results obtained will be presented.

7.1 Model description

The components of natural gas pipeline networks can be described using basic graphic elements, namely nodes and branches (Fig. 7.1). A branch represents an element with an inlet, an outlet and a flow direction. It can be of two types:

- **Pipe element:** symbolizes a limited section of the pipeline, whose function consists in transporting natural gas from point a to b. Therefore, it constitutes

a short term gas storage;

- **Non-pipe element:** represents a compressor station, which compensates the pressure and head losses due to friction and heat transfer by increasing the gas pressure.

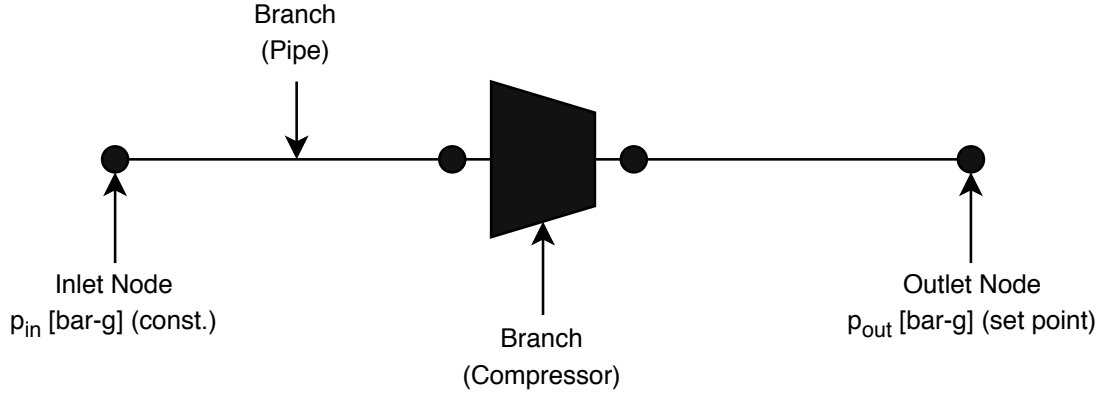


Figure 7.1. Simplified scheme of the elements represented in the model.

Pipelines are considered passive elements, since their behavior is completely defined by the physical equation:

$$\Delta P^{n+1} = R_f \cdot |G^{n+1}| G^{n+1} + R_i \cdot (G^{n+1} - G^n) \quad (7.1)$$

where

ΔP is the square pressure drop.

R_f and R_i are respectively the pipe resistance coefficient and the pipe inertia factor.

G is the mass flow rate through the pipe element.

On the other hand, compressors are regarded active elements, as their states can be controlled externally. The operation of a compression station is generally expressed by an equation describing the required compression power from the driver, defined as:

$$POW_d = \frac{\kappa Z_1 T_1 R \rho_n}{(\kappa - 1) \eta_{ad} \eta_{mech}} G \left[\left(\frac{p_o}{p_i} \right)^{\frac{\kappa-1}{\kappa}} - 1 \right] \quad (7.2)$$

where

POW_d is the power of the driver (i.e. a gas turbine).

κ is the isentropic exponent.

Z_1 is the compressibility factor.

R and ρ are respectively the gas constant and the gas density.

η_{ad} and η_{mech} are the adiabatic efficiency and the driver efficiency.

p_o and p_i are respectively the downstream pressure and the upstream pressure of compressor.

The interconnection points between the individual network elements are referred to as nodes. These are the only locations in the network where gas can be injected or extracted. Like for branches, it is possible to distinguish three types of nodes:

- **Demand node:** point where gas is extracted from the network, such as the entry points to the Italian gas pipeline grid (i.e. Mazara del Vallo and Gela). These are points connected to the local, low pressure distribution network.
- **Supply node:** point where gas is injected into the network, such as the access points to the gas transportation system in correspondence of production fields.
- **Junction node:** point where a topological change or a turn in pipe properties occurs (e.g. diameter, inclination).

The topology of the entire network is described by the following node-branch incidence matrix:

$$\mathbf{A} = [a_{i,j}]^{n \times m} \quad (7.3)$$

$$a_{i,j} = \begin{cases} +1, & \text{node } i \text{ is outlet of element } j \\ -1, & \text{node } i \text{ is inlet of element } j \\ 0, & \text{node } i \text{ and element } j \text{ are not connected} \end{cases}$$

where n is the number of nodes, m the number of elements and $a_{i,j}$ the elements of matrix \mathbf{A} . The latter can be decomposed in a node-pipe incidence matrix $\mathbf{A_P}$, describing only pipe connections, and a node-Non-pipe incidence matrix $\mathbf{A_{NP}}$, describing Non-pipe connections.

$$\mathbf{A} = [\mathbf{A_P} | \mathbf{A_{NP}}] \quad (7.4)$$

Each node in the network is characterized by its nodal pressure p_i and nodal load L_i , whereas each branch is distinguished by its gas flow rate G_j . The set of these quantities can be described by their corresponding vectors:

$$p = \begin{bmatrix} p_1 \\ p_2 \\ \vdots \\ p_n \end{bmatrix}, \quad P = \begin{bmatrix} p_1^2 \\ p_2^2 \\ \vdots \\ p_n^2 \end{bmatrix}, \quad L = \begin{bmatrix} L_1 \\ L_2 \\ \vdots \\ L_n \end{bmatrix}, \quad G = \begin{bmatrix} G_1 \\ G_2 \\ \vdots \\ G_m \end{bmatrix} \quad (7.5)$$

where

$$p_i \geq 0, \quad L_i : \begin{cases} > 0, & \text{demand node} \\ < 0, & \text{supply node} \\ = 0, & \text{junction node} \end{cases},$$

$$G_j : \begin{cases} > 0, & \text{flow direction is inlet to outlet} \\ < 0, & \text{flow direction is outlet to inlet} \end{cases}$$

Like for the incidence matrix \mathbf{A} , the flow vector G can be decomposed in a pipe and Non-pipe component:

$$G = [G_P | G_{NP}]^T \quad (7.6)$$

In this study, the number of pipe elements has been determined by the subdivision of the two natural gas pipeline networks considered in sections of 10 km length. For each of them it has been assigned a pipe roughness value typical for transport pipelines ($\epsilon = 0.014$ mm). On the other hand, the number of Non-pipe elements (i.e. compression stations) is known from information available for each pipeline network. Moreover, 1 km length branches have been used for their representation.

7.2 Operational logic of compressors

The major constraint considered in the simulations regards the set point pressure at the receiving terminals of the Italian gas pipeline network, which has to be maintained above 75 bar-g. Thus, the variable that has to be monitored every hour of simulation ($\Delta t = 3600$ s) is the pressure at the end of pipeline networks. In order to comply this constraint, it has been determined that the threshold value corresponds to 110 bar-g. The control logic described below has been applied for all the scenarios considered in Section 5.3.

Based on Eq. 7.2, compressors are characterized by three operational modes:

- **On (ON)**: it occurs when the pressure at the end of the pipeline network goes down below 110 bar-g. It means that $p_o \geq p_i$.
- **Bypass (BP)**: it happens when the downstream pressure and the upstream pressure of compressors are equal (i.e. $p_o = p_i$). In this situation the non-pipe element behaves as a pipe element.
- **Off (OFF)**: it occurs when the pressure at the end of the pipeline network overcomes the threshold value of 110 bar-g. It means that there is no gas flow rate through the non-pipe element ($G_j = 0$) and so the pipeline could be conceived as divided in two non-communicating trunks.

In the ON state, the driver power is expressed as:

$$POW_d = POW_{GT} \cdot NC \quad (7.7)$$

where POW_{GT} is the power of a single gas turbine driving a compressor and NC is the number of compressors switched on.

When the constraint is infringed, the first compressor is activated ($NC = 1$). If the pressure continues to decline, the compression work must be increased ($NC = 2$). This arrangement goes on until all compressors are activated ($NC = NC_{max}$) and, at this point, it is only possible to monitor the pressure trend. When the pressure start to increase, the number of compressors operating are gradually reduced, until all of them are switched off ($NC = 0$).

7.3 Findings and discussion

Due to the different layout of the two natural gas pipeline networks considered in this study, the results obtained will be presented and discussed separately for both Greenstream and Transmed. For each of them it has been selected representative time spans of summer and winter seasons, in which the behavior of compression stations has been investigated for all the scenarios analyzed in Section 5.3.

7.3.1 Greenstream

As seen in Section 4.2, the Libyan gas is pumped through the Mediterranean Sea by a single major Gas Compressor Station (GCS) located at Mellitah. The main input parameters provided to the model are summarized in Table 7.1 and Table 7.2.

Pipe section		Length [km]	Diameter [mm]	N° branches
From	To			
Wafa	Mellitah	530	793.7	53
Mellitah	Gela	540	793.7	54

Table 7.1: Input parameters regarding pipe elements for Greenstream.

CGS	NC	POW _{GT} [MW]	POW _d [MW]	p _{control} [bar-g]
Mellitah	5	32	160	110

Table 7.2: Input parameters regarding Non-pipe elements for Greenstream.

The periods that have been analyzed are comprised between July 7–18 and November 7–18. Thus, the total number of hours for each simulation is 264. The mass flow rates of the imported gas associated to these intervals are shown in Fig. 7.2.

The first discussion focuses on the constraint imposed in this analysis, regarding the set point pressure at the end of the pipeline network. It is shown in Fig. 7.3 for both the winter and summer season. The only case in which it is not respected regards Case C (i.e. Additional H₂) in the winter season. It occurs for a short period of 3 hours, and is due to a sharp increase of the gas flow rate imported. In all the other cases the power of existing compression stations is sufficient to respect the set point pressure at Gela. It is also possible to observe that in the summer period the pressures registered at Gela are comprised between 105–120 bar-g, and are higher than those for the winter season. This result is due to the lower import of gas during the colder months of the year. Moreover, the differences between the pressures for each scenario are more evident in winter, where lower pressures correspond for Case C and B (i.e. Constant energy), and slightly higher pressures for Case A (i.e. Constant volume) with respect to the Base case (i.e. no H₂ injection).

It is also interesting to analyze the pressure trend along the pipeline network (Fig. 7.4). In this graph the pressure trends for different time steps of the simulation are reported and are referred to the reference case. It can be seen that when compressors are switched on, the pressure at Gela is always higher than the imposed condition. Moreover, the downstream pressure of compressors decreases more with respect to the situations in which compressors are switched off. This behavior is more pronounced in the summer season, where there is a minor operation of compressors because of the lower amount of gas imported (upper graph of Fig. 7.5). Therefore, pressures lower than 50 bar-g can be registered downstream of compressors. Instead, when they are off, higher pressures characterize the gas before entering the non-pipe element, as the set point pressure at the end of the pipeline network is respected.

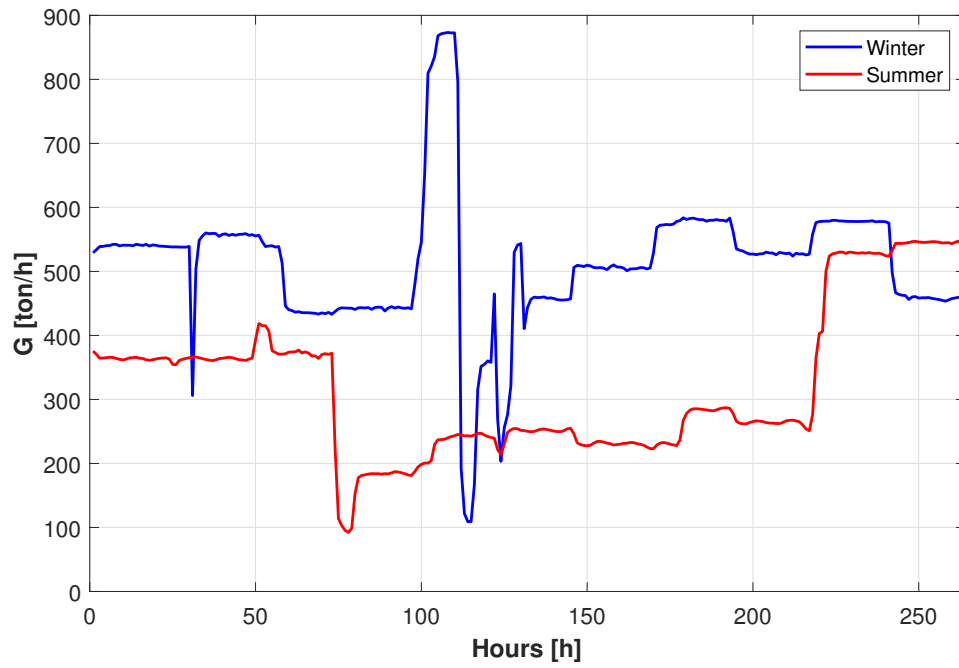


Figure 7.2. Gas flow rates through Greenstream in the Base case.

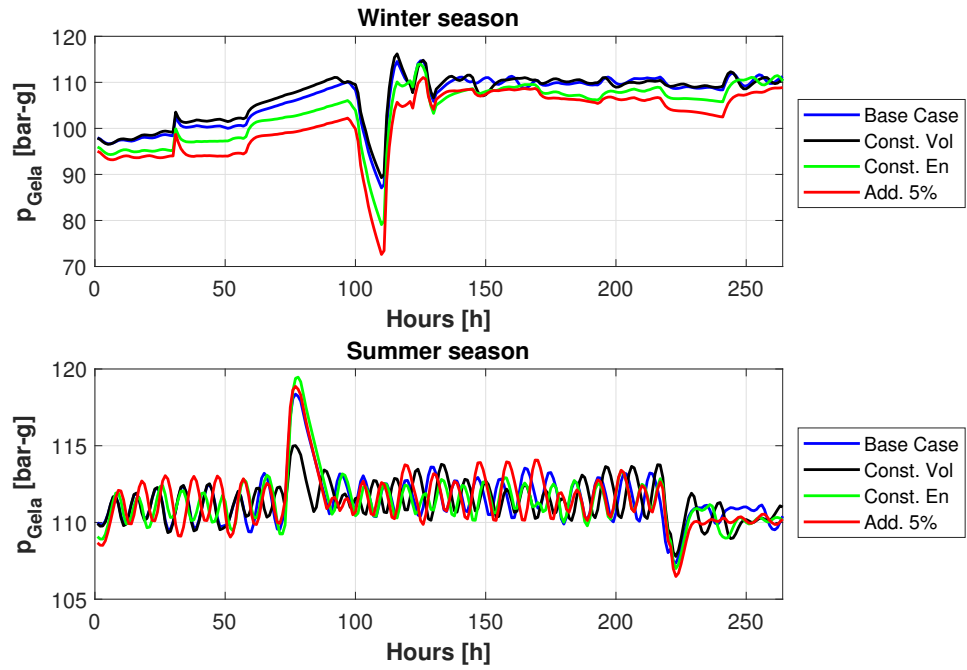


Figure 7.3. Pressure trends registered at Gela.

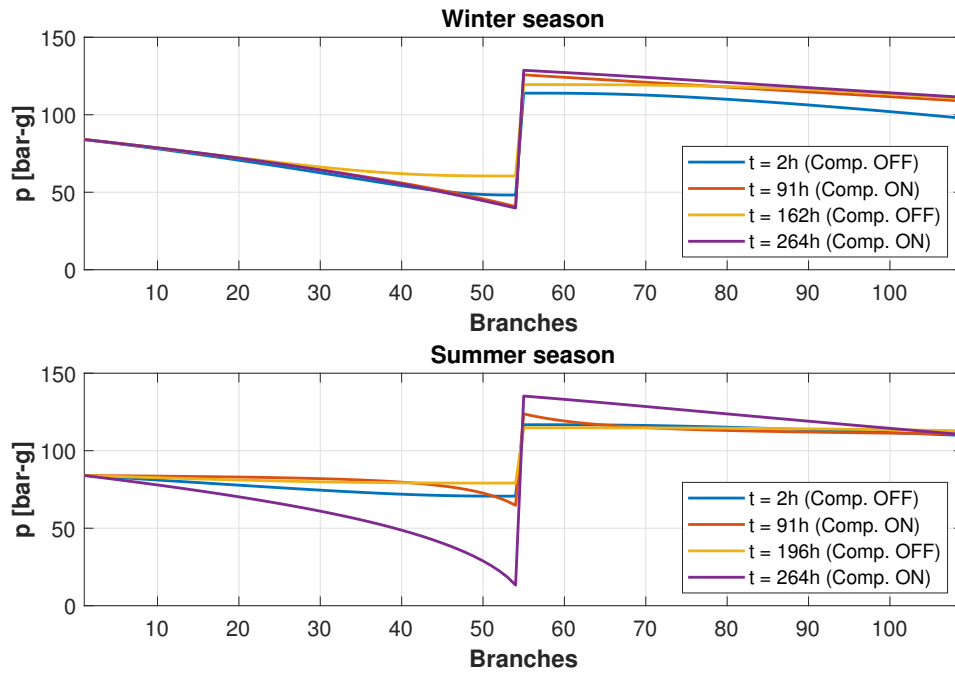


Figure 7.4. Pressure trends along Greenstream in the base case.

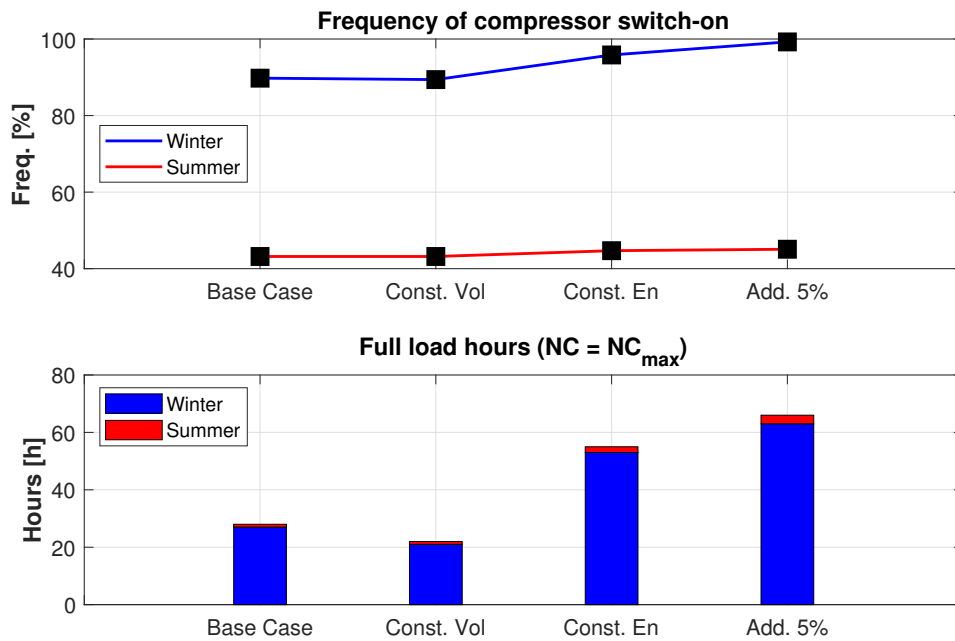


Figure 7.5. Characteristic of operation for the Mellitah CGS.

In the lower graph of Fig. 7.5 the number of hours in which all the compressors are working is shown. It is clear that the hydrogen content within the blend increases considerably the operation of compressors with respect to the transport of natural gas only. Again, this situation is more evident when a higher amount of gas is imported. For instance, out of 264 hours of simulations, the number of full load hours in Case C for the winter season is equal to 63 hours, more than twice with respect to the reference case. During summer the number of full load hours is practically unchanged for all scenarios, which means that less compressors are sufficient to compress the blend in the respect of the set point pressure.

Finally, to compare the performance of compressors in all the scenarios considered, it has been calculated the transport efficiency, defined as follows:

$$\eta_{trans} = \frac{E_{chem,blend}}{E_{GT,in} + E_{chem,blend}} \quad (7.8)$$

where

$E_{chem,blend}$ is the chemical energy associated to the gas imported.

$E_{GT,in}$ is the energy required at the inlet of the gas turbine to produce the driving power of compressors.

The energy in input to gas turbines is calculated from the gas consumption during the hours of simulation (Fig. 7.6) as follows:

$$E_{GT,in} = NG_{cons,GT} \cdot HHV_{gas} \quad (7.9)$$

Fig. 7.7 shows the percentage change in the transport efficiency for all scenarios with respect to the reference case in both winter and summer seasons. It is observed that in both periods Case A exhibits a higher transport efficiency. In fact, since the volume flow rate of gas is kept constant, the hydrogen volume fraction in the blend causes a reduction in its density, which implies a lower mass flow rate and consequently lower pressure losses. Moreover, compressors are less used (Fig. 7.5), mainly during winter, and thus also $E_{GT,in}$ decreases, causing the increase in η_{trans} . Concerning Cases B and C, the transport efficiency decreases due to the higher operation hours of compressors, implying a higher gas consumption which prevails on the increase of the chemical energy associated to the blends.

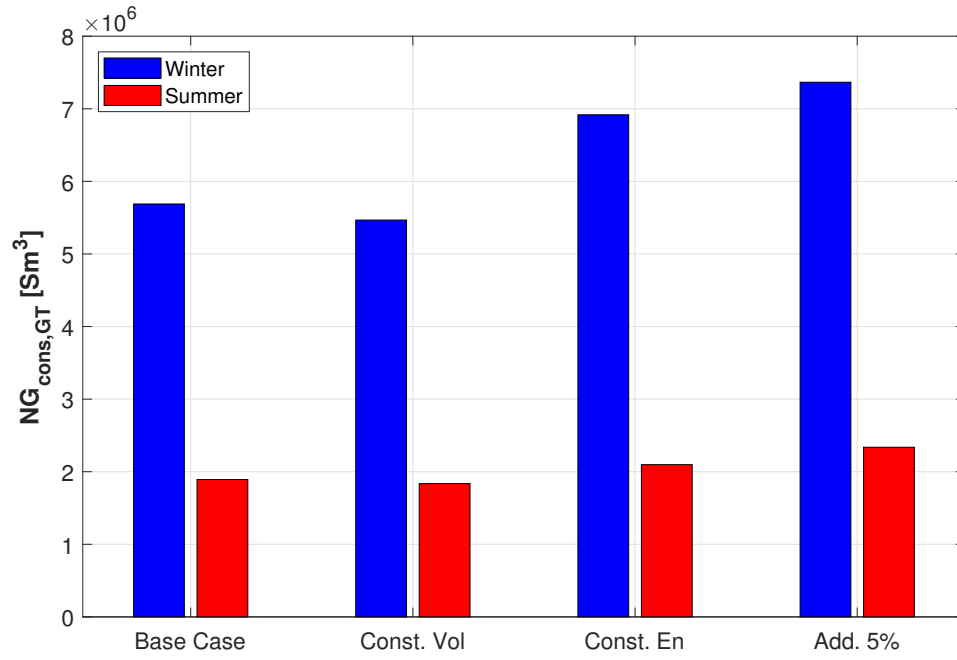


Figure 7.6. Gas consumption of turbines at Mellitah CGS.

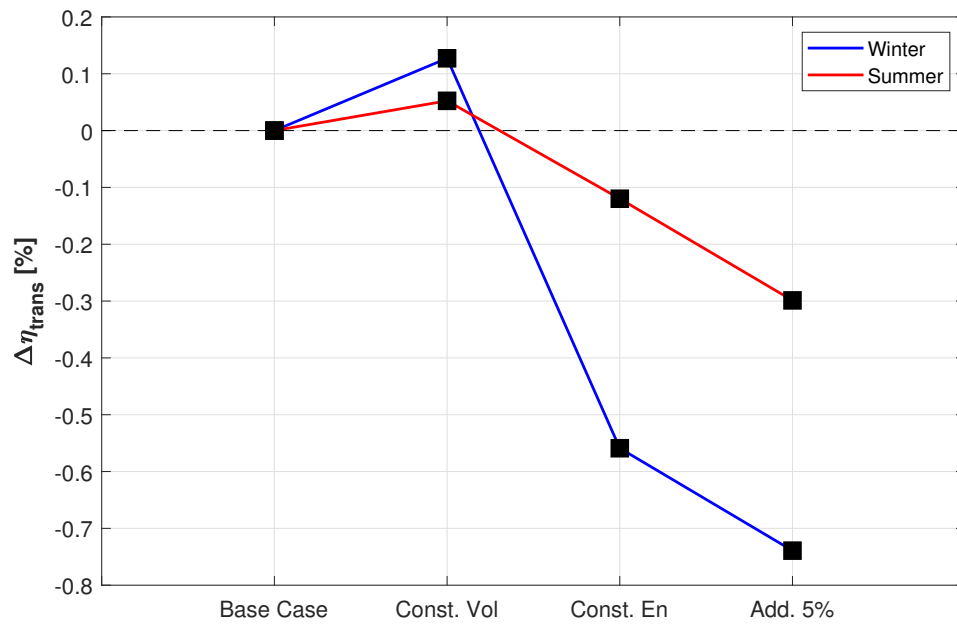


Figure 7.7. Percent variance of the transport efficiency for Greenstream.

7.3.2 Transmed

Unlike the previous case, Transmed is characterized by the presence of more than one compressor station along his route. Data used for simulations regarding these units are summarized in Table 7.3 and Table 7.4.

Pipe section		Length [km]	Diameter [mm]	N° branches
From	To			
Hassi R' Mel	Ain Naga	335	1200	34
Ain Naga	Feriana	215	1200	22
Feriana	Sbeitla	70	1200	7
Sbeitla	Sbikha	120	1200	12
Sbikha	Korba	115	1200	12
Korba	Cap Bon	65	1200	7
Cap Bon	Mazara del Vallo	155	641.3	16

Table 7.3: Input parameters regarding pipe elements for Transmed.

CGS	NC	POW _{GT} [MW]	POW _d [MW]	p _{control} [bar-g]
Ain Naga	1	25	25	65
Feriana	1	25	25	65
Sbeitla	3	23	69	65
Sbikha	1	25	25	65
Korba	3	23	69	65
Cap Bon	2	26	52	110

Table 7.4: Input parameters regarding Non-pipe elements for Transmed.

In this case the time frames considered are comprised between July 7–18 and January 7–18 and their corresponding mass flow rates of the imported gas are displayed in Fig. 7.8. Here the trend of the imported gas is almost constant and the contrast between winter and summer is more evident than in the case of Greenstream.

Concerning the pressures registered at Mazara del Vallo (Fig. 7.9), it is observed that all the scenarios maintained the set point pressure imposed. Moreover, because of the almost constant gas flow rate, the pressure trends after the transient are comprised within restricted intervals around 75–85 bar-g and 107–112 bar-g for the winter and summer season respectively. As for Greenstream, the lower pressures in the colder months of the year are due to the higher amounts of gas imported. Regarding the pressure trend for each scenario, it is observed that slightly lower pressures are registered when the amount of hydrogen injected into the pipeline network increases.

Due to the presence of more than one gas compression station, it has been also analyzed the pressure trends along the pipeline network for different time steps of the simulation (Fig. 7.10), in which a certain number of compression stations are in operation. The only case in which all the compression stations work simultaneously

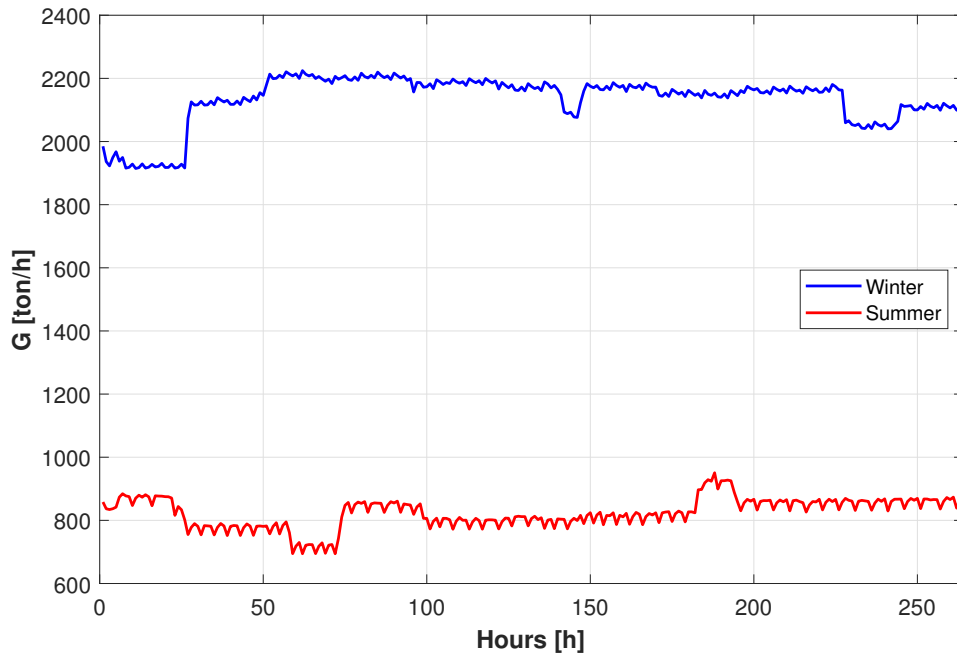


Figure 7.8. Gas flow rates through Transmed in the Base case.

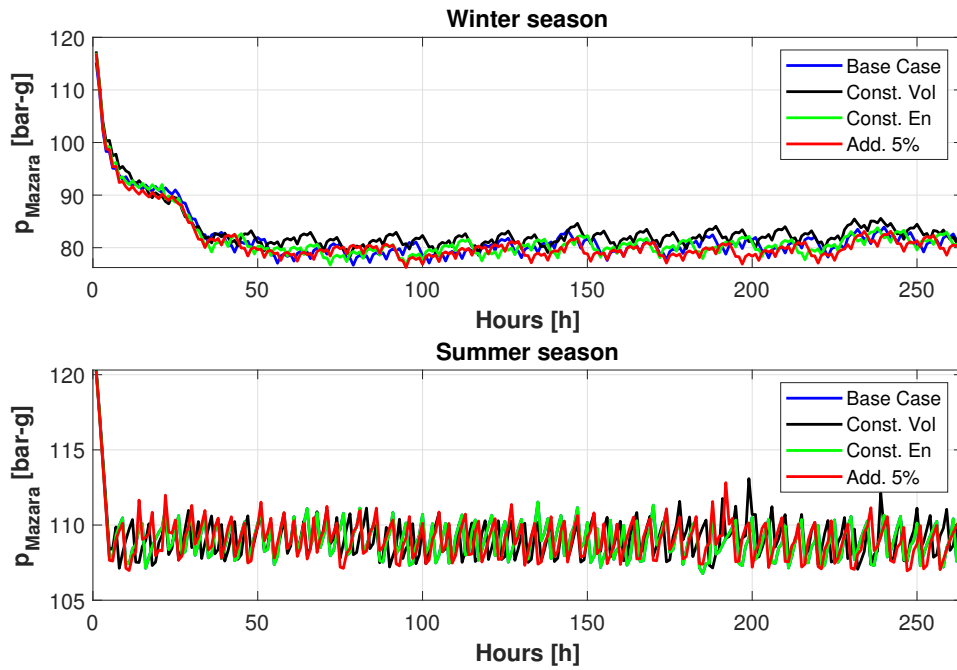


Figure 7.9. Pressure trends registered at Mazara del Vallo.

regards the winter season. Conversely, during the summer period at most 4 compression stations work at the same time. Thanks to the vast number of available compressors along the pipeline, the pressure is always maintained on values above 50 bar-g, and the lower pressures are encountered primarily during winter, due to the higher gas demand. Additionally, it is observed that the most used compressor stations are those placed far away from the gas extraction field, specifically in the last part of the pipeline network in the Tunisian territory. This fact is much more evident if the frequency of compressor stations switch on are analyzed (Fig. 7.11). During winter, Cap Bon CGS operates for almost the entire period evaluated in all scenarios, whereas the intermediate CGS are operative for almost 75%. The only CGS located in Algeria is the less active, working for around 60% of the time. The contrast in the operation of CGS is more evident during summer, where Cap Bon CGS remains the most active for around 75% of time in all the scenarios. For the remaining compression stations, the frequency of operation decreases drastically and progressively from Korba to Ain Naga, below 20% of activity. The corresponding gas consumption of the turbines is reported in Fig. 7.12. The higher operation of Cap Bon CGS is related to long offshore section of the pipeline network, in which higher pressure losses can take place.

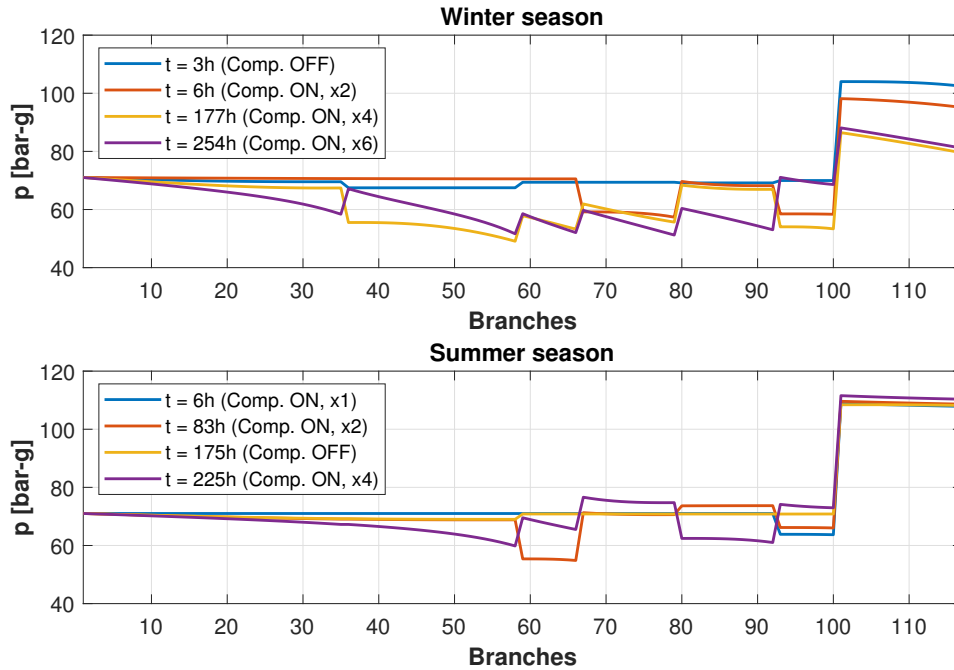


Figure 7.10. Pressure trends along Transmed in the base case.

Lastly, also in this case the transport efficiency has been estimated (Fig. 7.13). Unlike the results for Greenstream, unexpected values have been encountered. Whereas in the summer period the typical decreasing trend of the efficiency with a

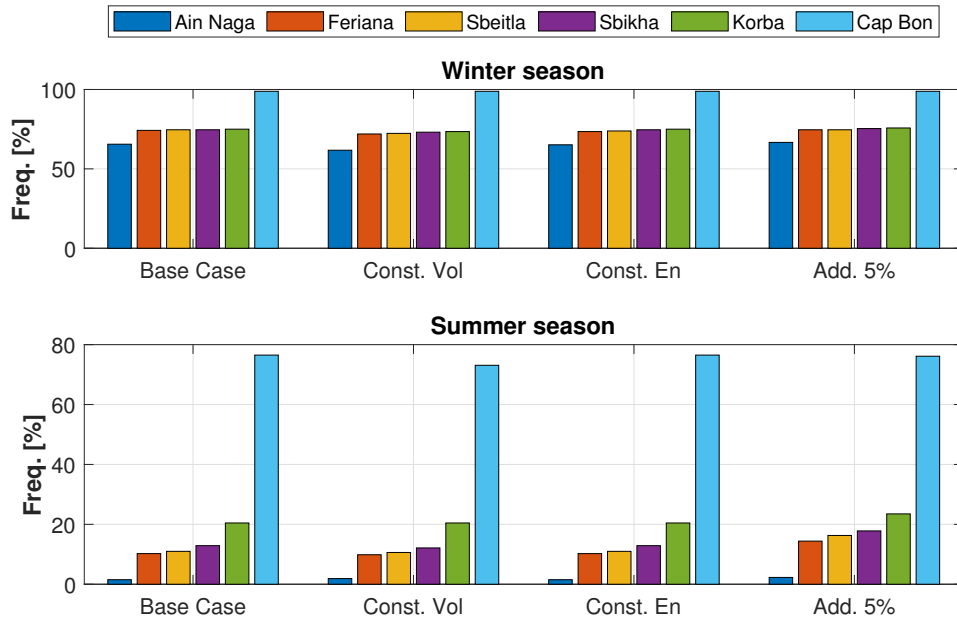


Figure 7.11. Frequencies of operation for all CGS.

higher amount of hydrogen imported has been found, in winter an opposite tendency has been detected. In fact, with higher hydrogen fractions there is an improvement in the transport efficiency. However, the percent variance in this case is considerably lower with respect to that for Greenstream, which could mean that the effect of hydrogen injection for Transmed is almost irrelevant, thanks to presence of several gas compression stations able to compensate pressure losses along the pipeline network effectively.

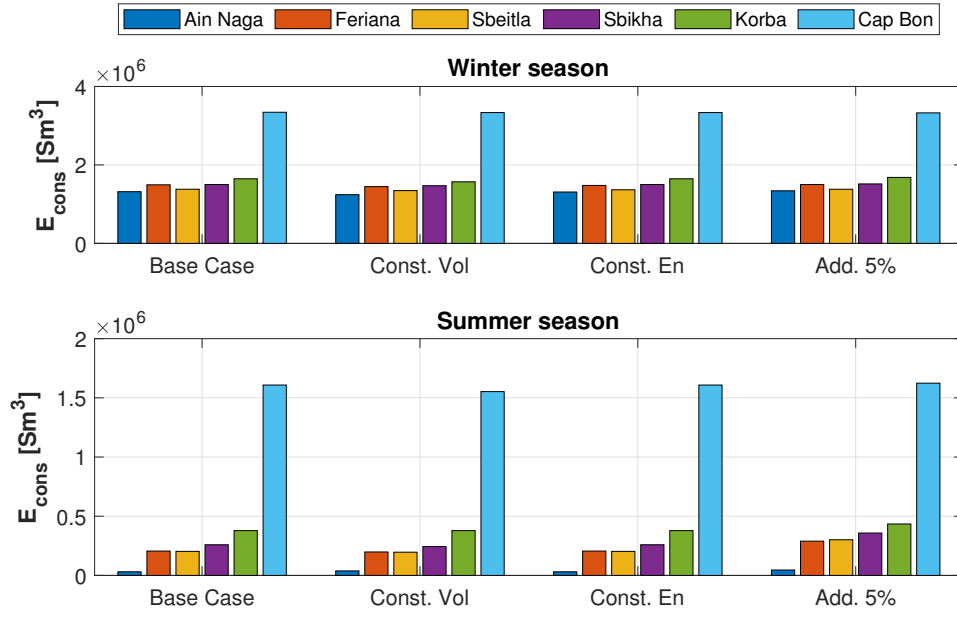


Figure 7.12. Gas consumption of turbines for all the CGS.

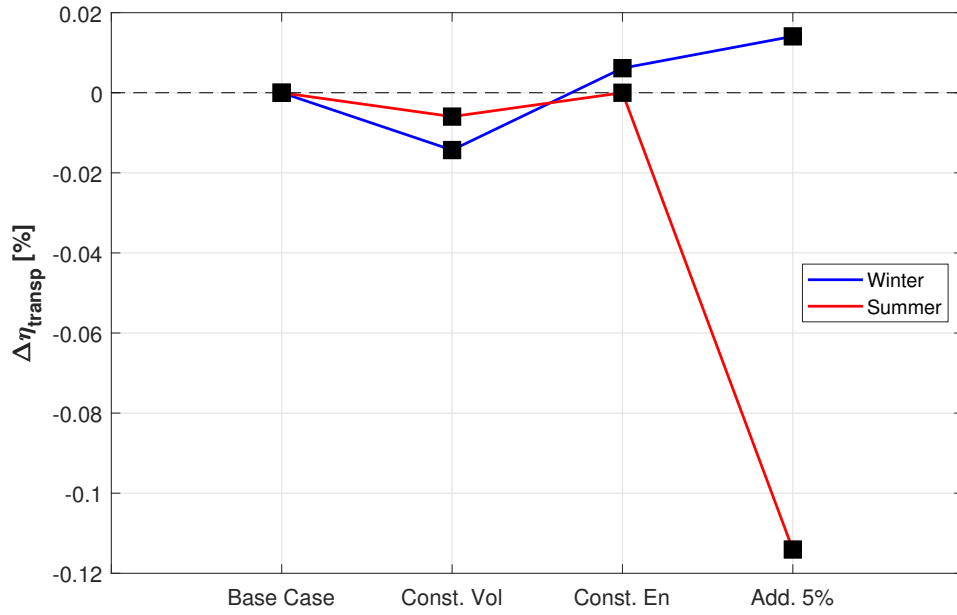


Figure 7.13. Percent variance of the transport efficiency for Transmed.

Chapter 8

Conclusions

The present work investigates the option of producing solar-based hydrogen from water electrolysis in North Africa, namely in Algeria, Tunisia and Libya. The final goal consists in transporting the hydrogen produced to Italy by injecting it into the existing natural gas pipeline systems crossing the Mediterranean Sea. To this end, the analysis focuses primarily on three system components: photovoltaic panels producing the electricity required by electrolyzers, hydrogen storage facilities and compression stations for blend transportation.

Firstly, a preliminary study on the main gas quality indicators has been conducted, in order to determine which hydrogen shares can be blended to natural gas imported through the pipeline networks Transmed and Greestream, in the respect of energy and safety constraints imposed by contract. Results showed that blends with a hydrogen volume below 10% are acceptable, which justified the choice of 5% of hydrogen adopted for the subsequent analyses.

For all simulations three scenarios have been considered: constant gas volume imported, constant energy imported and additional hydrogen injection to the actual trade of natural gas. For what concerns the sizing of photovoltaic systems, it turned out that nominal capacities comprised between 2.10–2.60 GW are required in Algeria and Tunisia in order to produce the total hydrogen demand associated to the natural gas imported through Transmed, which involves both the countries along its route. The corresponding occupied areas are in the range of 15–20 km², with lower values corresponding to Algeria. Regarding Libya, the installed capacities are even lower, in the range between 550–590 MW, with a required surface around 4 km². However, it is only due to the lower amount of natural gas imported through Greestream.

It was concluded that Algeria and Libya have better predisposition for the settlement of this technology. This is further confirmed by the subsequent step in the

analysis, consisting in the downsizing of the systems in order to decrease the produced hourly hydrogen shares. To do that, it was imposed the production of 5% hydrogen content in the blend with the maximum frequency over the year. Indeed, the process has been possible only for Algeria and Libya, which are the countries presenting better values of solar irradiation available throughout the year. It is thought that also the data extracted from Meteonorm has also affected this outcome, as it is referred to a predictive scenario. The production frequencies corresponding to the 5%vol H_2 are around 13% and 15% of the operative hours, respectively for Algeria and Libya. However, these frequencies goes up to 88% and 96% respectively regarding production of hydrogen below 10%vol, maximum injection limit found in this study. Moreover, it has been observed that a constant trend of the gas imported would affect positively on the size of these systems, decreasing the nominal capacities required as well as the maximum hydrogen shares produce, down to 8% vol. Anyhow, the main issue of this approach regards the partial supply of the hydrogen demand.

To deal with the intermittent nature of solar energy, it has been thought the integration of storage facilities in both the complete and partial supply systems of the hydrogen demand. Thus, it has been calculated the overproduced hydrogen that should be stored. Seasonal storage facilities have to be used for complete supply systems, as they are able to produce the entire amount of hydrogen requested over the year. Underground systems such as salt caverns, depleted gas reservoirs or aquifers are the most interesting solutions. However, operational experience of industrial hydrogen storage exists only in few locations and therefore further research has to be conducted. Concerning partial supply systems, the overproduced hydrogen can only be stored using daily storage systems. For that reason it has been calculated the number of tanks that would be necessary to store hydrogen in the compressed form. The considerable number of units together with the fact that only part of the hydrogen demand is fulfilled make this solution less attractive. In fact, the production frequency of 5%vol H_2 in the blend accounts for only 77% and 65% of the operative time, respectively for Algeria and Libya. Moreover, since no hydrogen is produced during periods in which there is no natural gas import, the operative hours of the plant are considerable reduced, decreasing in that way the capacity factor of the entire system.

Finally, from the analysis of compression stations along both natural gas pipeline networks considered, it has been demonstrated the feasibility of the hydrogen transport with the available nominal power of compressors. Thanks to the vast number of compression stations, Transmed presents very few variations in the transport efficiency in all the scenarios studied. Conversely, the effects of hydrogen injection are more evident in the case of Greenstream, where the power of compression required grows significantly with the increasing of the amount of hydrogen imported.

Bibliography

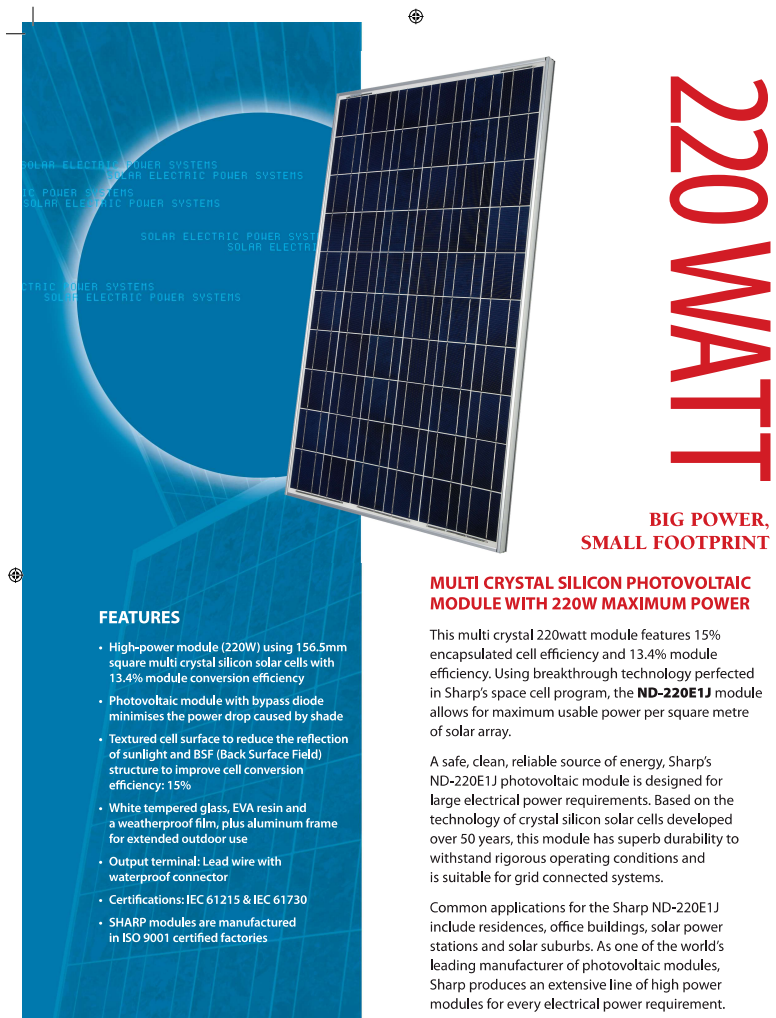
- [1] R. Boudries. “Techno-economic study of hydrogen production using CSP technology”. In: *International Journal of Hydrogen Energy* 43.6 (2018), pp. 3406–3417. ISSN: 03603199. DOI: 10.1016/j.ijhydene.2017.05.157.
- [2] R. Boudries and R. Dizene. “Prospects of solar hydrogen production in the Adrar region”. In: *Renewable Energy* 36.11 (2011), pp. 2872–2877. ISSN: 09601481. DOI: 10.1016/j.renene.2011.04.013.
- [3] Rafika Boudries. “Techno-economic Assessment of Solar Hydrogen Production Using CPV-electrolysis Systems”. In: *Energy Procedia* 93.March (2016), pp. 96–101. ISSN: 18766102. DOI: 10.1016/j.egypro.2016.07.155.
- [4] BP. *Full report – BP Statistical Review of World Energy 2019*.
- [5] Alexander Buttler and Hartmut Spliethoff. “Current status of water electrolysis for energy storage, grid balancing and sector coupling via power-to-gas and power-to-liquids: A review”. In: *Renewable and Sustainable Energy Reviews* 82.September 2017 (2018), pp. 2440–2454. ISSN: 18790690. DOI: 10.1016/j.rser.2017.09.003.
- [6] Anthony Dipaola. *Saudi Arabia Gets Cheapest Bids for Solar Power in Auction - Bloomberg*. <https://www.bloomberg.com/news/articles/2017-10-03/saudi-arabia-gets-cheapest-ever-bids-for-solar-power-in-auction>. 2017.
- [7] *ENTSOG - Transparency Platform*. <https://transparency.entsog.eu/>.
- [8] Markus Felgenhauer and Thomas Hamacher. “State-of-the-art of commercial electrolyzers and on-site hydrogen generation for logistic vehicles in South Carolina”. In: *International Journal of Hydrogen Energy* 40.5 (2015), pp. 2084–2090. ISSN: 03603199. DOI: 10.1016/j.ijhydene.2014.12.043.
- [9] Stephen Foster et al. *Non-renewable groundwater resources: a guidebook on socially-sustainable management for water-policy makers; IHP-VI series on groundwater; Vol.:10; 2006*. Tech. rep. 2006.
- [10] R. M. Goss. “BP statistical review of world energy 2019.” In: (2019).
- [11] H2tools. *Hydrogen Pipelines / Hydrogen Tools*. <https://h2tools.org/hyarc/hydrogen-data/hydrogen-pipelines>. 2016.
- [12] IRENA. *Renewable power generation costs in 2018*. Tech. rep. 2019.

- [13] Sophie Jablonski et al. “The Mediterranean Solar Plan: Project proposals for renewable energy in the Mediterranean Partner Countries region”. In: *Energy Policy* 44 (May 2012), pp. 291–300. ISSN: 03014215. DOI: 10.1016/j.enpol.2012.01.052.
- [14] Delf Rothe Jakob Horst, Annette Jünemann. *Euro-Mediterranean Relations after the Arab Spring: Persistence in Times of Change*. 2016.
- [15] S. Koumi Ngoh et al. “Design and simulation of hybrid solar high-temperature hydrogen production system using both solar photovoltaic and thermal energy”. In: *Sustainable Energy Technologies and Assessments* 7 (2014), pp. 279–293. ISSN: 22131388. DOI: 10.1016/j.seta.2014.05.002.
- [16] Bouziane Mahmah et al. “MedHySol: Future federator project of massive production of solar hydrogen”. In: *International Journal of Hydrogen Energy* 34.11 (2009), pp. 4922–4933. ISSN: 03603199. DOI: 10.1016/j.ijhydene.2008.12.068.
- [17] Amin Mohammadi and Mehdi Mehrpooya. “A comprehensive review on coupling different types of electrolyzer to renewable energy sources”. In: *Energy* 158 (2018), pp. 632–655. ISSN: 03605442. DOI: 10.1016/j.energy.2018.06.073.
- [18] Elena Quadri. *The Nubian Sandstone Aquifer System-A case of cooperation in the making*. Tech. rep.
- [19] Soumia Rahmouni et al. “Prospects of hydrogen production potential from renewable resources in Algeria”. In: *International Journal of Hydrogen Energy* 42.2 (2017), pp. 1383–1395. ISSN: 03603199. DOI: 10.1016/j.ijhydene.2016.07.214.
- [20] Joeri Rogelj et al. *Paris Agreement climate proposals need a boost to keep warming well below 2 °C*. June 2016. DOI: 10.1038/nature18307.
- [21] Hifa Salah, Adeen Embirsh, and Eng Yousuf Almkhtar Mathkour Ikshadah. “Future of Solar Energy in Libya”. In: *International Journal of Scientific and Research Publications* 7.10 (2017), p. 33. ISSN: 2250-3153.
- [22] Farid Sayedin et al. “Optimization of Photovoltaic Electrolyzer Hybrid systems; Taking into account the effect of climate conditions”. In: *Energy Conversion and Management* 118 (2016), pp. 438–449. ISSN: 01968904. DOI: 10.1016/j.enconman.2016.04.021.
- [23] Matthew R. Shaner et al. “A comparative technoeconomic analysis of renewable hydrogen production using solar energy”. In: *Energy and Environmental Science* 9.7 (2016), pp. 2354–2371. ISSN: 17545706. DOI: 10.1039/c5ee02573g.
- [24] *Snapshot of global photovoltaic markets*. Tech. rep. 2018.
- [25] *Sonatrach Solar Power Development Program*. Tech. rep. 2019.
- [26] Jamie Speirs et al. *A greener gas grid: What are the options?* Tech. rep. July. Sustainable Gas Institute, Imperial College London, 2017.
- [27] *The Future of Hydrogen*. Tech. rep. IEA, 2019.

- [28] Samir Touili et al. “A technical and economical assessment of hydrogen production potential from solar energy in Morocco”. In: *International Journal of Hydrogen Energy* 43.51 (2018), pp. 22777–22796. ISSN: 03603199. DOI: 10.1016/j.ijhydene.2018.10.136.

Appendix A

PV module specifications:



220 WATT

**BIG POWER,
SMALL FOOTPRINT**

FEATURES

- High-power module (220W) using 156.5mm square multi crystal silicon solar cells with 13.4% module conversion efficiency
- Photovoltaic module with bypass diode minimises the power drop caused by shade
- Textured cell surface to reduce the reflection of sunlight and BSF (Back Surface Field) structure to improve cell conversion efficiency: 15%
- White tempered glass, EVA resin and a weatherproof film, plus aluminum frame for extended outdoor use
- Output terminal: Lead wire with waterproof connector
- Certifications: IEC 61215 & IEC 61730
- SHARP modules are manufactured in ISO 9001 certified factories

MULTI CRYSTAL SILICON PHOTOVOLTAIC MODULE WITH 220W MAXIMUM POWER

This multi crystal 220watt module features 15% encapsulated cell efficiency and 13.4% module efficiency. Using breakthrough technology perfected in Sharp's space cell program, the **ND-220E1J** module allows for maximum usable power per square metre of solar array.

A safe, clean, reliable source of energy, Sharp's ND-220E1J photovoltaic module is designed for large electrical power requirements. Based on the technology of crystal silicon solar cells developed over 50 years, this module has superb durability to withstand rigorous operating conditions and is suitable for grid connected systems.

Common applications for the Sharp ND-220E1J include residences, office buildings, solar power stations and solar suburbs. As one of the world's leading manufacturer of photovoltaic modules, Sharp produces an extensive line of high power modules for every electrical power requirement.

ND-220E1J – MAXIMUM POWER

ELECTRICAL CHARACTERISTICS

Cell	156.5mm Square Polycrystalline silicon
No. of Cells and Connections	60 in series
Open Circuit Voltage (Voc)	36.5V
Maximum Power Voltage (Vpm)	29.2V
Short Circuit Current (Isc)	8.20A
Maximum Power Current (Ipm)	7.54A
Maximum Power (Pm) ¹	Typical 220W
Encapsulated Solar Cell Efficiency (ηc)	15%
Module Efficiency (ηm)	13.4%
Maximum System Voltage	DC 1000V
Series Fuse Rating	15A
Type of Output Terminal	Lead Wire with MC3 Connector

Specifications are subject to change without notice
¹ (STC) Standard Test Conditions: 25°C, 1 kW/m², AM 1.5

MECHANICAL CHARACTERISTICS

Dimensions	994 x 1652 x 46mm
Weight	21.0kg

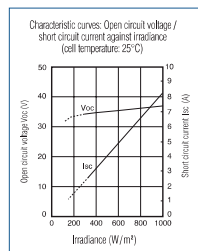
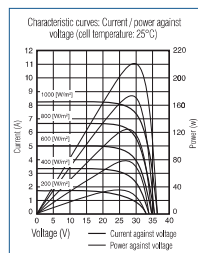
TEMPERATURE COEFFICIENT

Temp. Coefficient of Pmax	-0.485	% / °C
Temp. Coefficient of Voc	-0.13	V / °C
Temp. Coefficient of Isc	0.053	% / °C

ABSOLUTE MAXIMUM RATINGS

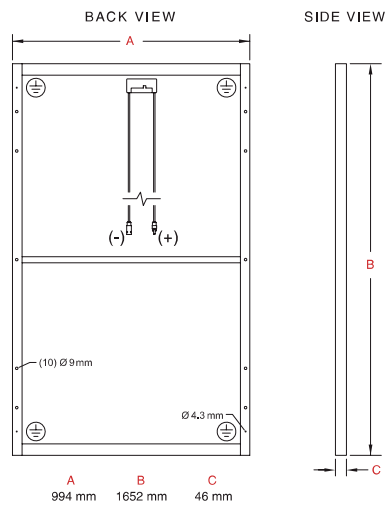
Parameters	Rating	Unit
Operating Temperature	-40 to +90	°C
Storage Temperature	-40 to +90	°C
Dielectric Voltage Withstood	3000 max.	V-DC

IV CURVES



Specifications are subject to change without notice

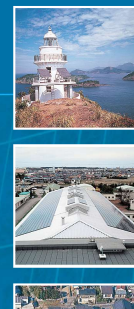
DIMENSIONS



Specifications are subject to change without notice

In the absence of confirmation by device specifications sheets, Sharp takes no responsibility for any defects that may occur in equipment using any Sharp devices shown in catalogues, data books, etc. Contact Sharp in order to obtain the latest device specification sheets before using any Sharp device.

- Design and specifications are subject to change without prior notice.
- Colour variations to products may occur due to printing.
- All information and technical details are correct as at product release date.



Appendix B

H₂ storage tank specifications:



DATASHEET

TANK – 60bar 850L

Type IV buffer tank at 60bar

The perfect solution to store H₂ after electrolyser



Can be installed/packaged in a rack by 1,2,3...*

SERVICE CONDITIONS	
Mass of hydrogen stored at 60bar (15°C)	4.2kg
Temperature of use	From -40°C to 65°C
Maximum working pressure (PS)	60bar
PRV (can be installed by MAHYTEC on request)	Maximum 60bar
Maximum refilling pressure	60bar
Position of use	Vertical or horizontal
DIMENSIONS	
Inner volume	850L
Mass of empty tank	215kg
External dimensions (cm) (without support)	Ø 84 x 187
MATERIALS	
Body material	Type IV polymer liner with composite materials
Nozzle stainless steel	A2
REGULATION TEST	
Service life	20 years / 10,000 cycles
Hydraulic pressure proof test	86bar
Approved according to	AD2000 - PED 2014/68/EU

Example of installation: two tanks in a rack*

CL-DS10
Update: 21/05/2019



All data are subject to change without notification

MAHYTEC - 6 rue Léon Bel, 39100 Dole - France / contact@mahytec.com - www.mahytec.com - +33 (0)3 84 80 17 20